AD-A127 840 ACTA AERONAUTICA ET ASTRONAUTICA SINICA(U) FOREIGN TECHNOLOGY DIV WRIGHT-PATTERSON AFB OH Y ZHENG ET AL. 04 MAR 83 FTD-ID(RS)T-1605-82 1/2

UNCLASSIFIED F/G 20/4 NL

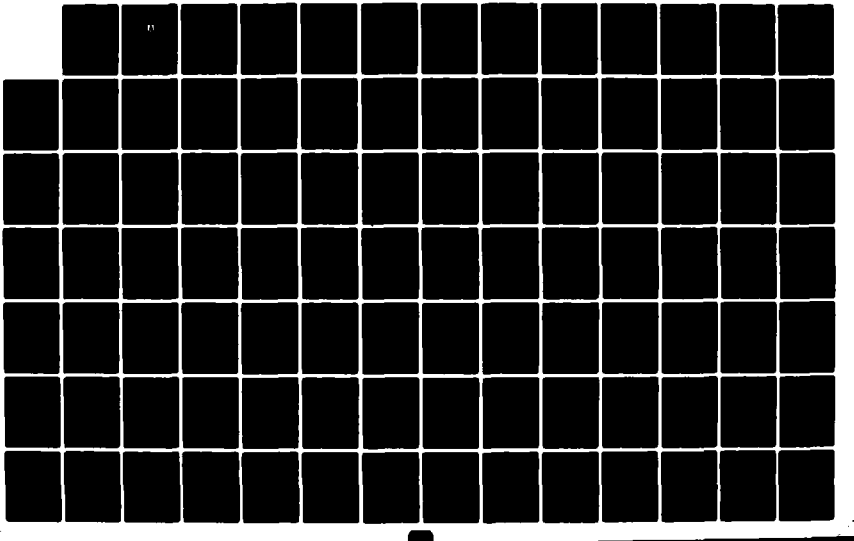

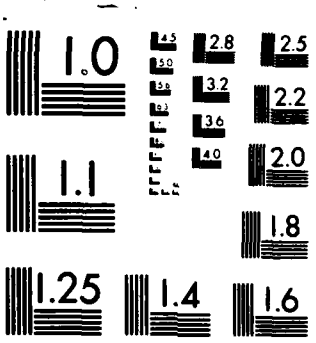

FTD-ID(RS)T-1605-82

AD A127840

FOREIGN TECHNOLOGY DIVISION

ACTA AERONAUTICA ET ASTRONAUTICA SINICA

Approved for public release;
distribution unlimited.

83 05 09-039

EDITED TRANSLATION

FTD-ID(RS)T-1605-82 4 March 1983

MICROFICHE NR: FTD-83-C-000334

ACTA AERONAUTICA ET ASTRONAUTICA SINICA

English pages: 162

Source: Hang Kong Xuebao, Vol. 3, Nr. 3, September 1982, pp. 1-105

Country of origin: China
Translated by: SCITRAN
F33657-81-D-0263
Requester: FTD/TQTA

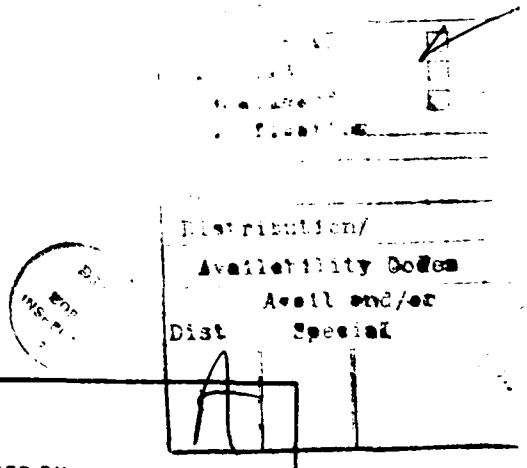

PREPARED BY:

TRANSLATION DIVISION
FOREIGN TECHNOLOGY DIVISION
WP-AFB, OHIO.

TABLE OF CONTENTS

SOCIETY NEWS

GRAPHICS DISCLAIMER

All figures, graphics, tables, equations, etc. merged into this translation were extracted from the best quality copy available.

RELAXATION COMPUTATION OF TRANSONIC FLOWS AROUND WINGS WITH BLUNT LEADING-EDGE AND DISCUSSION ON ITS STABILITY AND CONVERGENCE

Northwestern Polytechnical University*
/Zheng Yuwen and Luo Shijun

ABSTRACT

In this paper, the exact velocity potential equation and /1** the exact boundary conditions were used around the blunt leading-edge of a wing, and the velocity potential equation with small perturbation in the transverse direction and large perturbation in the longitudinal direction together with its corresponding boundary conditions were used in other areas to obtain the solution. Numerical example 1 was for a rectangular wing with an aspect ratio $\lambda=12$, airfoil NACA0012, free stream Mach number $M_\infty=0.63$, and attack angle $\alpha=2^\circ$. The calculated pressure distribution of the root section was close to the exact numerical subsonic solution (Sells, 1968). Example 2 was an experimental wing NACA RM A51G31 having airfoil NACA 64A010 which is perpendicular to the 1/4 chord line with a sweepback angle $\chi_{1/4}=45^\circ$, $\lambda=3$, taper ratio $\eta=2$, $M_\infty=0.4$, 0.8, 0.9, and $\alpha=2^\circ$. The computed results were very close to the experimental ones.

In this paper, we establish the stability conditions of the linear relaxation with improving iteration of the transonic velocity potential difference equation with small steady perturbation under the assumption of local linearization, and the conditions for the convergence of the relaxation solution to the original differential equation solution. These conditions more or less agree with the numerical experiments.

*Received December, 1981.

**Numbers in the margin indicate pagination of foreign text.

INTRODUCTION

The blunt leading-edge is a singular point of the classical small perturbation equation. There are numerous treatment methods in the literature. In Reference [1,2], the leading-edge was avoided, i.e., the leading edge was not taken as a mesh point. Thus, the arrangement of the mesh had a large effect on the calculated results. Reference [3], in the treatment of the leading-edge, used the following equation:

$$\int_{x_L}^{x_T} \frac{\partial y_\pm}{\partial x} dx = y_\pm(x_T, z) - y_\pm(x_L, z)$$

where x_L and x_T are the chord direction coordinates of the leading edge and the trailing edge; $y\pm$ are the vertical coordinates of the top and bottom surfaces of the wing; and z is the span direction coordinate. The integral on the left is calculated by the trapezoidal equation according to the mesh used. Using the above equation, it is possible to solve for $\frac{\partial y_\pm}{\partial x}$ at the leading edge. In Reference [4], based on the mesh used, $\frac{\partial y_\pm}{\partial x} = \pm 0.2$, was obtained at the leading edge using an extrapolation method. This type of treatment is equivalent to the sharpening of the leading edge which has some arbitrariness.

In the first part of this paper, the leading edge of the wing was taken as a mesh point. Using the directional derivative equation, the exact boundary condition of the blunt leading edge was inserted into the exact velocity potential equation. In other areas, the small transverse perturbation velocity potential equation and the small transverse pertubation boundary conditions were used. This method avoided the shortcomings of the above described method which is also easy to apply.

The results of several numerical tests showed that: whether the linear relaxation of transonic small perturbation

potential flow converges or not and the convergence speed (if it converges) are related to the relaxation factor ω.[3,5] /2
Here we need to use theoretical analysis guidance. In the second part of this paper, under the assumption of local linearization, the stability of linear relaxation with improving iteration was analysed using the von Neumann method. Furthermore, the convergence of linear relaxation improving iteration was discussed using the separation of variables method for the corresponding differential equation.

1. RELATION COMPUTATION OF TRANSONIC POTENTIAL FLOW AROUND WINGS WITH BLUNT LEADING EDGE

1. Basic Equations

Let us choose a rectangular coordinate system oxyz. The x-axis is parallel to the wing chord and the z-axis is parallel to the wing span. At the blunt leading edge, the exact perturbation vel city potential equation was used:

$$(a^2-u^2)\varphi_{xx}+(a^2-v^2)\varphi_{yy}+(a^2-w^2)\varphi_{zz}-2uv\varphi_{xy}-2uw\varphi_{xz}-2vw\varphi_{yz}=0 \tag{1}$$

where

$$a^2=a_\infty^2+\frac{\gamma-1}{2}(q_\infty^2-u^2-v^2-w^2)$$

$$u=q_\infty\cos\alpha+\varphi_x,\quad v=q_\infty\sin\alpha+\varphi_y,\quad w=\varphi_z$$

γ is the adiabatic index; q_∞ and a_∞ are the velocity and sonic speed of the free stream; and (u,v,w) and a are the local velocity and the sonic speed.

At a non-leading edge point, assuming that velocity perturbation components in the y and z directions are small and that in the x-direction may not be small, then equation (1) can be simplified as

$$(1-M^2)\varphi_{xx}+\varphi_{yy}+\varphi_{zz}=0 \tag{2}$$

where

$$1-M^2=\frac{1-M_\infty^2\cos^2\alpha-\frac{\gamma+1}{q_\infty}M_\infty^2\cos\alpha\varphi_x-\frac{\gamma+1}{aq_\infty^2}M_\infty^2\varphi_x^2}{1-\frac{\gamma-1}{q_\infty}M_\infty^2\cos\alpha\varphi_x-\frac{\gamma-1}{aq_\infty^2}M_\infty^2\varphi_x^2} \tag{3}$$

M is the local Mach number.

2. Boundary Conditions

Let us choose the coordinate plane oxz in the wing plane. The boundary condition of the wing surface with the exception of the leading edge can be simplified, under the assumption of small transverse perturbation, as

$$\varphi_y(x,\pm 0,z)=(q_\infty\cos\alpha+\varphi_x(x,\pm 0,z))\frac{\partial y_\pm}{\partial x}-q_\infty\sin\alpha \tag{4}$$

Similarly, the conditions on the free vortex behind the wing can be simplified as

$$\varphi_y(x,+0,z)=\varphi_y(x,-0,z) \tag{5}$$

$$\varphi(x,+0,z)-\varphi(x,-0,z)=\varphi(x_T,+0,z)-\varphi(x_T,-0,z) \tag{6}$$

The exact boundary condition at the blunt leading edge is

$$\varphi_n=-q_\infty\cos\alpha\cos\chi \tag{7}$$

where χ - the sweepback angle of the leading edge of the wing.
n - the normal direction of the leading edge (Figure 1).

Inserting equation (7) into the directional derivative equation of the leading edge, we get

$$\left.\begin{aligned}\varphi_s &= \varphi_t \sin\chi - q_\infty \cos\alpha \cos^2\chi \\ \varphi_n &= \varphi_t \cos\chi + q_\infty \cos\alpha \sin\chi \cos\chi\end{aligned}\right\} \tag{8}$$

where t is the direction of the leading-edge (Figure 1).

By isolating the boundary condition of the leading edge of the root of the wing, equation (8) can be transformed into

$$\left.\begin{aligned}\varphi_s &= -q_\infty \cos\alpha \\ \varphi_n &= 0\end{aligned}\right\} \tag{9}$$

Similarily, the boundary condition of the leading edge of the wing tip is also equation (9).

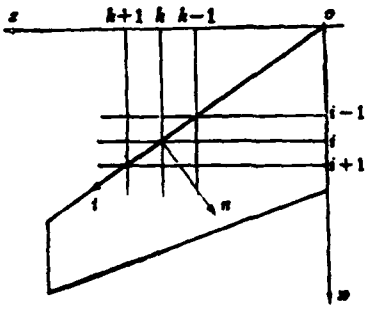

Figure 1. Wing plane.

The boundary condition of the far field of the wing can use the small perturbation condition which is shown in §1.6 of Reference [6].

3. The Difference Equation

Let us choose the sequential symbols for the mesh nodal points in the x,y,z directions to be i,j,k. At the blunt leading-edge of the wing, the first order partial derivatives φ_x and φ_z are calculated from equation (8) in which φ_t uses the central difference scheme. This means that it is assumed that at the leading edge it is subsonic:

$$\varphi_t = \frac{\Delta t_{i-1}^2 \varphi_{i+1,j,k+1} + (\Delta t_i^2 - \Delta t_{i-1}^2)\varphi_{i,j,k} - \Delta t_i^2 \varphi_{i-1,j,k-1}}{\Delta t_{i-1}\Delta t_i(\Delta t_{i-1} + \Delta t_i)} \tag{10}$$

(11)

where $\Delta t_i = \Delta x_i / \sin\chi$, Δx_i and Δt_i are the step lengths.

The first order partial derivative φ_y, similar to φ_t, is calculated using the central difference equation. The second order partial derivatives can be calculated as follows:

$$\left.\begin{aligned}
\varphi_{xx} &= \frac{2}{\Delta x_{i-1}}\left(\varphi_x - \frac{\varphi_{i,j,k}-\varphi_{i-1,j,k}}{\Delta x_{i-1}}\right)\\
\varphi_{zz} &= \frac{2}{\Delta z_k}\left(\frac{\varphi_{i,j,k+1}-\varphi_{i,j,k}}{\Delta z_k} - \varphi_z\right)\\
\varphi_{yy} &= 2\,\frac{\varphi_{i,j+1,k}\Delta y_{j-1} - \varphi_{i,j,k}(\Delta y_{j-1}+\Delta y_j) + \varphi_{i,j-1,k}\Delta y_j}{\Delta y_{j-1}\Delta y_j(\Delta y_{j-1}+\Delta y_j)}\\
\varphi_{xx} &= \frac{1}{\Delta x_{i-1}}(\varphi_x|_{i,j,k} - \varphi_x|_{i-1,j,k})\\
\varphi_{xy} &= \frac{1}{\Delta x_{i-1}}(\varphi_y|_{i,j,k} - \varphi_y|_{i-1,j,k})\\
\varphi_{yz} &= \frac{1}{\Delta z_k}(\varphi_y|_{i,j,k+1} - \varphi_y|_{i,j,k})
\end{aligned}\right\} \qquad (12)$$

where φ_x and φ_z are computed based on equation (8). Other first order partial derivatives, similar to φ_t, are calculated using the central difference equation. Δ_{yi} and Δ_{zk} are the step lengths.

With the exception of the leading edge, the small transverse perturbation velocity potential equation (2) is used. The Murman-Cole mixed difference format is used in the difference equation. On the surface of the wing and the upper surface j=jw+o of the free vortex:

$$\varphi_{yy}|_{i,j_w+o,k} = \frac{2}{\Delta y_{j_w}}\left(\frac{\varphi_{i,j_w+1,k}-\varphi_{i,j_w+o,k}}{\Delta y_{j_w}} - \varphi_y|_{i,j_w+o,k}\right) \qquad (13)$$

Similarily, the expression for the lower surface can be written.

4. Linear Relaxation and Iteration Computation

The set of difference equations is solved using the linear relaxation and improved iteration method. The details of the method will be shown in Section II. Numerical example 1 is a rectangular wing having airfoil NACA0012 with an aspect ratio of λ=12. Choose a mesh which is 31x13x33. The wing chord is equally divided into 20 blocks and the half wing span is divided into 29 blocks. It takes 20 seconds per iteration on the 655 computer. M_∞=0.63, $\alpha=2^\circ$. By choosing a relaxation factor ω=1.0, where the number of iteration reached n=1045, we obtained /4

$$\max|\varphi^{(n)}_{i,j,k}-\varphi^{(n-1)}_{i,j,k}|=0.15\times10^{-4}$$, which is noted as /$\Delta\varphi$/

The pressure distribution of the wing root section obtained is very close to the exact numerical subsonic solution[1] as shown in Figure 2.

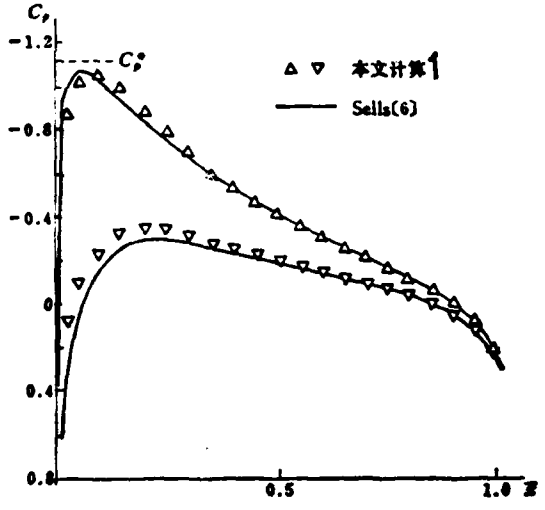

Figure 2. Pressure distribution of the root section of a rectangular wing.

Key: 1) calculation in this work.

Example 2 is the experimental wing in Reference [8]. The airfoil perpendicular to the 1/4 chord line is NACA 64A010. $X_{1/4}=45^{\circ}$, $\lambda=3$, $\eta=2$. Choose a mesh of 31x13x19. There are 15 sections along the half wing span. Each section has 11 points. It takes 10 seconds for each iteration on the 655 machine. The computational results are shown in Table 1. The computed results agree with the experimental ones [8] as shown in Figures 3-5. The calculated results are better than those reported in Reference [4]. In Reference [4], the small perturbation velocity potential equation and $\frac{\partial y_{\pm}}{\partial x}=\pm 0.2$ were used at the blunt leading-edge.

Table 1. Computed cases of NACA RM A51G31 Wing.

M_∞	α	$\omega(M<1)$	$\omega(M>1)$	n	$\lvert\Delta\varphi\rvert$
0.4	2°	1	1	258	0.7×10^{-3}
0.8	2°	0.9	0.7	481	0.13×10^{-3}
0.9	2°	0.9	0.7	667	0.15×10^{-3}

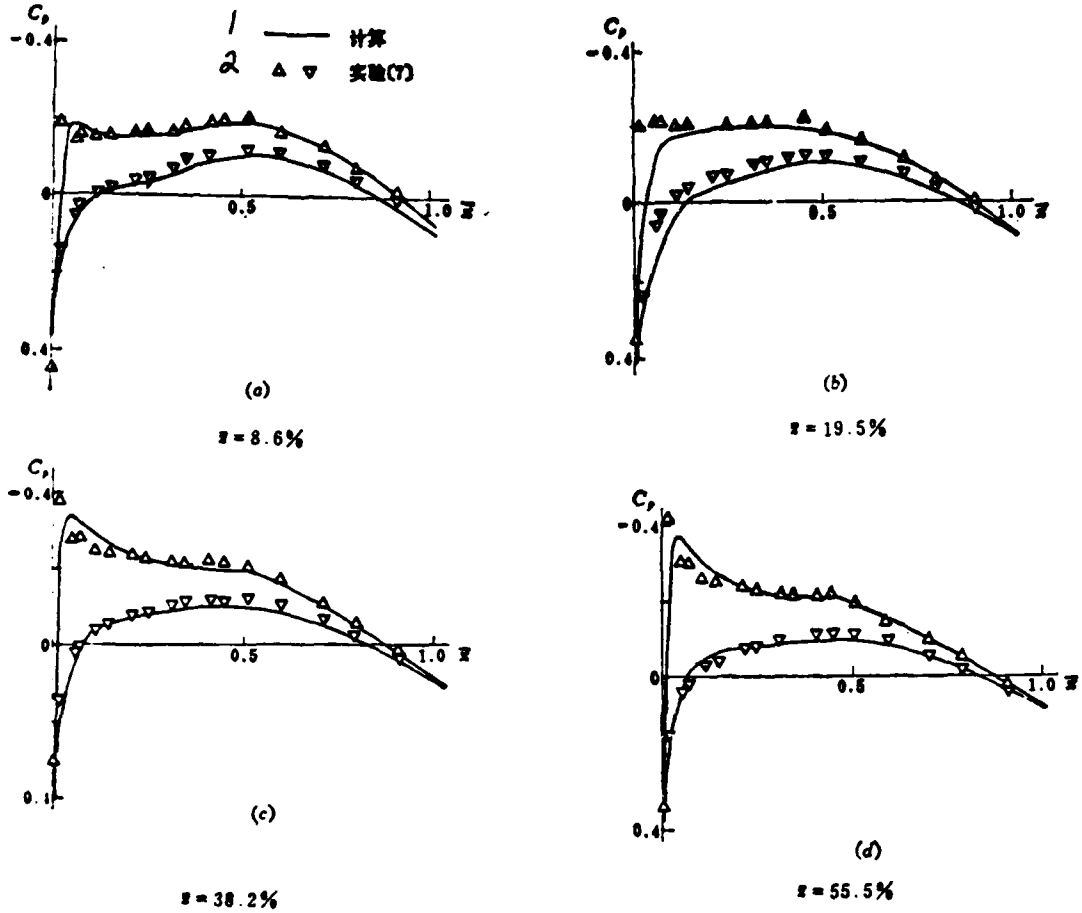

Figure 3. Pressure distribution of NACA RM A51G31 wing $M_\infty = 0.4$, $\alpha = 2^\circ$.
Key: 1) computed; 2) experimental [7].

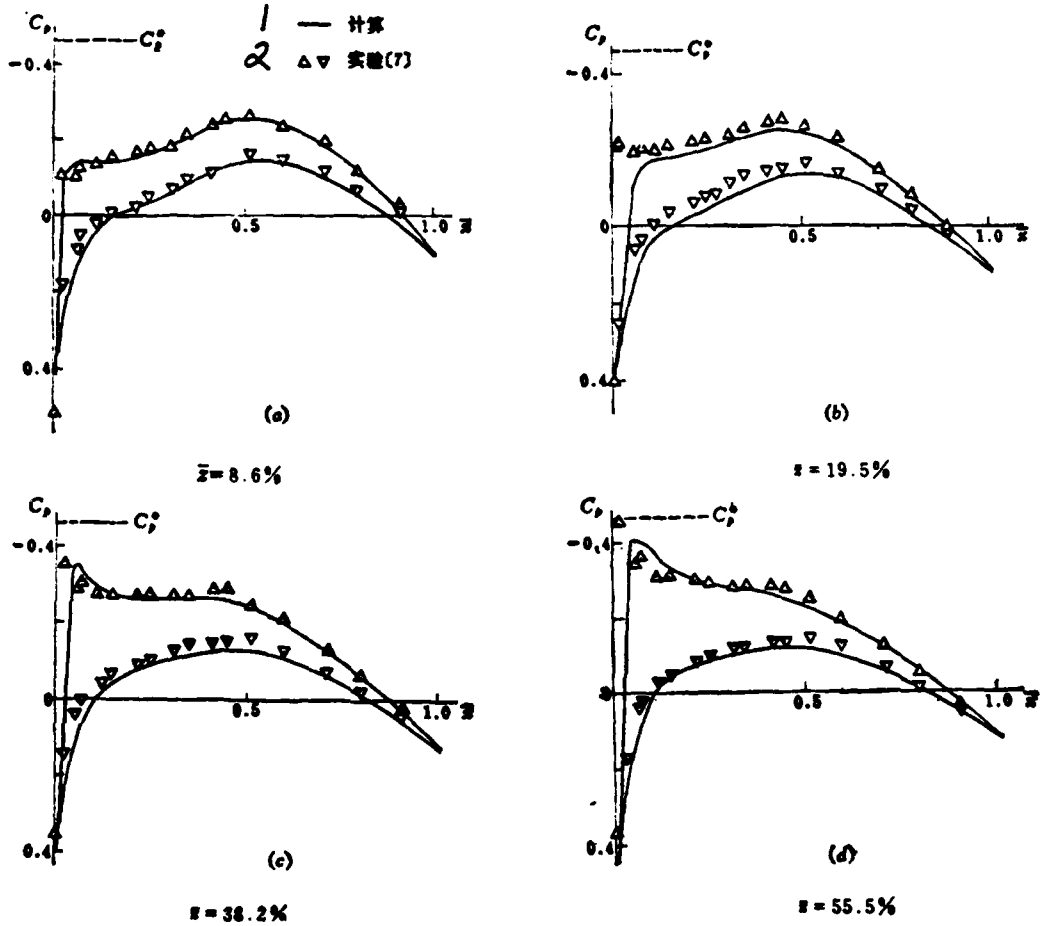

Figure 4. Pressure distribution of NACA RM A51G31 wing $M_\infty = 0.8$, $\alpha = 2^\circ$.

Key: 1) computed; 2) experimental [7].

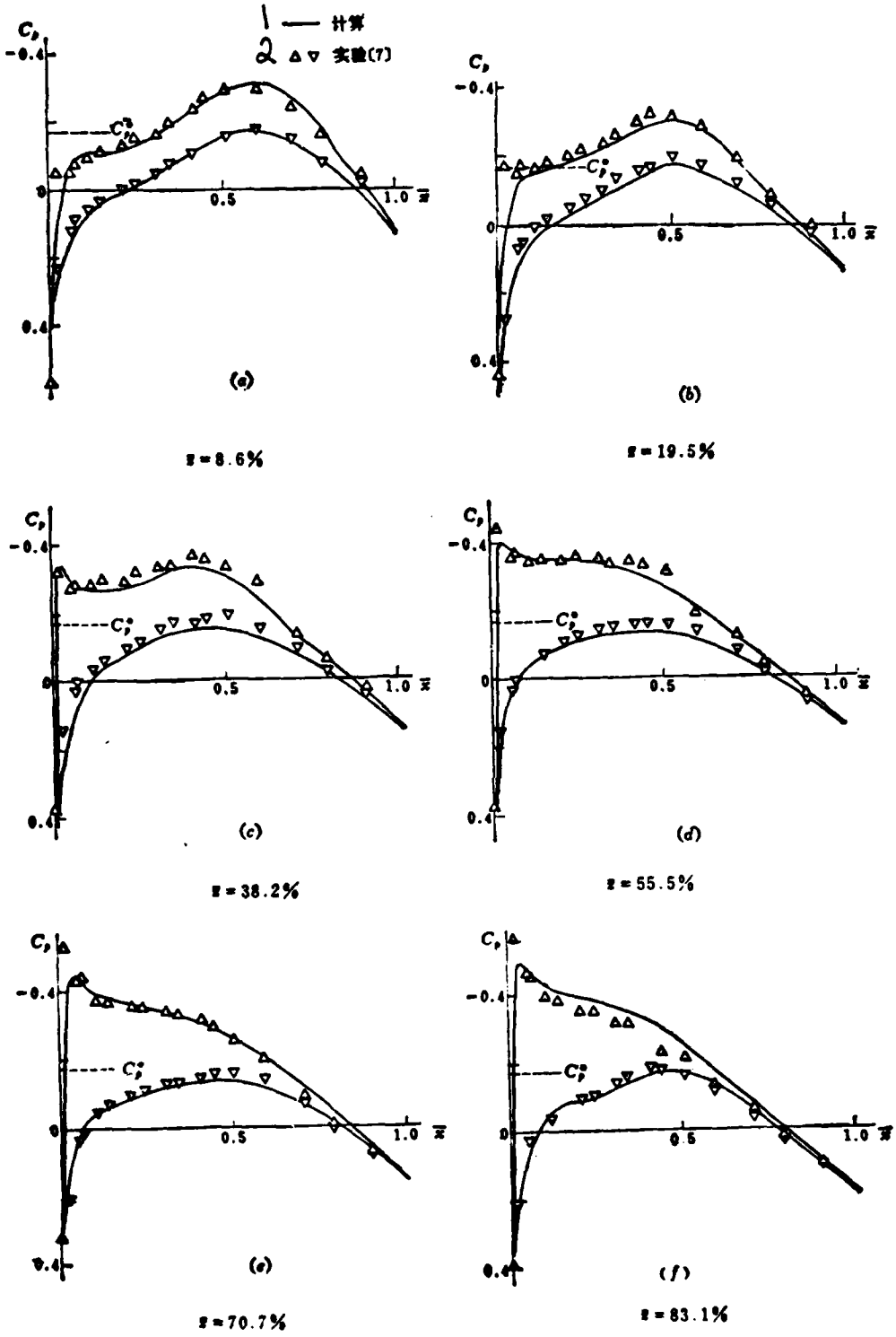

Figure 5. Pressure Distribution of NACA RM A51G31 wing M_∞=0.9, $\alpha=2^0$.

Key: 1) computed; 2) experimental [7].

2. DISCUSSION ON THE STABILITY AND CONVERGENCE OF LINEAR RELAXATION AND IMPROVING ITERATION /8

1. Discussion on Stability

In order to analyze the stability of the difference equation of the linear relaxation improving iteration of the small transverse perturbation velocity potential equation (2), it is assumed that the coefficient $1=M^2$ of the φ_{xx} term in equation (2) is a constant, i.e., local linearization. Thus, at the local subsonic point and the local supersonic point, equation (2) can be transformed into

$$\varphi_{xx}+\varphi_{yy}+\varphi_{zz}=0 \tag{14}$$

$$-\varphi_{xx}+\varphi_{yy}+\varphi_{zz}=0 \tag{15}$$

By choosing the relaxation line which is parallel to the y-axis, the difference equations of linear relaxation and iteration of equations (14) and (15) are

$$\frac{\varphi^{(n-1)}_{i+1,j,k}-2\bar{\varphi}^{(n)}_{i,j,k}+\varphi^{(n)}_{i-1,j,k}}{\Delta x^2}+\frac{\bar{\varphi}^{(n)}_{i,j+1,k}-2\bar{\varphi}^{(n)}_{i,j,k}+\bar{\varphi}^{(n)}_{i,j-1,k}}{\Delta y^2}+\frac{\varphi^{(n-1)}_{i,j,k+1}-2\bar{\varphi}^{(n)}_{i,j,k}+\varphi^{(n)}_{i,j,k-1}}{\Delta z^2}=0 \tag{16}$$

$$-\frac{\bar{\varphi}^{(n)}_{i,j,k}-2\varphi^{(n)}_{i-1,j,k}+\varphi^{(n)}_{i-2,j,k}}{\Delta x^2}+\frac{\bar{\varphi}^{(n)}_{i,j+1,k}-2\bar{\varphi}^{(n)}_{i,j,k}+\bar{\varphi}^{(n)}_{i,j-1,k}}{\Delta y^2}+\frac{\varphi^{(n-1)}_{i,j,k+1}-2\bar{\varphi}^{(n)}_{i,j,k}+\varphi^{(n)}_{i,j,k-1}}{\Delta z^2}=0 \tag{17}$$

where

$$\bar{\varphi}^{(n)}_{i,j,k}=\frac{1}{\omega}\varphi^{(n)}_{i,j,k}+\left(1-\frac{1}{\omega}\right)\varphi^{(n-1)}_{i,j,k} \tag{18}$$

Substituting (18) into (16) and (17), we get

$$\frac{\varphi^{(n-1)}_{i+1,j,k}-\frac{2}{\omega}\varphi^{(n)}_{i,j,k}-2\left(1-\frac{1}{\omega}\right)\varphi^{(n-1)}_{i,j,k}+\varphi^{(n)}_{i-1,j,k}}{\Delta x^2}+\{\quad\}=0 \tag{19}$$

$$-\frac{\frac{1}{\omega}\varphi^{(n)}_{i,j,k}+\left(1-\frac{1}{\omega}\right)\varphi^{(n-1)}_{i,j,k}-2\varphi^{(n)}_{i-1,j,k}+\varphi^{(n)}_{i-2,j,k}}{\Delta x^2}+\{\quad\}=0 \tag{20}$$

where

$$\{\quad\}=\frac{\frac{1}{\omega}(\varphi^{(n)}_{i,j+1,k}-2\varphi^{(n)}_{i,j,k}+\varphi^{(n)}_{i,j-1,k})+\left(1-\frac{1}{\omega}\right)(\varphi^{(n-1)}_{i,j+1,k}-2\varphi^{(n-1)}_{i,j,k}+\varphi^{(n-1)}_{i,j-1,k})}{\Delta y^2}+\frac{\varphi^{(n-1)}_{i,j,k+1}-\frac{2}{\omega}\varphi^{(n)}_{i,j,k}-2\left(1-\frac{1}{\omega}\right)\varphi^{(n-1)}_{i,j,k}+\varphi^{(n)}_{i,j,k-1}}{\Delta z^2} \tag{A}$$

Introduce a new variable t which corresponds to the separation variable n. Then:

$$\varphi = \varphi(x, y, z, t) \tag{B}$$

Let the step length of t be Δt. $\frac{\partial \varphi}{\partial t}$ should choose the leading difference form:

$$\varphi_t|^{(n)}_{i,j,k} = \frac{\varphi^{(n)}_{i,j,k} - \varphi^{(n-1)}_{i,j,k}}{\Delta t} \tag{21}$$

The difference equations (19) and (20) are equivalent to the following differential equations:

$$\varphi_{xx} + \varphi_{yy} + \varphi_{zz} - \left(\frac{\Delta t}{\Delta x^2} + \frac{\Delta t}{\Delta z^2}\right)\left(\frac{2}{\omega} - 1\right)\varphi_t - \frac{\Delta t}{\Delta x}\varphi_{xt} - \frac{\Delta t}{\Delta z}\varphi_{zt} = 0 \tag{22}$$

/9

$$-\varphi_{xx} + \varphi_{yy} + \varphi_{zz} - \left[\left(\frac{1}{\omega} - 1\right)\frac{\Delta t}{\Delta x^2} + \left(\frac{2}{\omega} - 1\right)\frac{\Delta t}{\Delta z^2}\right]\varphi_t - \frac{\Delta t}{\Delta z}\varphi_{zt} = 0 \tag{23}$$

The above equations are different from equations (14) and (15). They are time dependent equations.

Now, let us analyze the stability of equations (19) and (20). Let the exact solution of the difference equation be φ, and the numerical solution of the difference equation be $\varphi + \delta$ where δ is the error introduced by the numerical computation. φ and $\varphi + \delta$ satisfy the same difference equation. Because the difference equation is linear, therefore, δ also satisfies the same difference equation. Based on the superposition principle of linearity, δ can be decomposed into the basic solution with an expression such as

$$\delta(x, y, z, t) = e^{\alpha_0 t + i_0(\beta_1 x + \beta_2 y + \beta_3 z)} \tag{24}$$

where $i_0 = \sqrt{-1}$, β_1, β_2, and β_3 are arbitrary real numbers and α_0 is a function of these numbers.

Substituting equation (24) into (19) and (20), we get

$$|e^{s\Delta t}| = \left| \frac{\left(\frac{2}{\omega}-1\right)\left(\frac{1}{\Delta x^2}+\frac{2}{\Delta y^2}\sin^2\frac{\beta_2\Delta y}{2}+\frac{1}{\Delta z^2}\right)-\frac{1-\cos\beta_1\Delta x}{\Delta x^2} - \frac{2}{\Delta y^2}\sin^2\frac{\beta_2\Delta y}{2}-\frac{1-\cos\beta_3\Delta z}{\Delta z^2}+i_0\left(\frac{\sin\beta_1\Delta x}{\Delta x^2}+\frac{\sin\beta_3\Delta z}{\Delta z^2}\right)}{\left(\frac{2}{\omega}-1\right)\left(\frac{1}{\Delta x^2}+\frac{2}{\Delta y^2}\sin^2\frac{\beta_2\Delta y}{2}+\frac{1}{\Delta z^2}\right)+\frac{1-\cos\beta_1\Delta x}{\Delta x^2} + \frac{2}{\Delta y^2}\sin^2\frac{\beta_2\Delta y}{2}+\frac{1-\cos\beta_3\Delta z}{\Delta z^2}+i_0\left(\frac{\sin\beta_1\Delta x}{\Delta x^2}+\frac{\sin\beta_3\Delta z}{\Delta z^2}\right)} \right| \tag{25}$$

$$|e^{s\Delta t}| = \left|\frac{A}{B}\right| \tag{26}$$

where

$$A = \left(\frac{1}{\omega}-1\right)\left(\frac{1}{\Delta x^2}+\frac{4}{\Delta y^2}\sin^2\frac{\beta_2\Delta y}{2}+\frac{2}{\Delta z^2}\right)+\frac{\cos\beta_3\Delta z}{\Delta z^2}+i_0\frac{\sin\beta_3\Delta z}{\Delta z^2}$$

$$B = \left(\frac{1}{\omega}-1\right)\left(\frac{1}{\Delta x^2}+\frac{4}{\Delta y^2}\sin^2\frac{\beta_2\Delta y}{2}+\frac{2}{\Delta z^2}\right)-\frac{4}{\Delta x^2}\cos\beta_1\Delta x\sin^2\frac{\beta_1\Delta x}{2}+\frac{4}{\Delta y^2}\sin^2\frac{\beta_2\Delta y}{2} + \frac{2}{\Delta z^2}-\frac{\cos\beta_3\Delta z}{\Delta z^2}+i_0\left(\frac{4}{\Delta x^2}\sin\beta_1\Delta x\sin^2\frac{\beta_1\Delta x}{2}+\frac{\sin\beta_3\Delta z}{\Delta z^2}\right)$$

According to the stability condition $|e^{s\Delta t}| \leqslant 1$, from equation (25) we obtain

$$0 < \omega \leqslant 2 \tag{27}$$

For equation (26), it is not possible to find an ω to satisfy the stability condition. The proof is shown in the Appendix.

2. Discussion on Convergence

Convergence means the converging of the solution of the time dependent differential equations (23) and (24) to the solution of the steady state differential equations (14) and (15). Perform variable transformations for equations (22) and (23),

$$\tau = t + \frac{1}{2}\cdot\frac{\Delta t}{\Delta x}x + \frac{1}{2}\cdot\frac{\Delta t}{\Delta z}z$$

and

$$\tau = t + \frac{1}{2}\cdot\frac{\Delta t}{\Delta z}z$$

We obtain

$$\varphi_{xx}+\varphi_{yy}+\varphi_{zz}-\frac{1}{4}\left[\left(\frac{\Delta t}{\Delta x}\right)^2+\left(\frac{\Delta t}{\Delta z}\right)^2\right]\varphi_{tt}-\left(\frac{2}{\omega}-1\right)\left(\frac{\Delta t}{\Delta x^2}+\frac{\Delta t}{\Delta z^2}\right)\varphi_t=0 \tag{28}$$

$$-\varphi_{xx}+\varphi_{yy}+\varphi_{zz}-\frac{1}{4}\left(\frac{\Delta t}{\Delta z}\right)^2\varphi_{tt}-\left[\left(\frac{1}{\omega}-1\right)\frac{\Delta t}{\Delta x^2}+\left(\frac{2}{\omega}-1\right)\frac{\Delta t}{\Delta z^2}\right]\varphi_t=0 \tag{29}$$

/10

Equation (28) is hyperbolic and equation (29) is super hyperbolic.

By using the variable separation method, let

$$\varphi=F(\tau)G(x,y,z) \tag{A}$$

From equation (28), we get

$$\frac{\frac{1}{4}\left[\left(\frac{\Delta t}{\Delta x}\right)^2+\left(\frac{\Delta t}{\Delta z}\right)^2\right]F''+\left(-\frac{2}{\omega}-1\right)\left(\frac{\Delta t}{\Delta x^2}+\frac{\Delta t}{\Delta z^2}\right)F'}{F}=\frac{G_{xx}+G_{yy}+G_{zz}}{G} \tag{B}$$

The solution is

$$\varphi(x,y,z,\tau)=G_0(x,y,z)+\sum_{m=1}^{\infty}(A_m e^{-p_m\tau}+B_m e^{-q_m\tau})G_m(x,y,z) \tag{30}$$

where

$$\left.\begin{aligned} p_m&=\frac{2}{\Delta t}\left(\frac{2}{\omega}-1\right)-\sqrt{\frac{4}{\Delta t^2}\left(\frac{2}{\omega}-1\right)^2-\frac{4k_m^2}{\left(\frac{\Delta t}{\Delta x}\right)^2+\left(\frac{\Delta t}{\Delta z}\right)^2}}\\ q_m&=\frac{2}{\Delta t}\left(\frac{2}{\omega}-1\right)+\sqrt{\frac{4}{\Delta t^2}\left(\frac{2}{\omega}-1\right)^2-\frac{4k_m^2}{\left(\frac{\Delta t}{\Delta x}\right)^2+\left(\frac{\Delta t}{\Delta z}\right)^2}} \end{aligned}\right\} \tag{31}$$

$G_m(x,y,z)$ is the characteristic function of the boundary value problem of the following equation

$$G_{xx}+G_{yy}+G_{zz}+k_m^2G=0 \tag{C}$$

K_m^2 is the corresponding characteristic value. Let

$$k_1^2<k_2^2<\cdots<k_{m-1}^2<k_m^2<\cdots \tag{D}$$

G_0 (x,y,z) is the solution of the Laplace equation

$$G_{xx}+G_{yy}+G_{zz}=0$$

From equation (30), we know that when $0<\omega<2$. Hence, the convergence condition of a local subsonic velocity point is $0<\omega<2$. The converging speed is determined by the minimum value of the real part of the exponents in equation (30), i.e. Re. (p_1). From equation (31)

$$\lim_{\tau\to\infty}\varphi(x,y,z,\tau)=G_0(x,y,z)$$

$$p_1=\frac{2}{\Delta t}\left(\frac{2}{\omega}-1\right)-\sqrt{\frac{4}{\Delta t^2}\left(\frac{2}{\omega}-1\right)^2-\frac{4k_1^2}{\left(\frac{\Delta t}{\Delta x}\right)^2+\left(\frac{\Delta t}{\Delta z}\right)^2}}$$

where Δx and $\Delta z\to 0$

$$p_1=\frac{k_1^2}{\left(\frac{2}{\omega}-1\right)\left(\frac{1}{\Delta x^2}+\frac{1}{\Delta z^2}\right)\Delta t}$$

We can see that along with increasing ω, p_1 increases monotonically. Under usual conditions, it is possible to choose ω so that the square root in the expression of p_1 is zero in order to raise the converging speed. This optimal relaxation factor is

$$\omega=\frac{2}{1+\frac{k_1}{\sqrt{\frac{1}{\Delta x^2}+\frac{1}{\Delta z^2}}}} \tag{32}$$

Similarly, the solution to equation (29) is found to obtain /11 the convergence condition of local supersonic velocity points

$$0<\omega<1+\frac{1}{1+\left(\frac{\Delta z}{\Delta x}\right)^2} \tag{33}$$

and the optimal relaxation factor

$$\omega=\frac{2+\left(\frac{\Delta z}{\Delta x}\right)^2}{1+\left(\frac{\Delta z}{\Delta x}\right)^2+k_1\Delta z} \tag{34}$$

Furthermore, with increasing ω, the converging speed increases monotonically. When $\Delta x = \Delta z\to 0$, the optimal relaxtion factor is 1.5.

3. Comparison With Numerical Tests

The analysis of the stabilization of the above local linearization pointed out that: For three dimensional supersonic stream, linear relaxation is always unstable. However, many numerical computations are stable. In addition, the results analyzed in the above two sections agree with the experience of numerical calculation.

In Reference [3], the isolated wing of experimental model NASA TND-830 was computed. The wing was triangular, $x=60^{\circ}$, the flow section is NACA 65 A 003, $M_{\infty}=1.05$, and $\alpha=2.2^{\circ}$. For various relaxation factors, the convergence conditions are shown in Table 2.

$$|\Delta\Phi|<10^{-6}$$

Table 2. Convergence cases of NASA TN D-830 wing, $M_{\infty}=1.05$, $\alpha=2.2^{\circ}$.

亚音速点的ω 1	1.0	1.7	1.0	1.0	1.7	1.7	1.0
超音速点的ω 2	0.7	0.7	0.9	1.0	1.0	1.3	1.5
停止振荡的n 3	349	333	231	191	184	148	70
达到收敛标准的n 4	465	459	365	339	335	218	153

Key: 1) ω subsonic velocity point; 2) ω of supersonic velocity point; 3) of n for stopping oscillation; 4) n for reaching the convergence standard.

When $\omega=1.6$ for a supersonic velocity point, the computation is divergent. When it is 1.5, convergence is the fastest. This agrees with the convergence analysis in Section 2.

3. CONCLUSIONS

In this paper, the exact velocity potential equation was used at the blunt leading-edge of the wing to overcome the

uncertainty at the leading edge using the small perturbation method. The pressure distribution of the wing plane obtained was improved. In this paper, in other parts of the flow field, the small transverse perturbation velocity potential operation was used. It saved considerable computer time as compared to the use of the exact potential flow of the entire flow field. It is also easier to be applied to the complex wing-body structure.

In this paper, under the assumption of local linearization, the stability and convergence conditions of linear relaxation and iteration were established. In addition to individual conclusions, it agreed with the numerical tests. It is meaningful in the sense of providing some guidance.

APPENDIX The proof of the constant instability of linear relaxation iteration in the local supersonic region.

From equation (26) /12

$$|B|^2-|A|^2=2\left(\frac{1}{\omega}-1\right)\left(\frac{1}{\Delta x^2}+\frac{4}{\Delta y^2}\sin^2\frac{\beta_2\Delta y}{2}+\frac{2}{\Delta z^2}\right)\left(\frac{4}{\Delta y^2}\sin^2\frac{\beta_2\Delta y}{2}-\frac{4}{\Delta x^2}\cos\beta_1\Delta x\sin^2\frac{\beta_1\Delta x}{2}+\frac{2}{\Delta z^2}-\frac{2\cos\beta_3\Delta z}{\Delta z^2}\right)+\left(\frac{4}{\Delta x^2}\sin\beta_1\Delta x\sin^2\frac{\beta_1\Delta x}{2}+\frac{\sin\beta_3\Delta z}{\Delta z^2}\right)^2+\left(\frac{4}{\Delta y^2}\sin^2\frac{\beta_2\Delta y}{2}-\frac{4}{\Delta x^2}\cos\beta_1\Delta x\sin^2\frac{\beta_1\Delta x}{2}+\frac{2}{\Delta z^2}-\frac{\cos\beta_3\Delta z}{\Delta z^2}\right)^2-\frac{1}{\Delta z^4}$$

(1) When $\omega=1$, choose $\beta_1\Delta y=\beta_3\Delta z=0$ and $\Delta x=\Delta z$,

$$|B|^2-|A|^2=\frac{8}{\Delta x^4}\sin^2\frac{\beta_1\Delta x}{2}\left(2\sin^2\frac{\beta_1\Delta x}{2}-\cos\beta_1\Delta x\right)$$

When $0<\beta_1\Delta x<\frac{\pi}{3}$ 时, $|B|^2-|A|^2<0$

Hence, when $\omega=1$, it is unstable.

(2) When $\omega<1$, choose $\beta_2\Delta y=\beta_3\Delta z=0$ and $\Delta x=\Delta z$

$$|B|^2-|A|^2=-\left(\frac{1}{\omega}-1\right)\frac{24}{\Delta x^4}\cos\beta_1\Delta x\sin^2\frac{\beta_1\Delta x}{2}$$
$$+\frac{8}{\Delta x^4}\sin^2\frac{\beta_1\Delta x}{2}\left(2\sin^2\frac{\beta_1\Delta x}{2}-\cos\beta_1\Delta x\right)$$

when $0<\beta_1\Delta x<\frac{\pi}{3}$, $|B|^2-|A|^2<0$

Therefore, when $\omega<1$, it is unstable.

(3) when $\omega>1$, let $\frac{1}{\omega}=1-\varepsilon$, $\varepsilon>0$

Choose $\beta_1\Delta x=\beta_2\Delta y=0$ and $\Delta x=\frac{\Delta z}{\sqrt{2}}$

$$|B|^2-|A|^2=(1-4\varepsilon)\frac{4}{\Delta z^4}(1-\cos\beta_3\Delta z)$$

when $\varepsilon>1/4$, $|B|^2-|A|^2<0$.

Choose $\beta_2\Delta y=\beta_3\Delta z=0$ and $\Delta x=\Delta z$

$$|B|^2-|A|^2=\frac{8}{\Delta x^4}\sin^2\frac{\beta_1\Delta x}{2}\left[2\sin^2\frac{\beta_1\Delta x}{2}+(3\varepsilon-1)\cos\beta_1\Delta x\right]$$

When $\varepsilon\leq 1/4$ and $\beta_1\Delta X$ is sufficiently close to zero, $|B|^2-|A|^2<0$.
Therefore, when $\varepsilon>0$, i.e., $\omega>1$, it is unstable.

REFERENCES

[1] Ballhaus, W. F. Some Recent Progress in Transonic Flow Computations, Numerical Methods in Fluid Dynamics, Ed. by Wirz, H. J. and Smolderen, J. J. (1978) Chapter 3, page 160.

[2] Schmidt, W. Progress in Transonic Flow Computations : Analysis and Design Methods for Three-Dimensional Flows, Numerical Methods in Fluid Dynamics, Ed. by Wirz, H. J. and Smolderen, J. (1978) Chapter 5, Page 313.

[3] Luo Shijun, Zheng YuWen, Qian Hong, and Wang Die Qian, The Difference Computation of the Longitudinal Aerodynamics of Transonic Composit Structure, Acta Aeronautica et Astronautica Sinica, Volume 1, 1978, pp. 1-13.

[4] Ling He-yao and Luo Shijun, "The Finite Difference Computation of Transonic Blunt Leading-edge", Technical Information of Northwestern Polytechnical University, Volume 252 (1975), pp. 32-44.

[5] Zhang Yuwen, "The Difference Computation of Steady State Transonic Small Perturbation Potential Flow Around Blunt Leading-edge Wings", Technical Information of Northwestern Polytechnical University, SHJ8035 (1980).

[6] Luo Shijun, Zheng Yuwen, Wang Die Qian, and Qian Hong, "The Mixed Difference Method of Transonic Steady State Potential Flow", Defense Industrial Publication (1979).

[7] Krupp, J. A. and Murman, E. M. Computation of Transonic Flows Past Lifting Airfoils and Slender Bodies. AIAA J. 10 (1972) 880-6.

[8] Kolbe, C. D. and BoHz, F. W. The Force and Pressure Distribution at Subsonic Speeds on a Plane Wing Having 45° of Sweepback, an Aspect Ratio of 3 and a Taper Ratio of 0.5. NACA RMA51 G31 (1951).

RELAXATION COMPUTATION OF TRANSONIC FLOWS AROUND WINGS WITH BLUNT LEADING-EDGE AND DISCUSSION ON ITS STABILITY AND CONVERGENCE

Zheng Yuwen and Luo Shijun

(*Northwestern Polytechnical University*)

Abstract

In this paper, the blunt leading-edge of a wing is taken as mesh points, and there the exact velocity potential equation with central difference scheme and the exact boundary condition are used, while in the other places, the approximate velocity potential equation, which assumes small perturbation in the transverse plane but allows large perturbation in the longitudinal direction, and the corresponding boundary condition are employed.

Two numerical examples are following:

(1) A rectangular wing having airfoil NACA0012, aspect ratio $\lambda = 12$, angle of attack $\alpha = 2^\circ$, free stream Mach number $M_\infty = 0.63$. The computed pressure distribution of the root section agrees with the exact numerical subsonic solution given by Sells (1968).

(2) The sweepback wing tested by NACA RM A51G31 having airfoil NACA64A010 which is perpendicular to 1/4 chord line with sweepback angle $\chi_{1/4} = 45^\circ$, $\lambda = 3$ and taper ratio $\eta = 2$, $\alpha = 2^\circ$, $M_\infty = 0.4$, 0.8 and 0.9. The computed pressure distributions agree well with those obtained by tests.

Under the assumption of local linearization, the stability of the difference equation in line relaxation with Seidel iteration is studied by the von Neumann method and the convergence of the solution of the differential equation equivalent to the above difference equation to the solution of the original differential equation is discussed by the method of separation of variables.

The following conclusions are obtained:

(1) The stability condition for the line relaxation with Seidel iteration is $0 < \omega \leq 2$ at locally subsonic points, where ω is the relaxation factor.

(2) At locally supersonic points, the relaxation is always unstable. The convergence conditions are as follows. Let the steps Δx (chordwise) and Δz (spanwise) perpendicular to the relaxation line.

(3) $0 < \omega < 2$, at locally subsonic points.

(4) $0 < \omega < 1 + \dfrac{1}{1 + \left(\dfrac{\Delta z}{\Delta x}\right)^2}$, at locally supersonic points.

The numerical experiences agree with the conclusions (1), (3) and (4), but do not agree with the conclusion (2).

DETERMINATION OF AERODYNAMIC COEFFICIENTS FOR A RE-ENTRY BODY BY MEANS OF AN EXTENDED KALMAN FILTER

AERODYNAMIC RESEARCH AND DEVELOPMENT CENTER OF CHINA

Jiang Quanwei, Xu Jinzhi, and Zhou Shuying *

ABSTRACT

In this paper, an extended Kalman filter method was used to determine the major aerodynamic coefficients of re-entry bodies. The emphasis was placed on estimating states and parameters using the measured data during the re-entry flight under the condition that trajectory observation data was absent.

The data included body axial angular rate and acceleration obtained from the rate gyros and accelerameters. A mathematical model was established based on six-degree-of-freedom motion equations. Both ballistic and maneuvering re-entries were considered. Numerical simulation and actual measurement conversion showed that the present method provided more satisfactory results.

SYMBOLS

C_{x0}	resistance coefficient
$C_{x\alpha}$, $C_{y\beta}$	derivatives of normal force and lateral force
$C_{m\alpha}$, $C_{n\beta}$	derivatives of pitch moment and yaw moment
$C_{m\delta_z}$, $C_{n\delta_y}$	control moment derivatives
C_{mz}, C_{ny}	damping moment derivatives
$C_{x\delta_x}$, $C_{y\delta_y}$	roll and roll damping derivatives
C_{1b}, C_{1p}	bottom diameter
d	gravitational acceleration
g	flight altitude

* Received in March, 1981.

H	rotational moment of inertia
I, I_e	atmospheric model parameter
k_e	mass of the re-entry body
m	accelerations
$\tilde{n}_x$, $\tilde{n}_y$, $\tilde{n}_z$	angular speeds
p, q, r	reference area
$s = \pi d^2/4.0$	flight time
t	velocity components
u, v, w	combined speed
V	distances from the accelerometers to the center of gravity
x_1, y_2, y_3, z_2, z_3	pose angles
ϑ, ψ, γ	

/16

ρ	density of the atmosphere
ρ_e	reference density
δq, δr	inclination angles of the control plane

1. INTRODUCTION

In recent years, the determination of aerodynamic characteristics of a space craft from measured data obtained in flight using various parametric identification methods is one of the important subjects in the astronautical industry. This work has important significance in the design and final planning processes for a spacecraft. First of all, it is based on the measured data obtained in an actual flight environment. Consequently, the shortcomings due to ground equipment such as insufficient wind tunnel simulation can be remedied. Secondly, it provides real data for the design of the guidance and control systems. This is especially true of re-entry spacecraft. There are very few experiments and the cost of experiment is high. Therefore,

it is extremely important to obtain the most possible useful information from the analysis of limited data.

Since the emergence of the Kalman filter method[1], it has been widely applied in aspects such as communications and control. Especially in astronautical engineering, its application is even more popular[2]. However, modern Kalman filter methods were only used to determine the aerodynamic coefficients of a flight vehicle in recent years. In Reference [3], based on the re-entry vehicle point mass differential equation of motion, several Kalman filter plans were presented. References [4,5,6] discussed the use of extended Kalman filter methods to determine the aerodynamic characteristics of tactical aircraft. Reference [7] presented the feasibility of real time estimation of aerodynamic coefficients using a Kalman filter method. These type of efforts in foreign countries have already obtained some progress. However, they all included trajectory measurement information such as altitude, velocity, and position. Their work did not involve the identification of the aerodynamic coefficient of a re-entry vehicle under the condition that trajectory observation data was absent.

The purpose of this work was to attempt to use the Kalman filter method to solve the problem of determining the aerodynamic coefficients of an re-entry vehicle in the absence of trajectory observation data. This problem has a background. Experience showed that, due to various reasons, the trajectory observation data of re-entry flight tests frequently could not be or could only be partially obtained. If an estimation method could be found to determine the important aerodynamic parameters based on the acceleration and angular rate data measured on-board, it would be alot more meaningful. This paper is the theoretical simulation and the actual measurement conversion specifically with respect to this problem.

The major differences between this paper and Reference [7] are as follows:

(1) In Reference [7], the flight altitude was already known. The H in this paper was unknown which was a state quantity.

(2) In addition to trajectory re-entry, maneuvering re-entry was also considered.

(3) The method in this paper has already been applied in practice while Reference [7] was a feasibility study.

2. EXTENDED KALMAN FILTERING UNDER EXPANSION CONDITION

The Extended Kalman Filtering method, abbreviated as EKF, extends the use of linear Kalman filtering to the non-linear secondary filter system. With regard to the study of re-entry flight, the dynamic equation can be written as

$$\dot{\underline{y}}(t)=\underline{g}(\underline{y}(t), \underline{C}, t) \tag{1}$$

where $\underline{y}$ represents the state vector of the vehicle, $\underline{C}$ represents the performance parameters such as the aerodynamic coefficients of the flight vehicle, and $\underline{g}$ is the non-linear differentiable function. During the period of consideration, let us assume that $\underline{C}$ does not vary

$$\dot{\underline{C}}=\underline{0} \tag{2}$$

Combine equations (1) and (2), then we get

$$\begin{bmatrix}\dot{\underline{y}}(t)\\ \dot{\underline{C}}\end{bmatrix}=\begin{bmatrix}\underline{g}(\underline{y}(t), \underline{C}, t)\\ \underline{0}\end{bmatrix} \tag{3}$$

Define a new expansion state vector $\underline{X}(t)$ /17

$$\underline{X}(t)=\begin{bmatrix}\underline{Y}(t)\\ \underline{C}\end{bmatrix} \tag{A}$$

Also assume that

$$\underline{f}(\underline{X}(t), t)=\begin{bmatrix} \underline{g}(\underline{Y}(t), \underline{C}, t) \\ \underline{0} \end{bmatrix} \tag{4}$$

Then, we have the usual state equation

$$\dot{\underline{X}}(t)=\underline{f}(\underline{X}(t), t)+G(t)\underline{W}(t) \tag{5}$$

where $\underline{W}(t)$ is the Gaussian white noise whose average value is 0 and spectrum density is $Q(t)$. It is used to simulate process noise.

Let us assume that the observation vector is a set of discrete values which is a non-linear differentiable function of the state vector

$$\underline{Z}_K=\underline{h}_K(\underline{X}(t_K))+\underline{V}_K, \quad K=1, 2, \cdots \tag{6}$$

where $\underline{V}_K$ is the measurement noise, which is expressed by the positive state random vector with an average equal to 0. Its joint square difference matrix is R_K. Then, there are the following extended Kalman filtering iteration equations:

$$\left.\begin{aligned} &\dot{\hat{\underline{X}}}(t)=\underline{f}(\hat{\underline{X}}(t), t) \\ &\dot{P}(t)=F(\hat{\underline{X}}(t), t)P(t)+P(t)F^T(\hat{\underline{X}}(t), t)+G(t)Q(t)G^T(t) \\ &K_K=P_K(-)H_K^T\{H_KP_K(-)H_K^T+R_K\}^{-1} \\ &\hat{\underline{X}}_K(+)=\hat{\underline{X}}_K(-)+K_K\{\underline{Z}_K-\underline{h}_K(\hat{\underline{X}}_K(-))\} \\ &P_K(+)=\{I-K_KH_K(\hat{\underline{X}}_K(-))\}P_K(-) \end{aligned}\right\} \tag{7}$$

where

$$F(\hat{\underline{X}}(t), t)=\left.\frac{\partial \underline{f}(\underline{X}(t), t)}{\partial \underline{X}(t)}\right|_{\underline{X}(t)=\hat{\underline{X}}(t)} \tag{B}$$

$$H_K(\hat{\underline{X}}_K(-))=\left.\frac{\partial \underline{h}_K(\underline{X}(t_K))}{\partial \underline{X}(t_K)}\right|_{\underline{X}(t_K)=\hat{\underline{X}}_K(-)} \tag{C}$$

and the initial condition of state $\hat{x}_0$ and P_0.

In the simulation computation, equations (5) and (6) are used to produce the observation data.

III. STATE MODEL AND OBSERVATION MODEL

The mathematical model of this work has the following characteristics:

(1) It is based on the usual body axis six-degree-of-freedom equations of motion;

(2) The measured data only includes the acceleration and angular rate data on-board;

(3) The re-entry body can perform maneuvering flight, i.e., the aerodynamic rudder can carry out control;

(4) It has asymmetric aerodynamic characteristics;

(5) It considers the effect that the accelerometer is not located at the center of gravity.

The mathematical model in this paper has the following limitations:

(1) In the small attack angle flight trajectory section, the aerodynamic coefficients can be expressed as a linear function of the attack angle;

(2) Atmospheric density varies exponentially with altitude and its mathematical model is already known;

(3) There is no systematic error in the measurement.

Corresponding to equation (1), the actual form is /18

$$
\left.\begin{aligned}
\dot{u} &= vr - wq + \frac{QS}{m} C_{x_0} - g\sin\vartheta \\
\dot{v} &= wp - ur + \frac{QS}{m}\left(C_{y\beta}\frac{v}{V} + C_{yb_r}\delta r\right) + g\cos\vartheta\sin\gamma \\
\dot{w} &= uq - vp - \frac{QS}{m}\left(C_{z_\alpha}\frac{w}{u} + C_{zb_q}\delta q\right) + g\cos\vartheta\cos\gamma \\
\dot{p} &= \left(\frac{QSd}{I_x}\right)\left[\left(\frac{d}{2V}\right)C_{l_p}\cdot p + C_{l_\delta}\right] \\
\dot{q} &= \left(\frac{QSd}{I}\right)\left[C_{m_\alpha}\left(\frac{w}{u}\right) + \left(\frac{d}{2V}\right)C_{m_q}q + C_{mb_q}\delta q\right] + \left(1 - \frac{I_x}{I}\right)rp \\
\dot{r} &= \left(\frac{QSd}{I}\right)\left[C_{n\beta}\left(\frac{v}{V}\right) + \left(\frac{d}{2V}\right)C_{n_r}r + C_{nb_r}\delta r\right] - \left(1 - \frac{I_x}{I}\right)pq \\
\dot{\vartheta} &= q\cos\gamma - r\sin\gamma \\
\dot{\psi} &= (q\sin\gamma + r\cos\gamma)/\cos\vartheta \\
\dot{\gamma} &= p + \mathrm{tg}\,\vartheta\,(q\sin\gamma + r\cos\gamma) \\
\dot{H} &= V\sin\vartheta - V\frac{w}{u}\cos\vartheta\cos\gamma - v\cos\vartheta\sin\gamma
\end{aligned}\right\} \qquad (8)
$$

The auxiliary relations are

$$
\begin{aligned}
\rho &= \rho_0 \exp(-H/k_0) \\
V^2 &= u^2 + v^2 + w^2 \\
Q &= 0.5\rho V^2
\end{aligned}
$$

The actual form corresponding to equation (6) is

$$
\underline{h}(\underline{X}(t)) = (\tilde{n}_x \tilde{n}_y \tilde{n}_z pqr)^T
$$

where

$$
\left.\begin{aligned}
\tilde{n}_x &= \frac{QS}{mg}C_{x_0} - \frac{x_1}{g}(q^2 + r^2) \\
\tilde{n}_y &= \frac{QS}{mg}\left(C_{y\beta}\frac{v}{V} + C_{yb_r}\delta r\right) - \frac{y_1}{g}(r^2 + p^2) + \frac{z_1}{g}rq \\
\tilde{n}_z &= \frac{QS}{mg}\left(C_{z_\alpha}\frac{w}{u} + C_{zb_q}\delta q\right) - \frac{z_1}{g}(p^2 + q^2) + \frac{y_1}{g}qr
\end{aligned}\right\} \qquad (9)
$$

where x_1, y_2, z_2, y_3, z_3 are known constants. At this place, an acceleration sensor is installed in the following manner:

the axial sensor is placed on the longitudinal axis and the transverse sensor is in the cross-section passing through the center of gravity.

IV. RESULTS OF NUMERICAL SIMULATION AND PRELIMINARY REAL DATA EXTRACTION

The numerical simulation corresponds to the maneuvering re-entry situation. The control plane moves regularly according to $\underline{\delta q}=\delta r=0.1\sin(20t)$. The flight, aerodynamic and observation characteristics of this computational example are shown in Tables 1-4.

Table 1. Physical Constants

1 g (米/秒)	2 ρ_0 (公斤秒²/米⁴)	3 h_0 (米)	4 x_1 (米)	5 y_2 (米)	6 y_3 (米)	7 z_2 (米)	8 z_3 (米)
9.81	0.123	7660.0	-0.2	0.01	0.05	-0.2	-0.3

Key: 1) g (m/sec); 2) ρ_0 ($Kgsec^2/m^4$); 3) k_0(m); 4) X_1(m); 5) y_2(m); 6) y_3(m); 7) z_2(m); 8) z_3(m).

Table 2. Initial Condition for Trajectory and Filtering.

1 动力学状态	2 动态方程组初始条件	3 滤波初值		4 单位
		$\hat{X}_0$	$\sqrt{P_0}$	
u	4000.0	3879.56	400.0	5 米/秒
v	0.0	148.06	80.0	6 米/秒
w	0.0	68.8	80.0	7 米/秒
p	1.3	1.203	0.36	8 1/秒
q	0.0	0.3007	0.36	9 1/秒
r	0.0	-0.3761	0.36	10 1/秒
θ	-0.6284	-0.5728	0.0625	
ψ	0.0	0.0097	0.0625	
γ	0.0	-0.0546	0.0625	
H	21500.0	22000.0	3225.0	11 米

Key: 1) dynamic state; 2) initial condition of dynamic state functions; 3) initial value of filtering; 4) unit; 5-7) m/sec; 8-10) 1/sec; 11) m.

Table 3. Standard Deviation for Measurement and Process Noise.

12 符号	13 数值	14 噪声定义	15 注
σ_R	0.4	19 过载测量	全量程的1% 23
σ_α	16 0.0942/秒	20 角速率测量	
σ_2	17 2.0米/秒²	21 线加速过程	
σ_5	18 0.5 1/秒²	22 横向角加速过程	

Key: 12) symbol; 13) numerical value; 14) noise definition; 15) remark; 16) 0.0942/sec; 17) 2.0 m/sec^2; 18) 0.5 1/sec^2; 19) acceleration measurement; 20) angular rate measurement; 21) linear acceleration process; 22) transverse angular acceleration process; 23) 1% of the entire processed quantity.

Table 4. True Values, Filtering Initial Values and Filtering Results for Aerodynamic Coefficients.

24 气动系数	25 真值	26 滤波初值			27 滤波结果		
		$\hat{\underline{X}}_0$	$\sqrt{P_0}$	$K=1$ $E_c(E_f)$	$K=50$ 最优估值	$K=50$ $E_c(E_f)$	$K=80$ $E_c(E_f)$
C_{x_0}	-0.1075	-0.1	0.025	-7.0(23)	-0.1074	-0.155(7.0)	0.303(6.8)
$C_{x\alpha}$	-2.13	-2.0	0.5	-5.3(23)	-2.12	-0.817(7.0)	-0.52(6.8)
$C_{y\beta}$	-1.075	-2.0	0.5	86.0(47)	-1.061	-1.24(6.9)	-0.24(6.7)
C_{mz}	-0.883	-0.7	0.175	-20.7(20)	-0.88	-0.34(7.0)	-0.37(6.7)
$C_{z\beta}$	0.547	0.7	0.175	28.0(32)	0.543	-0.7(6.9)	-0.58(6.7)
$C_{m\delta_z}$	0.485	0.467	0.117	-3.7(24)	0.487	0.45(7.1)	-0.32(6.8)
$C_{x\delta_y}$	-0.47	-0.467	0.117	-0.64(25)	-0.472	0.43(7.2)	-1.38(6.9)
C_{mz}	-0.778	-1.0	0.25	28.5(32)	-0.909	16.9(31)	22.9(30)
$C_{z\omega}$	-0.799	-1.0	0.25	25.0(31)	-0.948	18.6(27)	17.2(25)
$C_{x\delta_z}$	-0.0791	-0.1	0.025	26.4(32)	-0.0947	19.7(21)	15.0(17)
$C_{y\delta_y}$	-0.0785	-0.1	0.025	27.4(32)	-0.0853	8.6(19.3)	-1.15(16)
C_{l_p}	-0.024	-0.015	0.015	-37.5(63)	-0.0028	-88.3(60)	-79.4(59)
C_{l_β}	1.3×10^{-8}	0.0	1.3×10^{-8}	-100(100)	2.7×10^{-8}	109.7(72)	81.7(62)

Key: 24) aerodynamic coefficient; 25) real value; 26) initial values of filtering; 27) results of filtering; 28) optimum estimation.

From equations (5) and (6), and the relevant data in Tables 1-4, we obtained the discrete values of acceleration and angular rate $\tilde{n}_x$, $\tilde{n}_y$, $\tilde{n}_z$, p,q,r. The sampling interval was chosen to be 0.02 second as shown in Figure 1. These data are stored in the machine to be used as the observation data for filtering. /20

Using equation set (7) and the relevant data in Tables 1-4, the optimum estimated value $\hat{C}_K$ and filtering computation square deviation $P_K(+)$ of various aerodynamic coefficients were obtained based on filtering iteration.

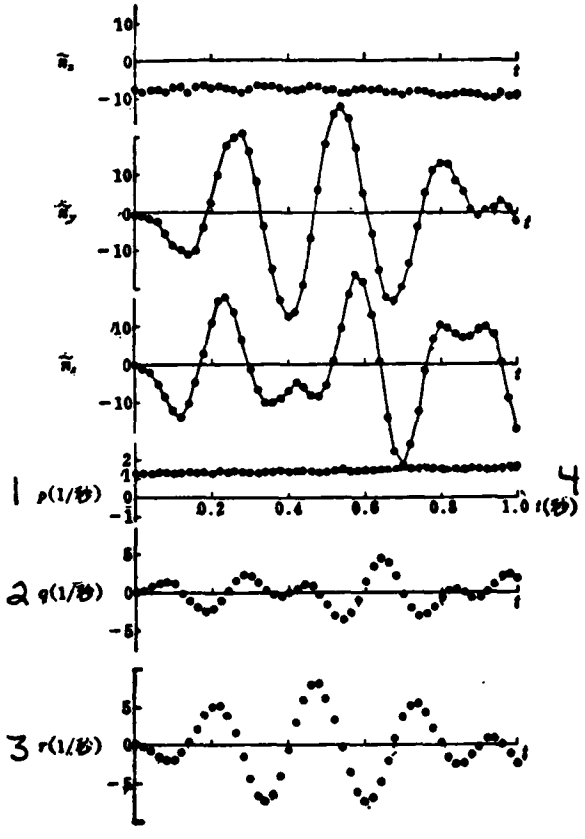

Figure 1. Measurement data.
Key: 1) p(1/sec); 2) q (1/sec); 3) r(1/sec); 4) t(sec).

The computed results are shown by two indicators; one is the actual estimated error E_e of filtering and the second is the computed error of filtering E_{f0}. The formulas are as follows:

$$(E_e)_k = 100(\hat{c}_k - C)/C \tag{10}$$

$$(E_f)_k = \pm 100\sqrt{\bar{P}_k(+)}/|C| \tag{11}$$

where $\hat{C}_K$ represents the optimum estimated value of an aerodynamic coefficient at the K^{th} observation point, C represents the actual value corresponding to the aerodynamic coefficient (see Table 4), and $P_K(+)$ represents the square deviation corresponding to the aerodynamic coefficient which is calculated from the filtering equation (7). Basic filtering theory points out that if the two indicators are in agreement statistically then it indicates the filtering is normal. The $(E_e)_K$ obtained after converging can be used as the actual estimated error.

The last 3 columns in Table 4 give the filtering results. /21
The first column shows the optimum estimated values when K=50. The two latter columns represent the E_e and E_f values of the 13 aerodynamic coefficients corresponding to K=50 and K=80, respectively.

Figures 2-4 plot the filtering process of 7 major aerodynamic coefficients. The solid lines in the figures represent the actual estimated error E_e. The symmetrical dotted lines are the filtering calculated error E_f.

Figure 5 shows the preliminary extraction results of a certain actual measured data which corresponds to the trajectory re-entry condition. In the figure, the analytical solution extraction results of K>30 with trajectory measured data are also plotted.[8]

The above figures reflected the following facts:

(1) For all the aerodynamic coefficients, regardless of whether it is the actual estimated error E_e or the filtering calculated error E_f, there is no divergence effect. $|E_e/E_f| \lesssim 2$.
For the major aerodynamic coefficients, such as $C_{xx}, C_{xz}, C_{yb}, C_{mx}, C_{mb}, C_{mbx}, C_{mbz}$, the values of E_e and E_f converge very rapidly. This indicates that filtering is normal.

(2) Through a 50 point filtering computation (which is the flight data in 1 second), the actual estimated error of the above described 7 major aerodynamic coefficients converges to within 1.5%. The filtering computation error is approximately 7%.

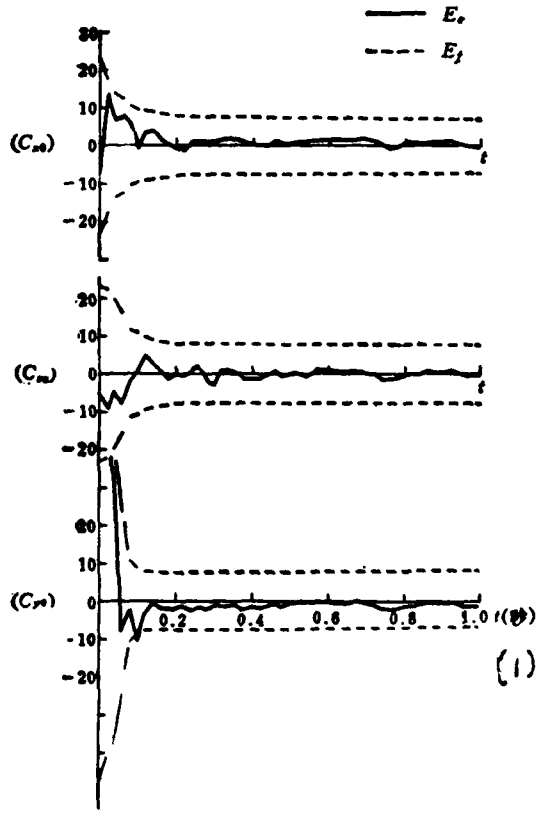

Figure 2. Filtering Results for Aerodynamic Force Coefficients. (C_{mx}, C_{my}, C_{yr}).

Key: 1) t (sec).

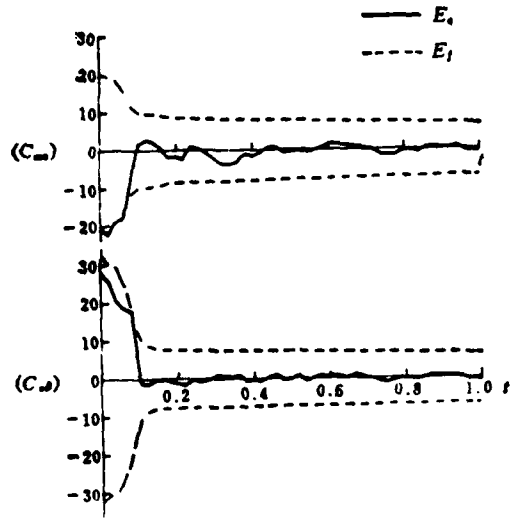

Figure 3. Filtering Results for Aerodynamic Moment Coefficients. (C_{ma}, $C_{n\beta}$).

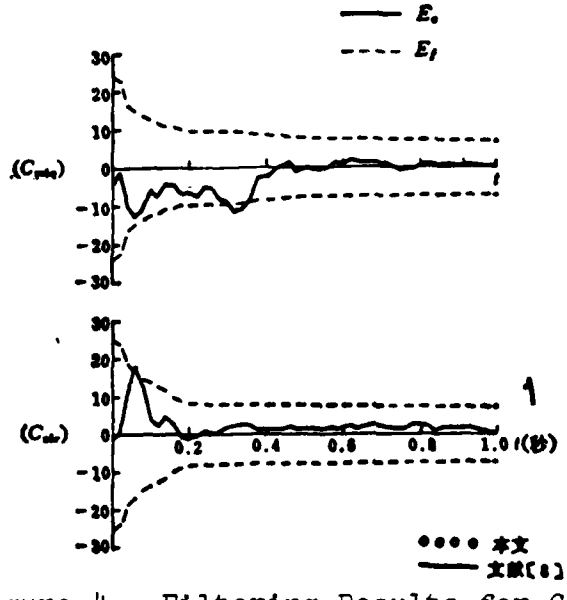

Figure 4. Filtering Results for Control Moment Coefficients ($C_{m\delta q}$, $C_{n\delta r}$).

Key: 1) t(sec); 2) this work; 3) Reference [8].

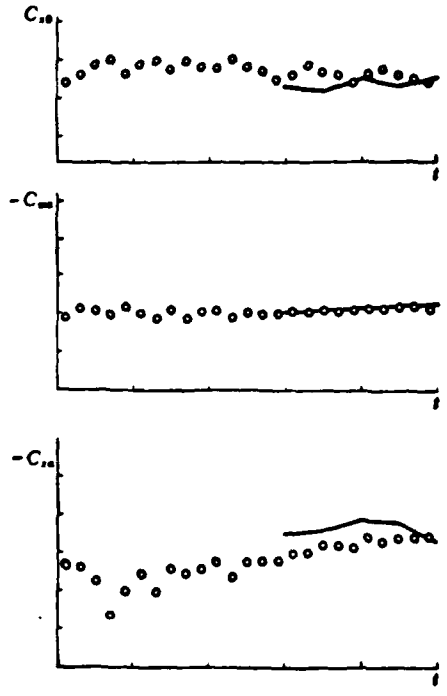

Figure 5. Real Data Extraction.

/22

For coefficients such as C_{mq}, C_{nr}, $C_{l\delta_r}$, $C_{l\delta_a}$, $C_{n\delta_a}$, $C_{y\delta_r}$ etc., although E_f varies convergently, yet they do not converge as quickly as the 7 major aerodynamic coefficients described above. The actual estimated error E_e does not have any significant improvement. This indicates that under given conditions these coefficients do not significantly affect the motion in this time period.

(3) Preliminary extraction of real data showed that the mathematical model and filtering program in this paper

could adequately suit real flight data. The results of this work are very close to those of the analytical solution with trajectory measured data.

In addition, several points are explained as follows:

(1) Rigorously speaking, it should provide many initial values of $\hat{x}_0$ randomly and through Monte Carlo simulation, the final statistical average value is given. However, the above set of classical situation computation is already capable of reflecting the major characteristics of filtering.

(2) For the real flight data, to provide the initial square deviation P_0 is undoubtedly an important problem. The P_0 corresponding to an aerodynamic coefficient can be given based on wind tunnel experiment data or from approximations. The P_0 corresponding to a dynamic state variable was given by an existing extraction method.[8]

(3) Although the analysis in this paper has the various assumptions described in the previous section, this basic method may be extended to a more generalized situation such as the aerodynamic non-linear effect, non-exponent type of atmospheric density; various types of measurement errors, etc.

4. CONCLUSIONS

1. This paper analyzed the use of an extended Kalman filtering method to determine the aerodynamic coefficients of a re-entry body from angular rate and acceleration data on-board in the absence of trajectory observation data. Numerical simulation and preliminary real data extraction showed that the solution of this problem is practical.

2. As long as no stringent initial state estimation is required, after the treatment of 1-2 second flight data, the error of a major aerodynamic coefficient can converge to a small range.

3. In the selection of parameters and analysis of error, more in depth work is needed.

We wish to thank Vice Chief Zhang Hauxiu and Associate Professor Zhang Jinghuai for their valuable opinions.

References

[1] Kalman, R.E., "A New Approach to Linear Filtering and Prediction," Journal of Basic Engineering (ASME), Vol. 82D, March 1960, pp. 35~45.

[2] Leondes, C.T., "Theory and Application of Kalman Filtering", AGARD ograph 139, Feb. 1970. AD-704306.

[3] Chang, C.B., Whiting, R.H., Athans, M., "On the State and Parameter Estimation for Maneuvering Reentry Vehicles," IEEE Tran. on Automatic Control. Vol. AC-22, No. 1, Feb. 1977, pp. 99~105.

[4] Brown, C.M., "An Extended Kalman Filter for Estimating Aerodynamic Coefficients," ADA 40594, Dec. 1978.

[5] Kain, J.E., Brown, C.M., Lee, J.G., "Missile Aerodynamic Parameter and Structure Identification from Flight Test Data", AIAA Paper 78~1341

[6] Kain, J.E., "An Evaluation of Aeroballistic Range Projectile Parameter Identification Procedures," AIAA Paper 79~1687.

[7] Kelsey, J.R., Petersen, D.P., "Aerodynamic Coefficient Estimation By Means of An Extended Kalman Filter", AIAA Paper 79~1686.

[8] Jiang Quanwei, Shang Yongshan, Song Chaoqin, et al, "A method to identify pressure center, attack angle, and aerodynamic coefficients". Journal of Aerodynamics, Volume 1 1980.

DETERMINATION OF AERODYNAMIC COEFFICIENTS FOR A RE-ENTRY BODY BY MEANS OF AN EXTENDED KALMAN FILTER

Jiang Quanwei, Xu Jinzhi, Zhou Shuying
(*Aerodynamic Research Center of China*)

Abctract

An extended Kalman filter is used to determine the major aerodynamic coefficients of a re-entry body in this paper. The emphasis is put on estimating the states and parameters only on the basis of the re-entry on-board measurement data in the absence of trajectory observation data. The measured data include angular rates and acceleration obtained from the rate gyros and accelerometers installed in the vehicle. A mathematical model presented is based upon the 6-degree-of-freedom motion equations. Both ballistic and maneuvering re-entries are considered. The numerical simulation and real data extraction show that the presented method can provide satisfactory results.

A PROGRAM SYSTEM FOR DYNAMIC ANALYSIS OF AERONAUTICAL STRUCTURES - HAJIF-II

TEAM FOR DEVELOPING HAJIF-II

Institute of Aeronautical Research of China
Written by Guan De *

ABSTRACT

HAJIF-II is the dynamic analysis system for aeronautical structures developed under the leadership of the Institute of Aeronautic Research of China. It is capable of carrying out the calculation of natural dynamic characteristics of structures as well as the calculation of aircraft flutter with an active control system and the calculation of gust response. It has 31 fixed flow routes and 2600 FORTRAN statements. It allows the use of 99 elementary substructures and each substructure can have 7000 degrees of freedom. In the flutter and gust response computation, it is possible to use 50 modes. The panel number in nonsteady aerodynamic calculation can reach 300. In the management of the stiffness matrix and mass matrix, the hypermatrix method is used for "macroscopic treatment" and the effective column method is used for "microscopic treatment" to develop a new simultaneous iteration algorithm to improve the efficiency of the calculation of real characteristic values. A more complete state synthesis method computation program has been designed. In addition to fixed and free interface methods, multilevel synthesis and step-by-step computation, a curve-fitting method is introduced to transform the harmonic oscillation aerodynamic force into the Laplace plane technique. This system has been used to calculate a number of typical aircraft structures. Good results are obtained.

*Received on December 15, 1981.

1. INTRODUCTION

HAJIF-II is the aeronautical structure dynamic analysis system developed by the Institute of Aeronautics Research of China. Its function includes the calculation of the natural dynamic characteristics of structures, the calculation of aircraft flutter with an active control system and the calculation of gust response.

In the development of the system, a series of measures has been adopted to satisfy generality, flexibility, reliability, automation, high efficiency, expandability, ease of correction, and diagnostic capability requirements. Furthermore, special attention has been paid to the guiding principle of advancing on the basis of practicality.

2. CAPABILITIES AND SIZE

In the calculation of structural natural dynamic characteristics of HAJIF-II, it is allowed to use 99 elementary substructures and each substructure has no more than 7000 degrees-of-freedom. In nonsteady aerodynamic calculation, the total number of panels can reach 300. In the flutter and gust response calculations, it is possible to use 50 modes.

HAJIF-II provides 31 fixed flow routes. That is, there are 7 computational flows in the calculation of the natural dynamic characteristics of structures (whole structure, fixed interface method single synthesis, free interface method single synthesis, fixed interface method multi-level synthesis, free interface method multi-level synthesis, fixed interface method step-by-step synthesis, free interface method step-by-step synthesis), 2 flows in the flutter calculation flow, (v-g method, p-k method), 1 gust response calculation flow, and 21 combination flow rates to calculate natural dynamic characteristics, flutter, and gust response.

3. STIFFNESS AND MASS MATRIX

In the natural dynamic characteristics calculation of structures of HAJIF-II, a finite element displacement method is used. A structure can be discretized into a finite element model, or can be approximated by a single beam. A structure can be analyzed as an entity, or can use the mode synthesis method. /26

In the element warehouse of HAJIF-II, there are 11 types of bar, plate, beam, and film elements to simulate the wing, body, external attachment, and their corrections.

In order to improve the efficiency of calculation, the following measures are taken:

(1) The technique to vary the degree of freedom. Regardless of whether it is an elementary or higher level substructure, the program automatically determines the real degree of freedom of each nodal point to eliminate ineffective degrees of freedom.

(2) The Cuthill-Meckec method[1] is used in the re-labeling of multi-level substructural nodal points and the optimized utilization of band width. In addition, some special treatments are also performed.

(3) A compact assembly method is used to only assemble non-zero nodal point panels.

(4) The improved hypermatrix technique. In an usual hypermatrix method, there are considerable zero elements in a non-zero submatrix. For this, HAJIF-II first conducts a "macroscopic treatment" to the submatrix in the hypermatrix method, and then carries out a "microscopic treatment". For

the stiffness matrix, the effective column concept is used to eliminate the useless zero elements in a non-zero submatrix. For a mass matrix, because it is unchanged in the entire iteration process, a nodal point control method is used. The improved hypermatrix method can effectively reduce the storage requirement as shown in Table 1.

Table 1. Comparison between the internal storage used by HAJIF-II and that by the conventional hypermatrix technique.

1 算例	2 阶数	4 刚度矩阵存贮量		5 质量矩阵存贮量	
		3 一般超元矩阵	HAJIF-Ⅱ	6 一般超元矩阵	HAJIF-Ⅱ
1	870	107712	78557	21312	1594
2	210	11520	5596	9590	1930
3	138	6336	1458	5357	979

Key: 1) example; 2) order; 3) conventional hypermatrix; 4) storage of the stiffness matrix; 5) storage of the mass matrix; 6) conventional hypermatrix.

In the constraint treatment area, HAJIF-II can perform single point or multiple constraint treatment with regard to the degree of freedom of a nodal point[2]. The function of the former is to designate the displacement values of certain degrees of freedom to simulate the symmetric and asymmetric conditions and boundary conditions, as well as to conduct zero stiffness direction treatment. The latter's function is to express the displacements of part of the degrees of freedom as the linear combination of the displacement of other degrees of freedom in order to treat the coordinating and stiffness elements between the degrees of freedom.

IV. ANALYSIS OF REAL CHARACTERISTIC VALUES

In the natural dynamic characteristics calculation of structures, the following equation is used

$$ku = \lambda mu \tag{1}$$

where k and m are the stiffness matrix and mass matrix, respectively, λ and u are characteristic value (circular frequency square) and characteristic vector (natural mode), respectively.

In order to improve the calculation efficiency, a new algorithm is developed on the basis of theoretical analysis of existing simultaneous iteration methods and large amounts of numerical tests by combining the advantages of these methods. Its special point is that the mass matrix is not decomposed. Rather, a "dimension lowering" treatment and other improvements /27
are used. Therefore, compared to the existing algorithms, this new algorithm has the same converging rate. However, the calculation load in each iteration step is the least and the efficiency is high as shown in Table 2.

When using projection matrix to solve the characteristic value problem, the QR or Jacobi method is used. The Chebyshev polynominal or origin displacement is used to perform acceleration treatment. The characteristics of the Sfurm series[3] are used to carryout the missing root check. This can be carried out in combination with the determination of the number of trial vectors. The wave array element elimination method with a buffer is used to solve the matrix.

Table 2. Comparison of efficiencies of various simultaneous iteration algorithms.

1 算例	2 阶数	3 半带宽	试向量个数 4	5 计算时间 (秒)					
				Rutishauer	Reinsch	McCormick	Nicolai	Bathe	HAJIF-I
1	500	301	13	1106	1069	992	973	980	758
2	100	5	30					194	93
3	200	20	33					363	234
4	500	10	38					986	558

Key: 1) example; 2) order; 3) half band width; 4) calculation time (second).

V. MODE SYNTHESIS

In HAJIF-II, a more complete mode synthesis program has been designed. In addition to the two major methods — fixed interface and free interface method[4,5], we also developed a level synthesis and step-by-step synthesis method of our own to form six types of synthesis methods as described in Section 2.

In the free interface method, we should consider the residual stiffness and residual inertia effects in higher order modes. Through trial calculation, it was discovered that the residual inertia effect could be neglected. Hence, in HAJIF-II only the algorithm considering the residual stiffness effect is used.

The free interface method of HAJIF-II processes the attached mode into a "quasi constraint mode" and the free interface main mode into a "quasi fixed interface main mode"[6] so that the calculation format of the free interface method is unified with that of the fixed interface method.

In the search for the softness matrix of the free interface main mode and free structure, the "imaginary structure" concept is used. The stiffness matrix of the imaginary structure is $k^*=k+m$, and the mass matrix is still m. Hence, the softness matrix of a free structure is $(k^*)^{-1}$.

The differences among single synthesis, multi-level synthesis and step-by-step synthesis are shown in Figure 1. The multi-level synthesis is, in principle, an extension of the single synthesis. However, in each level of synthesis in the step-by-step synthesis method, there are two substructures participating. Among them, one substructure participates using the reduced generalized degree of freedom and the other substructure directly participates with the physical degree of freedom.

In order to suit the requirements of multi-level synthesis and step-by-step synthesis, some development is needed with regard to frequency selection judgement in HAJIF-II.

HAJIF-II can treat rigid substructures. Only when using multi-level synthesis, it is required to process it during the first synthesis.

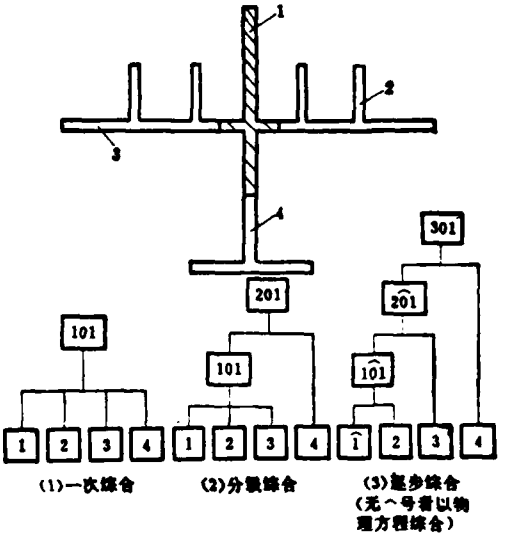

Figure 1. Models for calculation of various modal synthesis techniques.

Key: 1) single synthesis; 2) multi-level synthesis; 3) step-by-step synthesis (synthesized using the physical equation for those without the ^ symbol).

VI. NONSTEADY AERODYNAMIC FORCE CALCULATION

Serious flutter of modern aircraft mostly occurs in the near sonic speed region at low altitude. For wing surface with a medium or small aspect ratio, the results calculated based on the subsonic nonsteady aerodynamic theory could better reflect the basic flutter characteristics. In HAJIF-II we first established a subsonic horseshoe vortex — oscillating doublet mesh method[7] to treat multiwings in space.

In order to calculate the non-steady aerodynamic force, it is necessary to insert the vibrational mode at the structural nodal point to the point of aerodynamic force. HAJIF-II uses the two-way spline curves function method[8].

In HAJIF-II, a curve fitting method used by Rogai[9] was introduced which utilizes the resonating aerodynamic data to find the approximate expression of non-steady aerodynamic force on the Laplace plane.

VII. FLUTTER CALCULATION

In HAJIF-II, v-g and p-k methods are used to carryout flutter calculation[10]. The v-g method uses the following flutter equation

$$\begin{bmatrix} \bar{K}_{qq} & 0 \\ 0 & \bar{K}_{aa} \end{bmatrix} \begin{Bmatrix} q \\ a \end{Bmatrix} = \lambda \left(\begin{bmatrix} \bar{M}_{qq} & \bar{M}_{qa} \\ \bar{M}_{aq} & \bar{M}_{aa} \end{bmatrix} + \frac{\rho b_0}{2k^2} \begin{bmatrix} \bar{A}_{qq} & \bar{A}_{qa} \\ \bar{A}_{aq} & \bar{A}_{aa} \end{bmatrix} \right) \begin{Bmatrix} q \\ a \end{Bmatrix} \tag{2}$$

The p-k method uses the following flutter equation to be taken into account by the active control system

$$\left(\begin{bmatrix} \bar{K}_{qq} & 0 & 0 \\ 0 & \bar{K}_{aa} & 0 \\ 0 & 0 & \bar{K}_{\beta\beta} \end{bmatrix} + \lambda \begin{bmatrix} \bar{M}_{qq} & \bar{M}_{qa} & \bar{M}_{q\beta} \\ \bar{M}_{aq} & \bar{M}_{aa} & \bar{M}_{a\beta} \\ \bar{M}_{\beta q} & \bar{M}_{\beta a} & M_{\beta\beta} \end{bmatrix} + \frac{1}{2}\rho V^2 \begin{bmatrix} \bar{A}_{qq} & \bar{A}_{qa} & \bar{A}_{q\beta} \\ \bar{A}_{aq} & \bar{A}_{aa} & \bar{A}_{a\beta} \\ \bar{A}_{\beta q} & \bar{A}_{\beta a} & \bar{A}_{\beta\beta} \end{bmatrix} \right) \begin{Bmatrix} q \\ a \\ \beta \end{Bmatrix} = 0 \tag{3}$$

where $\overline{K}$, $\overline{M}$, and $\overline{A}$ are generalized stiffness, mass, and aerodynamic force, respectively; q,a, β are the generalized coordinates of the HAJIF-II users to add and control modes; ρ and V are the atmospheric density and flight velocity; λ is the complex characteristic value; b_0 is a reference length.

HAJIF-II uses LR, QR, and reverse root method with origin displacement to solve the complex characteristic value problem. They are available for the users to choose.

VIII. GUST RESPONSE CALCULATION

HAJIF-II uses the following equation to calculate the aerodynamic elastic frequency response[9]

$$\left([\overline{M}_{ee}\overline{M}_{e\beta}]+[\overline{K}_{ee}\,0]+\frac{1}{2}\rho V^2\,[\overline{A}_{ee}(s)\overline{A}_{e\beta}(s)]\right)\begin{Bmatrix} q \\ \beta \end{Bmatrix}=-\frac{1}{2}\,\rho V^2\{\overline{A}_{eg}(s)\} \qquad (4)$$

$$\{\beta\}=\frac{[R(s)]}{D(s)}\{q\}$$

where R/D is the transfer function of the active control system. The footnote g represents gust and s is the

In the calculation of gust response, it is possible to use the Karman power spectrum or to provide the users with a fixed form.

/29

IX. PROGRAM ORGANIZATION AND USER INTERFACE

HAJIF-II uses a two level management system. The first level is the monitoring control program which is composed of a series of dispatching languages. The second level is the processing program. In fact, it is dispatched by the monitoring

control program, which is the highest level subroutine capable of finishing a certain mathematical or mechanical function independently. It is not possible to be mutually dispatched between two processing programs. The input and output of each processing program are only related to data documentation.

In the monitoring control program of HAJIF-II, a common number group with a variable length is established to be given to various processing programs. In addition, to be able to establish a very small amount of the number group by the processing program, other numbers are formed completely from the above mentioned common number group.

For a calculation requiring a larger internal storage, the system can automatically judge whether external storage is necessary.

The entire data of HAJIF-II is called the "dictionary". The dictionary is formed by several volumes and the number of volumes can be expanded. Each volume has 100 books and each book is made up of 100 chapters. The volume, in principle, is divided according to the processing program. The major purpose of a book is to facilitate the performance of some repeated calculation. A chapter is the entire data of a "read" or "write" statement, which is the basis of data management.

The document management system of HAJIF-II can automatically conduct document distribution and correlated variable control. As long as the input, output table and the chapter address are provided, the system can independently complete reading and writing work.

In HAJIF-II, user-oriented broad command languages were designed. One is used to initiate leading fixed flow route and the other one is used to dispatch 21 processing programs for the users to form a "user flow". In view of the fact that flow organization of mode synthesis is more complicated, we also designed the special composite language.

In order to facilitate the preparation of data, the data generation system of HAJIF-II allows the use of two input forms: one is numerical data input and the other is a mixed input of numerical values, data, and topological description.

The function of topological description includes the simple description of nodal point coordinates of ideal parts and element information, data abbreviation with regularity, data correction, addition and elimination, etc.

As for the error diagnosis of HAJIF-II, the focus is placed on the checking of the original data. It is capable of providing over one hundred types of information according to the requirement of the users.

X. EXAMPLE

During the development of HAJIF-II, over ten examples were calculated. Now, let us introduce three types of combined examples.

(1) Calculation of the Natural Dynamic Characteristics and Flutter of a Triangular Wing. The wing is simulated by bars and shearing plates. The fuselage and flat tail are simulated by beams, and the wing-fuselage connection is simulated by transition beams. There are 315 nodal points and 1011 degrees

of freedom. The comparison of calculated natural dynamic characteristics and the resonance test results is shown in Figure 2. It coincides very well. In the meantime, v-g and p-k methods are used to calculate flutter and the results agree with the wind tunnel test results.

(2) The calculation of modal synthesis of the flat wing — fuselage — attachment combination. The structure is simulated entirely by beams. There are 46 nodal points, 138 degrees of freedom, and 4 substructures as shown in Figure 1. The calculated natural frequencies are shown in Table 3. It is obvious that all the synthesis methods have excellent accuracy.

(3) Calculation of Gust Response of B-47 Airplane. The computation data in Reference [11] was used. The wing and fuselage are simulated by beams and the flat tail is a rigid body. In the aerodynamic force calculation, the interference between the wing and the flat tail was included. In the calculation of the response, the atmospheric turbulence power spectrum measured in flight tests, provided in Reference [11], was used. The results are shown in Figure 3. Because the nonsteady aerodynamic force used in Reference [11] is different from the one used in HAJIF-II, the results of these two calculations are not quite the same. /30

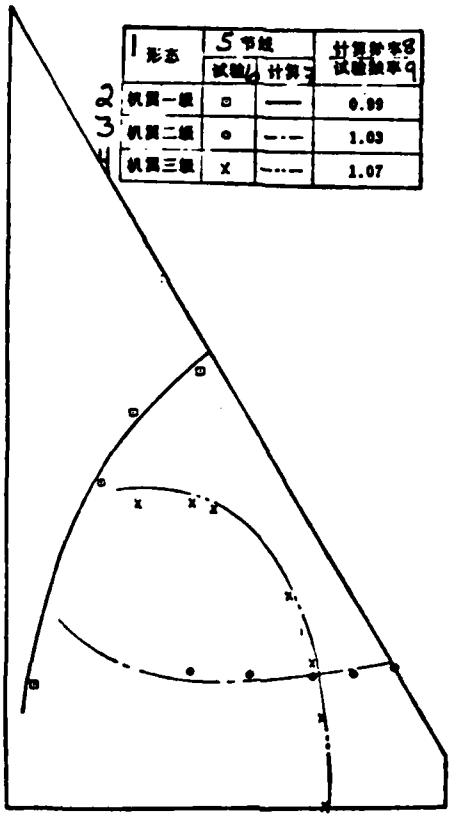

Figure 2. Comparison of calculated natural frequencies and modes with resonance test results.

Key: 1) mode; 2) first level wing; 3) second level wing; 4) third level wing; 5) nodal line; 6) experimental; 7) calculated; 8) calculated frequency; 9) experimental frequency.

Table 3. Comparison of various synthesis techniques.

形 态 10	全 结 构 11	固定界面一次综合 12	自由界面一次综合 13	固定界面分级综合 14	自由界面分级综合 15	固定界面逐步综合 16	自由界面逐步综合 17
1	2.5130	2.5130	2.5130	2.5146	2.5130	2.5130	2.5130
2	3.2683	3.2683	3.2683	3.2685	3.2684	3.2682	3.2683
3	4.0450	4.0450	4.0450	4.0605	4.0451	4.0450	4.0450
4	4.5917	4.5917	4.5917	4.5921	4.5917	4.5918	4.5917
5	4.9012	4.9012	4.9012	4.9013	4.9012	4.9012	4.9012
6	5.5063	5.5066	5.5063	5.5061	5.5063	5.5066	5.5063

Key: 10) mode; 11) whole structure; 12) fixed interface single synthesis; 13) free interface single synthesis; 14) fixed interface multilevel synthesis; 15) free interface multilevel synthesis; 16) fixed interface, step-by-step synthesis; 17) free interface, step-by-step synthesis.

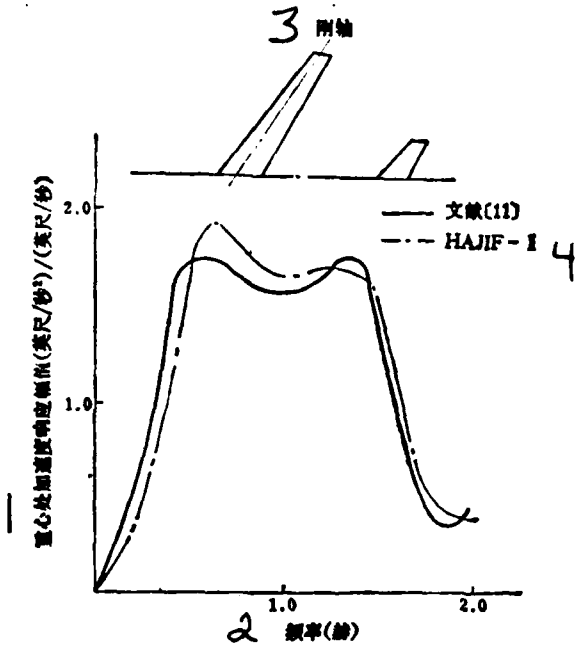

Figure 3. Comparison of calculated gust responses with the results of Reference [11].

Key: 1) acceleration response amplitude at center-of-gravity (foot/sec^2)/(foot/sec); 2) frequency (Hertz); 3) rigid axis; 4) Reference [11]. /31

CONCLUSION REMARKS

This paper briefly described the method and function of the HAJIF-II dynamic analysis system for aeronautical structures. The system incorporated several new measures and quite good trial calculation results were obtained. The system will be further developed. Due to the limitation in space, this paper might appear to be too oversimplified. The authors wish to apologize to the readers in this regard.

REFERENCES

[1] R. P. Tewarson, Spare Motrices, New York Academic, 1973.

[2] R. H. MacNeal, The NASTRAN Theorefical Manual (Level 15), NASA sp 221 (01), 1972.

[3] K. J. Bathe, E. L. Wilson, Numerical Methods in Finite Element Analysis, Englewood Cliffs, 1976.

[4] R. R. Craig Jr., C. J. Chang, On the Use of Attachment Modes in Substructure Coupling for Dynamic Analysis, AIAA Paper 77—405.

[5] Wang Wenliang, Du Zuo Run, Zhen Kang Ynan, "A short comment on simulated mode synthesis techniques and a new improvement", <<Acta Aeronautica et Astronautica Sinica>> 1979, 3.

[6] Zhu De mao, simulated mode synthesis technique in dynamic analysis of structures, <Journal of Naujing Aeronautical>> Institute 1979, 5.

[7] J. P. Giesing, T. P. Kalman, W. P. Rodden, Subsonic Steadyand Oscillatory Aerodynamics for Multiple Interfering Wings and Bodies, J. of Aircraft, Vol. 9, No. 10, 1972.

[8] G. T. S. Done, Interpolation of Mode Shapes, A Matrix Scheme Using Two-Way Spline Curves, Aeronautical QuarteHy, Vol. 16, Part 4, 1965.

[9] I. Abel, An Analytical Technique for Predicting the Characteristics of a Flexible Wing Equipped with an Active Flutter-Suppression System and Comparison with Wind Tunnel Data, NASA TP 1367, 1979.

[10] E. D. Bellinger, R. L. Harder, W. P. Rodden, Aeroelastic Addition to NASTRAN, NASA CR 3094, 1979.

[11] F V. Bennet, K. G. Pratt, Calculated Responses of a Large Sweptwing Airplane to Continuous Turbulance with Flight-Test Comparison, NASA R 69, 1960.

A PROGRAM SYSTEM FOR DYNAMIC ANALYSIS OF AERONAUTICAL STRUCTURES (HAJIF-II)

Team for Developing HAJIF-II

Penned by Guan De

Abstract

HAJIF-II is a program system developed by Chinese Aeronautical Establishment(CAE). It is able to accomplish the calculation of the modal characteristics of aircraft structures as well as the flutter and gust response analysis with the active control system taken into account. The structural model may be composed of 99 substructures each with 7000 degrees of freedom. 300 panels may be used in the calculation of nonsteady aerodynamic forces and 50 modes in the flutter and gust response analysis. The data generation system permits the flexible use of numerical data and topological description. 31 prescribed computational flows are supplied and an user can also organize his own computational flows as he needs. A structure can be discretized into finite elements or simulated by single spar. For the management of the stiffness and mass matrix a modified hypermatrix method is employed to omit all of inactive zero elements more effectively. A new algorithm, called a revised simultaneous iteration procedure, has been developed to solve the real eigenvalue problem and is more effective than the current agorithm. Modal synthesis technique with both free and fixed interfaces is adopted. Besides, two new methods of synthesis have been developed from the concept of multilevel substructures. Nonsteady aerodynamic forces are calculated by means of subsonic doublet lattice method for multiwings and aerodynamic forces in Laplace plane can be approximated with a curve-fitting procedure based on sinusoidal data. Flutter equations are solved by V~g and p~k methods and the continuous atmosphere turbulance are used in the gust response analysis. The system consists of a sequence of functional modules so it can be modified and extended easily. An advanced file management system has also been developed. There are approximately 26000 FORTRAN IV statements in the system. The HAJIF-II was applied to analyzing a number of typical aircraft structures and gave good results.

SYSTEM IDENTIFICATION AND AIRCRAFT FLUTTER

Zhang Lingmi *
Nanjing Aeronautical Institute

ABSTRACT

After briefly describing the application of system identification technique to the study of aircraft flutter, this paper introduced three types of system identification methods. The emphasis was placed on the essence of the algorithm and its theoretical basis. The relevant data processing problem was also properly explained. The transfer function method, based on complex modal analysis and the optimization technique, could accurately identify all the modal parameters. It was successfully used in the flutter model experiment of a wing with external bodies. This method could be extended to the conditions for wind tunnel and flight tests with response data only. The correlation and least square techniques were adopted in the impulse response and auto-regressive moving average model method in order to obtain accurate results under strong interference. The latter could also obtain the mean square deviation between the estimated value and the actual value. Both time domain methods could directly use measured sampling data to perform system identification without special signal analysis equipment.

I. INTRODUCTION

The so-called system identification in structural dynamics establishes a mathematical dynamic model according to the response (output) of a known excitation (input) for a structural system, including the modal parametric model in the generalized coordinate system and the structural parameters model in the physical coordinate system. The more practical method is to provide the input, output data of an actual system to determine a model structure and its parameters, using a certain optimization method based on a type of model so that they are best matched with the system under certain guide lines. For a discretized linear steady system, the so-called model structure consists of the determination of the system (or degree of freedom). Once

*Received May 26, 1981

the order is determined, system identification is transformed into parameter identification or parameter estimation problems. In a complete system identification process, in addition to the structure determination and parameter estimation parts, it is also necessary to carry out model verification (for a linear system the main item is the verification of order) and parametric mean square deviation analysis. In order to further improve the effectiveness of identification, experimental design must also become one aspect in the theoretical study on identification [1].

In the recent decade, the ideas and methods of system identification have been fairly successful in structural dynamics. It has promoted the ground, wind tunnel and flight tests of aircraft significantly. In the ground and wind tunnel tests of models and flight tests of aircraft, it is possible to more accurately identify the relevant modal parameters [2,3]. For a windfall flutter, the method relying on the extrapolation of damping to determine the critical point has been proven ineffective. However, the adaptation of the system identification method can determine the coefficients of the flutter differential equation based on experimental data. From these coefficients, it is possible to more accurately obtain the flutter critical velocity [4,5]. For the ground vibration tests of the entire plane, the determination of the proper adjustable force is very difficult. Presently, the major solution is to identify the transfer function matrix based on the experimental data of a single point excitation and the shaker adjustment force of the pure mode [6,7]. In the meantime, the techniques which use the single point transient or random excitation transfer function to identify the modal parameters of the whole aircraft have been successfully developed [6,8].

System identification techniques not only can be used in the ground, wind tunnel and flight vibration tests, but also can further serve as flutter analysis and synthesis. From the modal parameters of the aircraft (parts or the whole plane), it is possible to further identify the stiffness and mass matrices of structures to be used for structure modification and model optimization [9,10]. For an aero- 34
dynamic elastic model, usually only numerical solutions can be given

at the present time. Using the identification method, it is possible to obtain the mathematical expression in a rational form [11] to facilitate the analysis and synthesis of the flutter of the stabilizer system with control and the flutter active control.

This paper mainly introduces three identification methods suitable for studying flutter, i.e., the transfer function method, impulse response method and the auto-regressive moving average (ARMA) model method. The emphasis is placed on the essence of the identification algorithm and its theoretical basis. With regard to the relevant data processing problem, it is also properly explained. These methods are not only suitable for the sine experimental data, but also transient and random experimental data, as well as the condition of using wide frequency band random natural excitation with response data available alone.

II. TRANSFER FUNCTION METHOD

After the discretization of a linear steady system, its dynamic equation can be described by a matrix differential equation in the following:

$$[M]\{\ddot{x}\}+[C]\{\dot{x}\}+[K]\{x\}=\{f(t)\} \tag{1}$$

$\{f(t)\}$, $\{x(t)\}$ are the N-dimensional external force and the displacement response vector, respectively. $[M]$, $[K]$, $[C]$ are the Nth order mass, stiffness and damping matrices, respectively. [M] is orthogonal and [K] and [C] are orthogonal or semi-orthogonal. N is the discretized degree of freedom.

By conducting Laplace transformation on both sides of the equation and assuming the initial condition is zero, we obtain

$$[s^2[M]+s[C]+[K]]\{X(s)\}=\{F(s)\} \tag{2}$$

where $\{F(s)\}$, $\{X(s)\}$ are the Laplace transform of $\{f(t)\}$ and $\{X(t)\}$ respectively; s is the Laplace multiplier (complex number). Then, equation (2) can be expressed as

$$[Z(s)]\{X(s)\}=\{F(s)\} \tag{3}$$

or

$$[H(s)]\{F(s)\}=\{X(s)\} \tag{4}$$

where

$$[Z(s)] = s^2[M] + s[C] + [K] \tag{5}$$

is the generalized dynamic stiffness matrix. Its inverse matrix

$$[H(s)] = [Z(s)]^{-1} = \text{adj}[Z(s)]/\det[Z(s)] \tag{6}$$

is the generalized dynamic softness matrix or the transfer function matrix.

Let s_r be the characteristic root corresponding to the equation (3) and let $\{\psi_r\}$ be the corresponding characteristic vector, i.e.,

$$[Z(s_r)]\{\psi_r\} = 0 \tag{7}$$

For a sub-critical damping system, s_r and $\{\psi_r\}$ are complex numbers which are complex conjugates appearing in pairs.

From equation (6), we know that the transfer function can be expressed as a rational function of s. Furthermore, it can be expanded around the characteristic root.

$$[H(s)] = \sum_{r=1}^{N} \frac{[A_r]}{s - s_r} + \frac{[A_r^*]}{s - s_r^*} \tag{8}$$

where $[A_r]$ is the residual number matrix corresponding to s_r. The symbol * represents the complex conjugate. It can be proven that $[A_r]$ and the characteristic vector $\{\psi_r\}$ have the following analytical relation [12,13]

$$[A_r] = \frac{\{\psi_r\}\{\psi_r\}^T}{\rho_r} \tag{9}$$

$$\rho_r = \{\psi_r\}^T(2s_r[M] + [C])\{\psi_r\}$$

When the system damp is the structure damp or proportionality damp, the complex vibrational vector $\{\psi_r\}$ becomes the real vibrational vector $\{\phi_r\}$. From equation (9), we can get

$$\rho_r = i2\beta_r m_r \quad (i = \sqrt{-1},\ \beta_r = I_m(s_r))$$

(m_r is the real mode mass of the r-th order). A_r is also a pure imaginary number. After substituting into equation (8), we obtain

$$[H(s)] = \sum_{r=1}^{N} \frac{\{\phi_r\}\{\phi_r\}^T}{s^2 m_r + sC_r + K_r} \tag{10}$$

K_r and C_r are the r-th order real mode stiffness and damp, respectively.

By letting $s_r = -\alpha_r + i\beta_r$, $A_r = u_r + iv_r$, and substituting $s = i\omega$ into the general relation of the transfer matrix of equation (8), we can get the analytical expression between the frequency repsonse and the modal parameters

$$[H(i\omega)] \sum_{r=1}^{N} \frac{(u_r + iv_r)}{\alpha_r + i(\omega - \beta_r)} + \frac{(u_r - iv_r)}{\alpha_r + i(\omega + \beta_r)} \qquad (11)$$

A row (corresponding to a single coordinate excitation multi-coordinate measurement) or a column (corresponding to the single point excitation single coordinate measurement of each respective coordinate) of $[H(i\omega)]$ can determine the whole modal parameters.

Note that $\{\tilde{H}\}$ is the measured frequency response data corresponding to various frequencies tested and $\{\theta\} = (\alpha_1, \beta_1, u_1, v_1 \cdots\cdots \alpha_N, \beta_N, u_N, v_N)^T$ is the modal parameter vector to be identified. Hence, the total square deviation $J(\theta) = \{H(\theta) - \tilde{H}\}^T \{H(\theta) - \tilde{H}\}^*$ of the frequency response data and model value $\{H(\theta)\}$ can be used as the identification guideline function. Note that H(θ) is the nonlinear function of the parameters to be determined (such as α_r, β_r). Therefore, the modal parameter identification problem is transformed into the optimization of J(θ) = min which can be solved by iteration: to first give the initial value of the parameter {θ} to be determined and to use the nonlinear least square multiplication method to obtain the increment {Δθ} as the optimizing direction and then to use an extrapolation method to find the step length factor. The actual algorithm can be referred to in [13].

The row data of parameter identification using the transfer function method--frequency response, can be obtained by two ways: one is to use steady state sinusoidal excitation, tracking filter data analysis, and the other is to use wide frequency band excitation (fast sinusoidal scanning frequency, impulse, pure random, pseudo-random or periodical random, etc.) fast Fourier transfer (FFT) data processing. The frequency response of the former represents the complex amplitude ratio of response and excitation force and the latter represents the ratio of the mutual power spectrum and the individual power spectrum of input and output.

The main advantage of steady state sinusoidal excitation, tracking filter analysis is the high data accuracy. For wind tunnel model flutter tests on wings with external bodies, the accuracy of the modal frequencies identified could reach 1%. The vibrational model orthogonality tests could reach the 10% level required by the finite element mathematical model actually used in the analysis, testing and modification of flutter [14].

The major advantages of the wide frequency bandwidth excitation, FFT analysis technique are the fast testing speed and the adaptation to the wind tunnel and flight test conditions. The disadvantages are the small signal-to-noise ratio and the low frequency resolution which affect the data accuracy. Presently, measures to improve the accuracy of data have been developed, such as the power spectrum data smoothing and bandwidth selectable FFT analysis (BSFA), etc.

In the subcritical wind tunnel and flutter tests, sometimes it is possible to directly use natural bandwidth random excitation (such as turbulence). At this time, the input is a multiple input which cannot be directly measured. Assuming that the external force frequency spectrum $F(\omega)$ near the modal frequency is a constant, then the response spectrum can be expressed as

$$\{X(\omega)\}=[H(i\omega)]\{F(\omega)\}=\left[\sum_{r=1}^{N}\frac{\{u_r+iv_r\}}{\alpha_r+i(\omega-\beta_r)}+\frac{\{u_r-iv_r\}}{\alpha_r+i(\omega+\beta_r)}\right]\{F(\omega)\}$$

$$=\sum_{r=1}^{N}\frac{\{U_r+iV_r\}}{\alpha_r+i(\omega-\beta_r)}+\frac{\{U_r-iV_r\}}{\alpha_r+i(\omega+\beta_r)} \qquad (12)$$

From this, it is not difficult to extend the above identification technique to the condition under which only output (response) data exists.

III. IMPULSE RESPONSE METHOD

The impulse response function of a discrete linear steady system with N degree of freedom can be expressed by the inverse Laplace transformation of the relation between the transfer function and the complex frequency s_r and the complex number A_r equation (8): 36

$$h_{qp}(t)=\sum_{r=1}^{N}(A_r^{qp}e^{s_r t}+A_r^{*qp}e^{s_r^* t}) \qquad (13)$$

p and q are the excitation and measurement coordinates respectively.

At time t_n, let $t_n = n\Delta t$, and note $X_r = e^{s_r \Delta t}$, t_n . The impulse response at time t_n can be expressed as (omitting the symbols p, q)

$$h(t_n) = 2\mathrm{Re}\left(\sum_{r=1}^{N} A_r X_r^n \right) \tag{14}$$

where n is the power. For each sampling time of equal difference $t_n (n = 0, 1, 2, \cdots\cdots, N)$, , we can write (2 N + 1) equations. Let

$$\prod_{r=1}^{N} (X - X_r)(X - X_r^*) = \sum_{n=0}^{2N} a_n X^n = 0 \tag{15}$$

where $X = e^{s\Delta t}$, and the coefficients $a_n (n = 0, 1, 2, \cdots\cdots, 2N)$, are the autoregressive coefficients of the equation. Once these coefficients are obtained, it is possible to obtain the complex frequency $s_r = -\alpha_r + i\beta_r$ by solving the complex root $X_r = e^{s_r \Delta t}$ using equation (15). From them, we can obtain the modal frequency ω_r and damp ratio $h_r (r = 1, 2, \cdots\cdots, N)$

$$\omega_r = \sqrt{\alpha_r^2 + \beta_r^2}, \quad h_r = \alpha_r / \omega_r \quad .$$

The method to obtain the auto-regressive coefficients is as follows: multiply both sides of equation (14) by a_n and let $n = 0, 1, 2, \cdots\cdots, 2N$, . After rearrangement, we get

$$\sum_{n=0}^{2N} a_n h(t_{m+n}) = 0 \qquad (m = 0, 1, 2, \cdots\cdots, 2N-1) \tag{16}$$

There are only 2N independent amplitude values in the impulse response data. Let us choose $a_{2N} = 1$ to standardize it. Then, we have

$$\sum_{n=0}^{2N} a_n h(t_{m+n}) = h(t_{m+2N}), \tag{17}$$

By considering random interference and testing errors, the total square deviation of impulse response corresponding to M sampling times is

$$J_1(a) = \sum_{m=1}^{M} \left(\sum_{n=0}^{2N-1} a_n h(t_{m+n}) + h(t_{m+2N}) \right)^2 \tag{18}$$

The extreme value $\{a\} = (a_0, a_1, a_2, \cdots\cdots, a_{2N-1})^T$ corresponding to $J_1(a) = \min$ can be obtained from the following set of equations

$$\sum_{n=0}^{2N-1} R_{i,n}a_n = -R_{i,2N} \qquad (i = 0,\ 1,\ 2,\cdots\cdots,2N-1) \tag{19}$$

where

$$R_{i,n} = \sum_{m=1}^{M} h(t_{m+i})\,h(t_{m+n})$$

is the correlation function of impulse response. The latter is an even function which only deviates from the time difference. Equation (19) can be written in the following matrix form

$$\begin{bmatrix} R(0) & R(1)\cdots\cdots R(2N-1) \\ R(1) & R(0)\cdots\cdots R(2N-2) \\ \vdots & \vdots \\ R(2N-1) & R(2N-2)\cdots R(0) \end{bmatrix} \begin{bmatrix} a_0 \\ a_1 \\ \vdots \\ a_{2N-1} \end{bmatrix} = - \begin{bmatrix} R(2N) \\ R(2N-1) \\ \vdots \\ R(1) \end{bmatrix} \tag{20}$$

The least square method is as follows: Express the impulse response in the form of sine and cosine function form (notice that $s_r = -\alpha_r + i\beta_r$, $A_r = u_r + iv_r$) 37

$$h(t_m) = 2\sum_{r=1}^{N} e^{-\alpha_r t_m}(u_r\cos(\beta_r t_m) - v_r\sin(\beta_r t_m)) \tag{21}$$

The actual measured impulse response value at time t_m is denoted as g_m; then the total square deviation of M sampling values is

$$J_2(u,\ v) = \sum_{m=1}^{M}\left(g_m - \sum_{r=1}^{N}(c_{rm}u_r - s_{rm}v_r)\right)^2 \tag{22}$$

where

$$c_{rm} = 2e^{-\alpha_r t_m}\cos(\beta_r t_m),\quad s_{rm} = 2e^{-\alpha_r t_m}\sin(\beta_r t_m)$$

The extreme value $(U,\ V)^T = (u_1,\ u_2\cdots u_N,\ v_1,\ v_2\cdots v_N)^T$ of $J_2(u,v) = \min$ can be obtained from the following set of linear functions

$$\begin{bmatrix} A & D \\ D^T & B \end{bmatrix}\begin{bmatrix} U \\ V \end{bmatrix} = \begin{bmatrix} X \\ Y \end{bmatrix} \tag{23}$$

where A, B, and D are Nth order matrices. The ith row jth column elements are

$$A_{ij} = \sum_{m=1}^{M} c_{im}c_{jm},\quad B_{ij} = \sum_{m=1}^{M} s_{im}s_{jm}$$

$$D_{ij} = \sum_{m=1}^{M} c_{im}s_{jm}$$

X and Y are N dimensional vectors whose element is related to the measured data

$$X_i = \sum_{m=1}^{M} c_{im} g_m, \quad Y_i = -\sum_{m=1}^{M} s_{im} g_m$$

The original data of impulse response system identification is the impulse response tested data which can be obtained using the following method

(1) if input and output data can be simultaneously measured, then the frequency response can be obtained first. Then, Fourier inverse transform can be used to obtain the impulse response data. Both can utilize FFT and BSFA techniques;

(2) if the input (excitation force) cannot be directly measured, then a random decay technique can be used which triggers the recording at a certain voltage with respect to the wide frequency band random response signal of the system. Then it is followed by the sampled data total average. Assuming that the forced response of the voltage triggering sampling signal after total averaging and the response caused by the initial triggering condition are close to zero, the obtained characteristic signal can be described by the impulse response.

IV. AUTOREGRESSIVE MOVING AVERAGE MODEL METHOD

The usual expressions of a dynamic system in a time domain are modal functions and output functions. For a time discretized system, the input/output relation can be expressed by the difference equation

$$\sum_{i=0}^{2N} a_i x(t-i) = \sum_{i=0}^{2N} b_i y(t-i) \qquad (24)$$

Assume that y(t) is an independent random serial input with an average zero, square deviation σ^2. After taking random measurement noise into account without losing generality, the above equation can be written as:

$$\sum_{i=0}^{2N} a_i x(t-i) = \sum_{i=0}^{2N} b_i y(t-i) \quad (a_0 = b_0 = 1) \tag{25}$$

The measured response value of a certain coordinate of the system at time t is

$$\begin{aligned} e(t) = &-a_1 x(t-1) - a_2 x(t-2) - \cdots\cdots - a_{2N} x(t-2N) + y(t) \\ &+ b_1 y(t-1) + b_2 y(t-2) + \cdots\cdots + b_{2N} y(t-2N) \end{aligned} \tag{26}$$

The first 2N terms are the sum of the measured values (autoregressing) before time t, and the last (2 N + 1) terms are the moving average of the input. Therefore, equation (25) is also called the autoregressive moving (ARMA) model. The autoregressive coefficients a_i and the characteristic values $s_i = -\alpha_i + i\beta$ have the following relation

$$\sum_{i=0}^{2N} a_i X^i = \prod_{i=1}^{N} (X - X_i)(X - X_i^*) \tag{27}$$

where $X_i = e^{-\alpha_i \Delta t + i\beta_i \Delta t}$

After identifying the autoregressive coefficients, it is possible to solve the attenuation coefficient α_i and damping free vibrational frequency β_i (from here we can obtain the damp ratio and modal frequency). The moving average coefficients b_i, however, are related to the vibration model information.

The coefficients of the ARMA model can be identified using the maximum approximation method. The standard function can be chosen as the total square deviation (approximation function) of the measurement noise

$$J(a, b) = \frac{1}{M} \sum_{t=1}^{M} y(t)^2 = cyy(0) \tag{28}$$

where y(t) is the measurement noise, cyy(0) is the auto-correlation function with zero time difference, and M is the sampling data points. It is possible to use the Newton-Raphson method to solve the coefficients a_i, b_i (i = 1,2,--2N) to be identified to make J(a,b) = min. If the input cannot be measured, cyy(0) can be calculated from the auto-correlation function cxx(i) of the response.

The advantages of maximum approximation parameter estimation are

approaching without deviation (the expected estimation value is equal to the real value), identical intensity (when the sampling point increases, the estimation value converges to the actual value with probability equal to 1), and statistically effective (the least square deviation between the estimation and real values can reach the Cramer-Lao lower limit). The shortcoming is that the computation is too complicated which is suitable for engineering applications.

Let us write equation (26) (corresponding to M sampling time inoervals) in the matrix form

$$\{x\}=[P]^T\{\theta\}+[\varepsilon] \tag{29}$$

where {x} is the vector formed by the sampled response values at t = 2N + 1, 2N + 2, ..., 2N + M, {ε} is the corresponding measurement error vector, $\{\theta\} = (b_1, a_1, \ldots b_{2N}, a_{2N})^T$ is the vectors to be identified. The coefficient matrix is

$$\begin{pmatrix} y(2N), & y(2N+1)\cdots\cdots & y(2N+M-1) \\ -x(2N), & -x(2N+1)\cdots\cdots & -x(2N+M-1) \\ \vdots & \vdots & \vdots \\ y(1) & y(2)\cdots\cdots\cdots\cdots & y(M) \\ -x(1) & -x(2)\cdots\cdots\cdots\cdots & -x(M) \end{pmatrix}$$

From equation (29), the least square estimation of the parameter to be identified can be obtained from the following equation:

$$\{\hat{\theta}\}=([P][P]^T)^{-1}[P]^T\{x\} \tag{30}$$

The standard square deviation between the estimated value and the real value can also be estimated

$$Cov(\hat{\theta},\ \theta)=E\{(\hat{\theta}-\theta)(\hat{\theta}-\theta)^T\}=\frac{\sigma^2}{M-2N}([P][P]^T)^{-1} \tag{31}$$

where [P] $[P]^T$ can be calculated from the correlation function of the testing data.

39

$$[P][P]^T=\begin{bmatrix} R(0) & R(1)\cdots\cdots\cdots R(2N-1) \\ R(1) & R(0)\cdots\cdots\cdots R(2N-2) \\ \vdots & \vdots \\ R(2N-1) & R(2N-2)\cdots\cdots R(0) \end{bmatrix}$$

$$R_i=\begin{bmatrix} cyy(i) & -cyx(i) \\ -cxy(i) & cxx(i) \end{bmatrix}$$

Under the condition that the input signal (such as atmospheric turbulence, gust) cannot be observed, the least square method can be used which involves the structuring of an autoregressive (AR) model first and then deriving the auto-correlation and mutual correlation functions of the input based on the auto-correlation function of the output data. Let the AR model be

$$\sum_{i=0}^{L} \alpha_i x(t-i) = y(t) \quad (\alpha_0 = 1) \tag{32}$$

where y(x) satisfies

$$E\{y(t)\} = 0; \; E\{x(t)x(s)\} = \sigma^2\delta_{ts}$$

α_i are the autoregressive coefficients to be identified and L is the order to be determined. Because y and x are not correlated, we find from equation (32) that

$$\sum_{i=1}^{L} \alpha_i cxx(k-i) = 0 \quad (k = 1, 2, \cdots\cdots, L) \tag{33}$$

From this we can find α_i. The order L can be identified from the Akaike information guideline. The square deviation estimation value of measurement error is

$$\delta^2 = \sum_{i=1}^{L} \alpha_i cxx(i) \tag{34}$$

From the relation between input and output

$$x(t) = \sum_{i=1}^{L} h(i)y(t-i) \tag{35}$$

h(i) is the impulse response function. The above expression is also called the moving average (MA) model. From equation (35) we can derive the mutual correlation function

$$cxy(i) = \begin{cases} \sigma^2 h(i) & i \geq 0 \\ 0 & i < 0 \end{cases} \tag{36}$$

h(i) can be obtained from the following recurrence formula

$$h(0) = 1, \; h(t) = -\sum_{i=1}^{L} \alpha(i)h(t-i) \quad (t = 1, 2, \cdots) \tag{37}$$

From this, the original data needed to identify the parameters and the square deviations of the real values of the ARMA model by equations (30) and (31) can be obtained from the sampled data.

V. CONCLUSIONS

1. Based on the frequency response data obtained in ground vibration measurements, it is possible to obtain sufficiently accurate structural modal coefficients using the transfer function identification method. It has been a success for the flutter model of a wing with external bodies. This technique can be extended to the testing of the entire aircraft or to determine the pure modal excitation shaker forces of multiple points through a transfer function. 40

In the wind tunnel and flight flutter tests, it is possible to obtain the original data using random or transient excitation FFT analysis, including the situation with response excitation alone.

In order to verify and modify the finite element structure dynamic modal mathematical model, more reliable and accurate complete modal parameters are required. We suggest using steady state sinusoidal excitation, tracking filtering to analyze the frequency response data for identification.

The transfer function method can also obtain the distribution of zero and extremum points based on the aerodynamic elasticity calculation of the aircraft or the rational transfer function model formed according to the experimental data in order to facilitate the analysis and synthesis of the flutter of the stabilizer system and the flutter active control system.

2. The impulse response method, in addition to the fact that it is possible to use the inverse Fourier transform of the measured data as the original data, is especially suitable for the condition with response data only. At this time, the random attenuation method can be used to obtain the original data without any data analyzer. It is suited for the identification in wind tunnel and flight tests.

3. The autoregressive moving average model method is an effective statistic parameter estimation technique. Because the random noise effect is confronted face-to-face in this method, and also

because a double smoothing correlation--least square method is used, it is expected to obtain higher identification accuracy with strong interference. This method can also simultaneously obtain the standard square deviation between the real and the estimated values to further ensure the reliability of the results. Furthermore, this method can be directly based on sampled data without the use of special analytical instruments.

REFERENCES

〔1〕 Goodwin G.C Payne R.L, Dynamic System Identification(Experiment Design and Data Analysis) Academic Press. 1977.

〔2〕 Gaukroger D.R.et al, "Numerical Analysis of Vector Response Loci" JS&V.29(3) 1973.

〔3〕 Chang C.S, "Study of Dynamic Characteristics of Aeroelastic System Utilizing Randomdec Signature" NASA CR-132563 (1975).

〔4〕 Heron K.H et al, "The Derivation of Equations of Motion from Response Data and its Applications in Flutter Testing" ARE TR No 73051 (1973).

〔5〕 Houbolt J.C, "Subcritical Flutter Testing and System Identification". NASA CR-132480 (1974).

〔6〕 Hamma G.A.et al, "An evaluation of Exciting and Analysis Method for Modal Testing".SAE 760872.

〔7〕 Hallauer W.L et al, "On the Distribution of Shaker forces in Multiple-Shaker Modal Testing" S& V Bull. V48.pt 1. (1978).

〔8〕 Gimmested D, "Your next Ground Vibration Test Doesn't have to Cost a Millian Dolars".AIAA/ ASME/AHS 22th SDM Conference. (1981).

〔9〕 Collins J.D et al, "Statistical Identification of Structures". AIAA 73-339.

〔10〕 Chen J.C, "Matrix Pertubation for Analytical Model Improvement" AIAA 79-0831.

〔11〕 Arthurs T.D et al, "Aeroelastic Airframe Transfer Function Synthesis" AIAA/ASME 17th SDM Conference (1976).

[12] Ha Hai Chang. "The Vibrational Problem of a Multiple Degree of Freedom Damping Linear System", Journal of Solid Mechanics, 1980, Trial Volume.

[13] Zhang Lingmi. "Identification of Transfer Function and Modal Parameters in Structural Dynamics", Technical information 653 of Nanjing Aeronautical Institute (1979), the modified manuscript was published in the Journal of Solid Mechanics, no. 1 1982.

[14] Zhang Lingmi. "Identification of parameters and transfer function of flutter model for a wing with external bodies", Journal of Nanjing Aeronautical Institute, no. 1, 1982.

SYSTEM IDENTIFICATION AND AIRCRAFT FLUTTER

Zhang Lingmi

(*Nanjing Aeronautical Institute*)

Abstract

After reviewing the application of system identification to aircraft flutter research, three methods of system identification are presented in this paper. Emphases are put on the main points of identification algorithm and its theoretical basis. The problems related to data processing are also discussed. The Transfer Function Method based on complex modal analysis and optimization technique can identify all of the modal parameters accurately. Furthermore, this method has been applied to the flutter model test of a wing with external bodies successfully, The method can be extended to the cases of wind tunnel and flight tests which provide response data only. Adopting the correlation and least square technique, Impulse Function Method and Autoregressive Moving Average Method can gain considerable accuracy in identification of measurement data conteminated with rather strong noise interference. In no need for a special signal analysis instrument, it is possible to make direct use of measurement sampled data from artificial random or transient excitation and response data from natural random excitation with these two time domain methods.

APPLICATION OF MULTIPLE DYNAMIC ABSORBERS TO REDUCE THE VIBRATION LEVEL OF A COMPLEX CANTILEVER STRUCTURE

Tian Qianli
Institute of Mechanics, Chinese Academy of Sciences

ABSTRACT

A complex cantilever structure has two closely positioned resonance peaks near 20 Hz causing the destruction of the root of the structure. This paper presents a method to use multiple dynamic absorbers to reduce its vibration level. In order to overcome the drawback of the usual tuned absorbers which are very sensitive to the structural frequency, six absorbers were hung in a given section of the structure. The absorbers can vibrate along any direction with the structure. Furthermore, the stiffness and damping parameters of these six absorbers could be different from one another so that the absorbing frequency range could be widened. In order to find the optimum parameters and to study the effect of parameter variation on the structure response, large amounts of response curves were calculated. Because the structural damping is very small and the absorber damping is large, therefore, it is a non-proportional damping dynamic analysis problem. In this paper, this problem was solved by an eigen solution method and a modal synthesis method.

I. INTRODUCTION

For a cantilever structure in resonance at the base frequency, a large stress is produced at its root which easily leads to destruction. Use of dynamic absorbers can solve this problem very well. However, for a complex cantilever structure, there are usually several resonance peaks in the vicinity of the base frequency. In addition, due to the fact that the direction of excitation vibration is not specified, these resonance peaks are frequently coupled. The frequency parameters in the long period of the working process of the cantilever and absorbers may deviate from the original designed numerical values. Hence, it is impossible to use classical tuned absorbers to treat this problem. We adopted the method of installing multiple absorbers with different parameters on a section of the structure in

Received April 14, 1981

order to widen its absorbing frequency band and to reduce the vibration level in any direction by vibrating in any direction following the structure.

We all know very well that the commonly used finite element analysis programs such as SAP can only calculate the dynamic problems with proportional damping. Here, our damping is concentrated on the absorbers and these absorbers are hung on a section of the structure which is apparently a non-proportional damping problem. Therefore, we used a complex eigen solution method and a modal synthesis method.

II. USING A MODAL SYNTHESIS METHOD TO CALCULATE THE DYNAMIC RESPONSE

The special feature of the modal synthesis method is that the modal solution of each substructure is obtained individually first. Then the eigen vectors of the substructures are synthesized into the Ritz vector of the structure in order to solve the eigen solution of the system in the subspace. Here, the damping of the structure itself is very small, while the damping of the absorbers is larger. Therefore, we divided them into two substructures. The dampless mode of the structure itself is solved by the SAPN program. A few lower order modes after the cutoff are combined with the concentrating parameters of the absorber to carry out the synthesis. Now, the first few terms of the natural frequencies calculated by the SAPN program and the experimental results are listed in Table 1 for comparison.

43

Table 1 The few terms of natural frequencies of a cantilever structure

frequency order	f_1	f_2	f_3	f_4	f_5	f_6
calculated value	20.25	20.63	88.3	148.0	148.8	259.3
sinusoidal-test	20.83	21.42	88	147	148	240
random test	20.23	21.48	83.19	150.41	158.23	259.87

Because f_1 and f_2 are very closely connected, they correspond to the bending vibrations in two main directions, respectively.

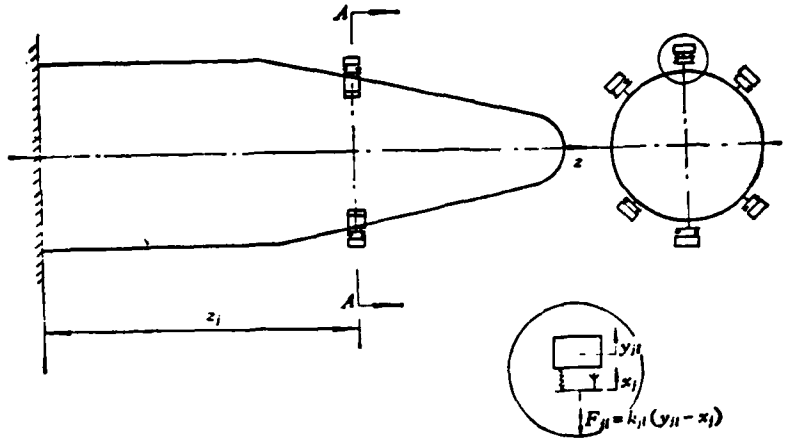

Fig. 1 Schematic of absorber

In order to demodulate them, we used the mechanical resistance testing method. In the 20-22 Hz frequency band, we used slow speed scanning and the phase and amplitude were recorded at high speed using an X-Y recorder. Then the resistance circle was plotted manually point-by-point. Therefore, in this frequency band, the frequency resolution could reach 0.01 Hz. The random excitation vibration was controlled by B·K 3380. The response was recorded on magnetic tape and spectral analysis was carried out on C·F 700.

The actual measured base frequency vibration model basically agrees with the calculated results. Therefore, we began the synthesis using the calculated modal parameters and the absorbers. As shown in Figure 1, after installing a dynamic absorber at point z of the cantilever structure, it is equivalent to the exertion of a concentrated force at that point

$$F_{j,l}=k_{j,l}(y_{j,l}-x_j)\,\delta(z-z_j) \qquad (1)$$

Here $k_{j,l}=k_{j,l}(1+i\beta)$ is the complex stiffness of the complex spring of the absorber, β is the damping coefficient, $i=\sqrt{-1}$.

In the finite element calculation, it is necessary to discretize the structure into several nodal points and each nodal point can have 0-6 degrees of freedom. If the beam element is one which neglects shear and rotational inertia, then each point has two degrees of freedom. Therefore, in the following we will use the jth degree of freedom to represent the z_j point mentioned above. By assuming the

total degrees of freedom after structural discretization to be N, then the displacement vector X is an N dimensional vector. In a structure with m degrees of freedom with p absorbers $(p \geqslant m)$, when the structure is under motion with a base acceleration equal to $\ddot{x}_0$ the equation of motion of the system is

$$M\ddot{X}+KX=M\{I\}\ddot{x}_0+F \tag{2}$$

where

$$F=\left\{\sum_l k^*_{j,l}(y_{j,l}-x_j)\right\} \tag{3}$$

The subscript j represents the jth degree of freedom, the subscript l represents the lth absorber, the superscript * represents the complex number of the quantity, $\{1\}^T=(1,1\cdots 1)$. Because we installed six absorbers of various parameters on a section of a structure, therefore, in equation (3) corresponding to the same x_j, it is possible to have l number of $y_{j,l}$. In order to unify the two in one coordinate system, let us introduce a matrix β 44

$$\beta=\begin{pmatrix} 1 & 0 & 0 & \vdots \\ 0 & 1 & 0 & \vdots \\ 0 & 1 & 0 & \vdots \\ \vdots & 0 & 1 & \vdots \\ \vdots & 0 & 1 & \vdots \\ \vdots & \vdots & 0 & \vdots \end{pmatrix} \tag{4}$$

β is a p x m matrix in which the number of rows corresponds to the number of absorbers and the number of columns is equal to the degrees of freedom of the added absorbers. Its element corresponding to x_j in each column is equal to 1, and the remaining elements are zero. Let

$$T^*=\begin{bmatrix} \ddots & & \\ & k_{j,l} & \\ & & \ddots \end{bmatrix} \tag{5}$$

T^* is a p x p diagonal matrix and its elements are the complex stiffness of the absorbers. Let y be a p dimensional vector whose elements are the displacements $y_{j,l}$ of the absorbers. The sequence corresponds to the diagonal elements of T^*. Therefore, the F in equation (3) can be written as

$$F=\beta^T T^*\{y-\beta X_j\} \tag{6}$$

X_j is the displacement vector corresponding to the part of degrees of freedom of the attached absorber in the total displacement vector of the structure X. It is related to X through the projection matrix P:

$$X_j = PX \tag{7}$$

$$P = \begin{bmatrix} 0 & 1 & 0 & 0 & \cdots\cdots \\ 0 & 0 & 0 & 1 & \cdots\cdots \\ 0 & 0 & 0 & 0 & 0 & 1 \cdots \end{bmatrix} \tag{8}$$

P is an m x N matrix [1]. Only the j^{th} element in each row which corresponds to the degree of freedom of the attached absorber is equal to 1, and other elements are zero.

From equation (6), we can see that F is an m dimensional vector. Multiply it by P^T from the front, so that it is extended into an N dimensional vector. Hence, equation (2) can be written as

$$M\ddot{X} + KX + P^T\beta^T T^* \beta PX - P^T\beta^T T^* y = -M\{I\}\ddot{x}_0 \tag{9}$$

Simultaneously, the equation of motion p absorbers can be written as

$$R\ddot{Y} + T^* Y - T^*\beta PX = -R\{I\}\ddot{x}_0 \tag{10}$$

where

$$R = \begin{bmatrix} \ddots & & \\ & R_{j,l} & \\ & & \ddots \end{bmatrix} \quad \text{is a p x p diagonal matrix} \tag{11}$$

$R_{j,l}$ is the mass of the l^{th} absorber attached to the j^{th} degree of freedom of the structure. Combining equations (9) and (10), we get the equation of motion of the synthesized structure:

$$\begin{bmatrix} M & 0 \\ 0 & R \end{bmatrix} \begin{Bmatrix} \ddot{X} \\ \ddot{Y} \end{Bmatrix} + \begin{bmatrix} K + P^T\beta^T T^* \beta P & -P^T\beta^T T^* \\ -T^*\beta P & T^* \end{bmatrix} \begin{Bmatrix} X \\ Y \end{Bmatrix} = -\begin{Bmatrix} M\{1\} \\ R\{1\} \end{Bmatrix} \ddot{x}_0 \tag{12}$$

In equation (12), T^* is a complex number diagonal matrix. Therefore, it is a $(N + p)^{th}$ order complex number matrix equation. The order N of a complicated structure is very high, and it takes a great deal of computer time to solve the complex eigen solution. For this, let us take the first n terms of modes of the structure as the Ritz vector of the synthesis system. Let $x = V_q$ and substitute it only into equation (9) where V is the matrix formed by the first n terms of the eigen vectors of the structure. Again, multiply it by V^T from the front. We notice that

45

$$V^T M V = I \qquad \text{(I is the unity matrix)}$$

$$V^T K V = \Lambda = \begin{bmatrix} \ddots & & \\ & \omega_r^2 & \\ & & \ddots \end{bmatrix} \omega_r^2 \text{ is the } r^{th} \text{ order eigen value of the structure}$$

Then, we have

$$I\ddot{q} + (\Lambda + V^T P^T \beta^T T^* \beta P V) q - V^T P^T \beta^T T^* Y = -V^T M \{1\} \ddot{x}_0 \qquad (13)$$

Let $PV = V_1$, $\beta^T T^* = T_1^*$, $\beta^T T^* \beta = T_2^*$

Then equation (12) becomes

$$\begin{bmatrix} I & 0 \\ 0 & R \end{bmatrix} \begin{Bmatrix} \ddot{q} \\ \ddot{y} \end{Bmatrix} - \left[\begin{array}{c|c} \Lambda + V_1^T T_2^* V_1 & -V_1^T T_1^* \\ \hline -T_1^{*T} V_1 & T^* \end{array}\right] \begin{Bmatrix} q \\ Y \end{Bmatrix} = - \left\{\begin{array}{c} V^T M \{1\} \\ \hline R\{1\} \end{array}\right\} \ddot{x}_0 \qquad (14)$$

Through the aforementioned cutoff modal transformation, the order of the square matrix decreases from (N + p) to (n + p) and usually n<<N. Therefore, the computational load is greatly reduced. This point is especially significant in dealing with the absorber problem. Because the base frequency component occupies an important portion in the cantilever structure vibration response, it is only necessary to keep the first few orders of modes to obtain a solution of sufficient accuracy. Here, our structure has 54 degrees of freedom after discretization, i.e., N = 54. The SAP program is used to obtain the first 10 orders of eigen values using an iteration method in the substructure space. The sixth, third and second order eigen vectors were selected to form the vector V to be substituted into the left side of equation (14). Use Q. R. Yugenmoyacoby's complex eigen solution program [2] to calculate the complex eigen values and complex eigen vectors, and the results obtained indicate that they are almost identical to those obtained when n = 6, 3, 2. The difference is smaller than one one-thousandth.

III. COMPLEX RESPONSE FUNCTION

Equation (14) is a complex number matrix equation; let $Q = \left\{\begin{array}{c} q \\ \hline y \end{array}\right\}$ From the complex eigen solution program, we can obtain the eigen solution of the homogeneous equations on the left end of equation (14).

$$Q = \Phi^* Z \qquad (15)$$

Φ^* is the complex eigen vector matrix.

Substituting equation (15) into equation (14) and multiplying it by Φ^{*T} from the front, we can obtain the following using orthogonality and normalization characteristics:

$$\ddot{Z}_r(t)+\omega_r^2(1+i\eta_r)Z_r(t)=-\Phi_r^{*T}\begin{Bmatrix} V^TM\{1\} \\ R\{1\} \end{Bmatrix}\ddot{x}_0 \qquad (16)$$

$r = 1, 2, \cdots\cdots n$

Φ_r^{*T} is the r^{th} row in Φ^{*T}

Let

$$\Phi_r^{*T}\begin{Bmatrix} V^TM\{1\} \\ R\{1\} \end{Bmatrix}\ddot{x}_0=P_r(t)=D_r^*\ddot{x}_0 \qquad (17)$$

Conducting Fourier transform on equation (16), we get

$$\bar{Z}_r(\omega)=\bar{H}_r(\omega)\bar{P}_r(\omega) \qquad (18)$$

Here

$$\bar{Z}_r(\omega)=\int_{-\infty}^{\infty}Z_r(t)e^{-i\omega t}dt \qquad (19)$$

$$\bar{P}_r(\omega)=D_r^*\int_{-\infty}^{\infty}\ddot{x}_0(t)e^{-i\omega t}dt=D_r^*\ddot{x}_0(\omega) \qquad (20)$$

$$\bar{H}_r(\omega)=\frac{1}{\omega_r^2(1+i\eta_r)-\omega^2} \qquad (21)$$

46

The denominator of $\bar{H}_r(\omega)$ has two roots, $\omega_{1,2}=\pm\omega_r+(1+i\eta_r)^{1/2}$ where $-\omega_r(1+i\eta_r)^{1/2}$ is located below the real number axis of the complex plane. Therefore, $\bar{H}_r(\omega)$ is unstable in the frequency region. For this purpose, we adopted the suggestion of [3] to use the sum of a pair of complex conjugate values to represent the real solution, i.e., to let

$$\bar{Z}_r(\omega)=\bar{H}_r(\omega)\bar{P}_r(\omega)|_{\omega>0}+\hat{H}_r(\omega)\hat{P}_r(\omega)|_{\omega<0} \qquad (22)$$

Here $\bar{H}_r(\omega)$, $\bar{P}_r(\omega)$ were taken from equations (21) and (22), respectively. $\hat{H}_r(\omega)$, $\hat{P}_r(\omega)$ are their complex conjugates.

Let us divide the Φ^* matrix in equation (15) into two parts which correspond to $\begin{Bmatrix} q \\ y \end{Bmatrix}$, respectively, i.e.,

$$\begin{bmatrix} \Phi_1^* \\ \Phi_2^* \end{bmatrix} Z = \begin{Bmatrix} q \\ y \end{Bmatrix}$$

then
$$\{q\} = \Phi_1^* Z \tag{23}$$

Hence, the displacement vector of the structure is

$$\bar{X}(\omega) = V(\bar{\Phi}_1^* \bar{Z}(\omega)|_{\omega>0} + \hat{\Phi}_1^* \hat{Z}(\omega)|_{\omega<0}) \tag{24}$$

IV. RANDOM VIBRATION RESPONSE

The Fourier transform of the bending moment of the root of a cantilever structure during random vibration is

$$\begin{aligned} \bar{M}(\omega) &= \{h\}^T M \Lambda V \bar{X}(\omega) \\ &= \sum_r \omega_r^2 \{h\}^T M V_r \left(\sum_m \bar{\phi}_{1r,m}^* \bar{Z}_m \Big|_{\omega>0} + \Sigma \hat{\phi}_{1r,m}^* \hat{Z}_m \Big|_{\omega<0} \right) \end{aligned} \tag{25}$$

Here $\{h\}^T$ is the transport of the vector formed by the root heights of all the nodal points after the discretization of the structure. V_r is the r^{th} column vector in the V matrix, and ϕ_{1r}^* is the r^{th} row m^{th} column element in the matrix Φ_1^*

Let
$$\omega_r^2 \{h\}^T M V_r = c_r \tag{26}$$

then
$$\sum_r c_r \bar{\phi}_{1r,m}^* = \bar{B}_m^*, \quad \sum_r c_r \hat{\phi}_{1r,m}^* = \hat{B}_m^* \tag{27}$$

$$\bar{M}(\omega) = \sum_m (\bar{B}_m^* \bar{Z}_m(\omega)|_{\omega>0} + \hat{B}_m^* \hat{Z}_m(\omega)|_{\omega<0}) \tag{28}$$

Its complex conjugate is

$$\bar{M}(\omega) = \Sigma(\hat{B}_m^* \hat{Z}_m(\omega)|_{\omega>0} + \bar{B}_m^* \bar{Z}_m(\omega)|_{\omega<0}) \tag{29}$$

The spectral density of the bending moment at the root of the structure is $S_{MM}(\omega) = \lim_{T\to\infty} \left(\frac{1}{T} \bar{M}\hat{M}\right) = \sum_n \sum_m (\bar{B}_n^* \hat{B}_m^* \bar{D}_n^* \hat{D}_m^* \bar{H}_n \hat{H}_m|_{\omega>0}$

$$+ \hat{B}_n^* \bar{B}_m^* \hat{D}_n^* \bar{D}_m^* \hat{H}_n \bar{H}_m|_{\omega<0}) S_{z_n z_m}(\omega) \tag{30}$$

Let
$$\bar{B}_n^* \hat{B}_m^* \bar{D}_n^* \hat{D}_m^* = A_{m,n} + iB_{m,n} \tag{31}$$

then
$$\hat{B}_n^* \bar{B}_m^* \hat{D}_n^* \bar{D}_m^* = A_{m,n} - iB_{m,n} \tag{32}$$

Substituting it into equation (30) and integrating with respect to ω from $-\infty$ to $+\infty$, the mean square value of the root bending moment can be obtained as

$$\sigma_m^2(t) = \frac{1}{2\pi}\int_{-\infty}^{+\infty} S_{mm}(\omega)\,d\omega$$

$$= \frac{1}{2\pi}\int_{-\infty}^{+\infty}\sum_m\sum_n\left[\frac{A_{m,n}+iB_{m,n}}{(\omega_n^2(1-i\eta_n)-\omega^2)(\omega_m^2(1+i\eta_m)-\omega^2)}\right|_{\omega>0}$$

$$+\left.\frac{A_{m,n}-iB_{m,n}}{(\omega_n^2(1+i\eta_n)-\omega^2)(\omega_m^2(1-i\eta_m)-\omega^2)}\right|_{\omega<0}\Bigg]S_{\ddot{x}_0\ddot{x}_0}(\omega)\,d\omega \qquad (33)$$

If $S_{\ddot{x}_0\ddot{x}_0}(\omega)$ varies slowly in the frequency band of interest, it may be approximated by the white noise spectrum S. Then

$$(t) \approx i\Sigma\Sigma\left[\frac{(B_{m,n}a_m - A_{m,n}b_m)(\omega_m^2-\omega_n^2)-(\omega_m^2\eta_m+\omega_n^2\eta_n)(A_{m,n}a_m+B_{m,n}b_m)}{2\omega_m(a_m^2+b_m^2)(\omega_m^4(1+\eta_m^2)+\omega_n^4(1+\eta_n^2)-2\omega_m^2\omega_n^2(1-\eta_m\eta_n))}\right]S \qquad (34)$$

where

$$a_m = \frac{1}{\sqrt{2}}\sqrt{\sqrt{1+\eta_m^2}+1}$$

$$b_m = \frac{1}{\sqrt{2}}\sqrt{\sqrt{1+\eta_m^2}-1}$$

When ω_m, ω_n are separated relatively far apart, and $\eta_m \approx \eta_n < 0.1$ the coupled term of m and n can be neglected. This caused the approximate expression in equation (2.130) of [4].

$$\sigma_m^2(t) = \sum_m \frac{A_{m,m}S}{4\eta_m\omega_m^3} \qquad (35)$$

V. APPLICATIONS

From equations (21) and (35), we can see that the response function and the mean square value of response are inversely proportional to the modal damping regardless, whether it is simple harmonic vibration or random vibration. Of course, it is also related to the vibrational model parameters. Basically, the stress is proportional to the square of vibration model. By adjusting the weight, position and parameters of the absorbers, it is possible to change the eigen solution of the system; i.e., it might change the response value. Here, due to the limitation in structure, the weights and positions of absorbers are defined. We are only able to change their stiffness and damping parameters. Because the base frequency of a cantilever structure has two major directions of bending vibration, therefore, the absorbers are divided into two groups. Each group has three absorbers corresponding to one major bending direction. Their stiffness and damping may be different. The stiffness coefficient $k_{j,1}$ ranges from

0.8-3.0 kg/cm and the damping coefficient β varies in the range of 0.05-1.0. With regard to various complex stiffness combinations, a large amount of numerical calculations has been carried out. We discovered that when the stiffness coefficients of the three absorbers are 1.5, 2.0 and 2.5 kg/cm, respectively, and when the damping coefficients are 0.2, the vibration absorbing effectiveness is optimal. Now, a comparison of these optimal response curves and another series of response curves obtained with identical stiffness coefficients and β equal to 1.0 is shown in Figure 2.

It is worthwhile mentioning that when this structure was calculated based on an equivalent single degree of freedom body system, the optimal stiffness coefficient is 1.64-1.66 kg/cm and the optimal damping coefficient is 0.19. However, due to the addition of six absorbers to reduce the vibration along the two major bending directions, the calculation formulas single degree of freedom system are no longer applicable. However, calculated results showed that a damping value of about 0.2 is still proper. Figure 2 explains that the effectiveness is reduced when the damping value is too large. When the frequency of the absorber is lower than the base frequency of the structure, the absorber consumes energy during resonance of the structure. [5] had used this property to solve the vibration problem of the SMS aircraft. In that case, the damping of the absorbers must be large. However, the effect was not as good as the multidimensional absorbers because there is always one absorber resonating when the structural frequency changes. Both calculated and experimental results showed that when the structural frequency and absorber frequency vary by 30%, the shock absorbing effect can still reach 50%.

The random tests and sinusoidal frequency scanningtest in this paper were completed by comrades Li Yen ping and Wang Danfung. The decomposition of the base frequency was performed by the author himself. The calculations were carried out by comrades Li Shen zhang and Liu Dekong.

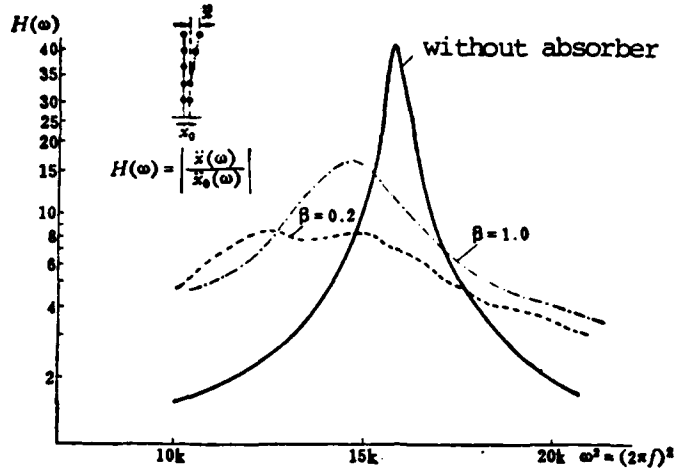

Fig. 2 The frequency response curves of a structure with absorbers having diffrent parameters

REFERENCES

[1] Hans, P. Geering, "New Methods in Substructuring" AIAA/ASME/ ASCE/AHS, 21st S.S.D.M. Conf. 1980, pp 801.

[2] Tian Qianli, Liu De kong, "Some Problems on Vibration Control", Intensity and Environment, vol. 3, 1980, pp 16-23.

[3] Y. Tsushima et al, "Analysis of Equations of Motion with Complex Stiffness Mode Superposition Method Applied to System with Many D.O.F." Nuclear Engng and Design vol. 37, no. 1, pp 47, 1976.

[4] G. B. Warburton, The Dynamical Behavior of Structures, Pergammon Press, pp 102, 1976.

[5] G. K. Hobbs, D. J. Kuyper and J. J. rooks, "Response Analysis of a System with Discrete Dampers", Shock and Vibration Bull. no. 46, Part 4, pp 137, 1976.

APPLICATION OF MULTIPLE DYNAMIC ABSORBERS TO REDUCING THE VIBRATION LEVEL OF A COMPLEX CANTILEVER STRUCTURE

Tian Qianli

(Institute of Mechanics, Chinese Academy of Sciences)

Abstract

In a complex cantilever structure there are some closed resonance peaks in the vicinity of 20Hz, causing a serious bending moment at its root. The application of multiple dynamic absorbers to reducing its vibration level is proposed in this paper. Six absorbers are hung on a given section of the structure to overcome the drawback of the usual tuned absorbers, i. e. excessive sensitivity to the tuning parameters. They can vibrate in all directions following the structure, but their stiffness and damping parameters of these absorbers are different from each other, so that their frequency range is made wide enough to cover the resonance frequencies.

In search of the conditions for minimizing the bending stress of the structure and for the sake of studying the effects of the parameters on the dynamic response, a great number of response curves at the top of the structure, bearing the harmonic excitation from the base movement, are calculated as the parameters of these absorbers vary in a considerable range. Since the damping of the structure is very small and that of absorbers are large enough, so it is a dynamic analysis problem with non-proportional damping. This problem has been solved by a complex eigen-solution method and a modal synthesis method in the present paper.

A SPECTRAL APPROACH FOR ANALYZING THE VIBRATION OF A PERIODIC STRUCTURE WITH RANDOM PARAMETERS

Huang Wen hu *
(Harbin Institute of Technology)

ABSTRACT

In order to explore the effect of fabrication deviation of the blades in a circumferentially closed turbine blade assembly on the vibration of the turbine blades, this paper used a structure model with periodic random parameters as an approximation of the blade structure. In addition, a spectral method was presented to analyze the vibration of this structure. Assuming the standard deviations of the structural parameters are small, therefore, it is possible to use a perturbation method. The periodic random structural parameters are expanded into Fourier series, so that the free vibration and forced vibration of the structure can be solved. Then, the frequency, vibration mode, resonance amplitude and square deviation estimate can be obtained. The orthogonality of the main vibration modes were proven. The special conditions for resonance of this structure were analyzed. The examples showed that the analyzed results and experimental results have the same order of magnitude.

MAJOR SYMBOLS

A, B, a, b, c, d ——amplitude coefficients

$f(\theta, t)$——excited vibration force

$F(\theta)$—— spatial function of the exciting vibration force

k ——number of harmonics of exciting force

l ——order of the Fourier series

m, n, r ——order of vibrational mode (nodal diameter no. of vibration mode)

$m_s(\theta), k_s(\theta), c_s(\theta), d_s(\theta)$— distributed mass, stiffness, stiffness of connecting and damping

$p(\theta), q(\theta)$—local frequencies of blade and connecting part

p_0, q_0——average values of aforementioned local frequencies

$P(\theta), Q(\theta), M(\theta)$— random functions of distribution stiffness, connecting part stiffness, mass parameters

$\sigma_p, \sigma_q, \sigma_m$—standard deviations of above random functions

f, g, h —Fourier coefficients of above random functions

$x(\theta, t)$—displacement

ξ, η, ζ — small parameters

$X(\theta) = y(\theta) + \xi u(\theta) + \eta v(\theta) + \zeta w(\theta)$——vibration mode function

$\omega^2 = \lambda^2 + \xi\mu^2 + \eta\nu^2 + \zeta\rho^2$—— natural frequency

$k\Omega$—exciting force frequency

$\alpha, \beta, \gamma, \delta$ — phase angles
ε — damping coefficient
θ, τ — spatial coordinates

*received October 1981

I. INTRODUCTION

The blades of a turbine are usually connected into a group. Sometimes through the use of various types of connecting parts, such as black crows, belts, shoulders, elastics, it is possible to circumferentially close the blades of the turbine disk to form a group. This type of circumferentially closely connected blade group has certain advantages in avoiding resonance. With regard to the vibration of such a structure, references [1-3] presented a method to calculate its vibrational characteristics under the assumption that all the blades had the same vibrational characteristics. In addition, a "triple point" condition for creating resonance on the rotating disk turbine blade group was also proposed. This means that resonance only occurs when (1) the exciting force frequency $k\Omega$ is equal to the natural frequency ω_m of the group of blades (i.e., $k\Omega = \omega_m$) and (2) the excitating force harmonic number k is equal to the nodal diameter number m of the natural vibration mode of the blade group (i.e., k = m). This conclusion could only be obtained under the assumption that the mechanical properties of all the blades and connectors were identical. However, in reality, it is unavoidable to have fabrication deviations between blades and their mechanical properties cannot be completely identical. Therefore, the above conclusion needs some correction. The purpose of this paper is to explore the effect of fabrication deviations of the blades on the vibration of the blade group.

In order to simplify the analysis, we chose the condition under which the blade distribution on the turbine was very dense as the limiting case. The closed loop with lateral spring support was selected as an approximate mechanical model to obtain a differential equation with random parameters.

In the random vibration problem, when the parameters on the left side of the differential equation are defined quantities and only the right side is a random function of time, this type of problem has been studied extensively in the literature with matured results. However, with regard to a dynamic structure system with random parameters, there is not too much available in the literature. Furthermore, there is a lack of a general treatment method. References [4] and [5] used a perturbation method to study the free vibration of a column beam with random structural parameters. The self-correlation and mutual correlation functions of random structural parameters in this paper were given manually in an exponential function form.

This paper discusses the free and forced vibrations of the aforementioned closed loop. First, by assuming that the standard deviations of the random structural parameters are infinitesimal quantities, a perturbation method is applied to obtain the solutions. By considering that the closed structure treated is a periodic structure, this paper proposes to use a spectral method to find the solutions. The random structural parameters are expanded into Fourier series to enable the solution of the differential equation to be expressed in terms of the Fourier coefficients of the structural parameters in order to obtain the natural frequencies, natural vibration modes, resonance amplitude and its square deviation estimation of the structure. The results of examples showed that the analyzed results were in the same order of magnitude as the experimental results obtained in [6,7].

II. BASIC EQUATIONS

The mechanical nodel discussed in this paper is a closed loop with lateral spring support (see Figure 1). The differential equation of motion is

$$m_0\frac{\partial^2 x}{\partial t^2}+k_0 x-\frac{\partial}{\partial\theta}\left(c_0\frac{\partial x}{\partial\theta}\right)+d_0\frac{\partial x}{\partial t}=f(\theta,t) \qquad (1)$$

the boundary condition is

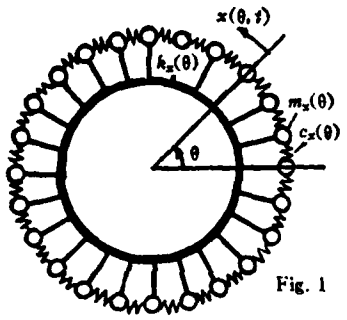

Fig. 1 Mechanical model

$$x(-\pi, t)=x(\pi, t),\ \left.\frac{\partial x}{\partial \theta}\right|_{(-\pi,\ t)}=\left.\frac{\partial x}{\partial \theta}\right|_{(\pi,\ t)} \tag{2}$$

the initial condition is

$$x(\theta, 0)=x_0(\theta),\ \left.\frac{\partial x}{\partial t}\right|_{(\theta,\ 0)}=\dot{x}_0(\theta) \tag{2'}$$

Let us assume that the system undergoes a harmonic oscillation under a harmonic exciting force. Let m_{xo} be the average value of the mass function; and the exciting force be

$$f(\theta, t)=m_{x_0}F(\theta)e^{i\omega t} \tag{3}$$

The solution to the differential equation (1) is

$$x(\theta, t)=X(\theta)e^{i\omega t} \tag{3'}$$

By introducing the symbols:

$$p^2(\theta)=\frac{k_x(\theta)}{m_{x_0}};\ q^2(\theta)=\frac{c_x(\theta)}{m_{x_0}};\ \varepsilon=\frac{d_x}{m_{x_0}} \tag{4}$$

then we can obtain the differential equation of the vibration mode from the partial differential equation (1) as

$$-\frac{d}{d\theta}\left(q^2\frac{dX}{d\theta}\right)+\left(p^2-\frac{m_x}{m_{x_0}}\omega^2\right)X+i\varepsilon\omega X=F(\theta) \tag{5}$$

The boundary condition is

$$X(-\pi)=X(\pi),\ X'(-\pi)=X'(\pi)$$

III. THE RANDOM STRUCTURAL PARAMETERS

Due to the fabrication deviation which exists in reality, the structural parameters $m_x(\theta)$, $k_x(\theta)$ and $c_x(\theta)$ are generally not constants. Instead, they are random functions oscillating around some constant values. Also because what is discussed here is a closed structure, these functions are also periodic functions. Parameters $p^2(\theta)$ and $q^2(\theta)$ are also periodic random functions oscillating around

their average values p_0^2 and q_0^2. For simplicity in this paper we assumed that the damping is a constant.

Let us assume that the scatter of a structural parameter is an infinitesimal quantity. Then these parameters can be expressed through the use of small parameters ξ, η, ζ as follows:

$$\begin{aligned} p^2(\theta) &= p_0^2[1+\xi P(\theta)] \\ q^2(\theta) &= q_0^2[1+\eta Q(\theta)] \\ m_z(\theta) &= m_{z_0}[1+\zeta M(\theta)] \end{aligned} \tag{6}$$

where $P(\theta)$, $Q(\theta)$ and $M(\theta)$--are periodically stable random processes with zero average values. We defined their square deviations to be 1. They satisfy the following periodic conditions:

$$\begin{aligned} P(-\pi) &= P(\pi),\ Q(-\pi) = Q(\pi) \\ Q'(-\pi) &= Q'(\pi),\ M(-\pi) = M(\pi) \end{aligned} \tag{6'}$$

In the following, we used the periodicities of these functions to expand these functions into Fourier series using the spectral method:

$$\begin{aligned} P(\theta) &= \sum_{l=-\infty}^{\infty} f_l e^{il\theta} \\ Q(\theta) &= \sum_{l=-\infty}^{\infty} g_l e^{il\theta} \\ M(\theta) &= \sum_{l=-\infty}^{\infty} h_l e^{il\theta} \end{aligned} \tag{7}$$

53

where $f_{-l}=f_l^*$; $g_{-l}=g_l^*$; $h_{-l}=h_l^*$ are the random Fourier coefficients. * represents the complex conjugate.

Let us assume that the random processes $P(\theta)$, $Q(\theta)$ and $M(\theta)$ are ergodic processes and their self-correlation functions can be obtained as follows:

$$\begin{aligned} R_p(\tau) &= E[P(\theta)P(\theta+\tau)] = \frac{1}{2\pi}\int_{-\pi}^{\pi} \sum_{l=-\infty}^{\infty} f_l e^{il\theta} \sum_{l'=-\infty}^{\infty} f_{l'} e^{il'(\theta+\tau)} d\theta \\ &= \sum_{l=-\infty}^{\infty} f_l f_l^* (e^{il\tau} + e^{-il\tau}) = 2\sum_{l=1}^{\infty} |f_l|^2 \cos l\tau \end{aligned} \tag{8}$$

When $\tau = 0$, the self-correlation function is equal to the square deviation. Furthermore, we have already defined the square deviation of $P(\theta)$ to be 1, therefore,

$$R_p(0) = 2\sum_{l=1}^{\infty} |f_l|^2 = 1 \tag{8'}$$

Similarly, we could obtain $R_q(\tau)$ and $R_m(\tau)$.

Let us assume that the standard deviations of the random processes $P(\theta)$, $Q(\theta)$ and $M(\theta)$ are σ_p, σ_q and σ_m, respectively. Then, from the above analysis, we know that the small parameters ξ, η and ζ are equal to these standard deviations, respectively, i.e.,

$$\xi=\sigma_p,\ \eta=\sigma_q,\ \zeta=\sigma_m \tag{9}$$

From equations (8) and (8'), we can see that the Fourier coefficients such as $|f_1|$ of a stable ergodic random function such as $P(\theta)$ can be determined. In fact, from equation (8'), we can see that: $|f_l|\leqslant 0.707\ (l=1,2,\cdots)$. Furthermore, with regard to a defined structure, the self-correlation function $R_p(\tau)$ can be experimentally obtained. As long as $R_p(\tau)$ is known, then the numerical value of $|f_1|$ can be obtained from equation (8).

In [4], the self-correlation function was artificially assumed to have the following form:

$$R_p(\tau)=e^{-\alpha|\tau|} \tag{10}$$

when the parameters α could be determined in combination with the experimental results. From the known equation (10), it is also possible to determine the actual numerical value of $|f_1|$.

IV. FREE VIBRATION

In the differential equation (5), when the exciting force is zero and damping is neglected, we get

$$-(q^2X')'+\left(p^2-\frac{m_x}{m_{x_0}}\omega^2\right)X=0 \tag{11}$$

The boundary conditions are

$$X(-\pi)=X(\pi),\ X'(-\pi)=X(\pi) \tag{11'}$$

By considering the randomness of the structural parameters, q, p and m_x, and by substituting equation (6) into (11), we get

$$-q_0^2[(1+\eta Q)X']'+[p_0^2(1+\xi P)-\omega^2(1+\zeta M)]X=0 \tag{12}$$

The obtained equation (12) is the free vibration differential equation of a periodic random parametric system. Because the variations of the random parameters are infinitesimal quantities and the differential equation contains small parameters ξ, η, ζ, it is possible to find its solution using a perturbation method. For this purpose, the frequencies and vibration modes are expressed as power series of the small parameters ξ, η, and ζ. As a first order approximation, let us keep the first order terms of these small parameters:

$$\omega^2=\lambda^2+\xi\mu^2+\eta\nu^2+\zeta\rho^2+\cdots\cdots$$
$$X(\theta)=y(\theta)+\xi u(\theta)+\eta v(\theta)+\zeta w(\theta)+\cdots\cdots \tag{13}$$

By substituting them into equation (12), neglecting higher order infinitesimal quantities, and making the coefficients of the small parameters ξ, η, ζ zero, we get the following equations:

54

$$\left.\begin{aligned}
&-q_0^2y''+(p_0^2-\lambda^2)\,y=0\\
&-q_0^2u''+(p_0^2-\lambda^2)\,u=-(p_0^2P-\mu^2)\,y\\
&-q_0^2v''+(p_0^2-\lambda^2)\,v=q_0^2(Qy''+Q'y')+\nu^2y\\
&-q_0^2w''+(p_0^2-\lambda^2)\,w=(\lambda^2M+\rho^2)\,y
\end{aligned}\right\} \tag{14}$$

The first equation in (14) is a well defined equation. By using the boundary conditions to solve this differential equation, we obtain the frequency λ_m^2 as

$$\lambda_m^2=p_0^2+m^2q_0^2 \tag{15}$$

where m is an integer and its physical meaning is the nodal diameter number of the vibration mode. The vibration mode $y_m(\theta)$ is

$$y_m(\theta)=A_me^{im\theta}+A_m^*e^{-im\theta} \tag{16}$$

where A_m and A_m^* are conjugating coefficients to be determined. We can formulate the vibration modes in such a way so that these coefficients can be determined. Considering the following orthogonal conditions:

$$\int_{-\pi}^{\pi} y_m(\theta)\,y_n(\theta)\,d\theta=\delta_{mn}=\begin{cases}1 & \text{when } m=n\\ 0 & \text{when } m\neq n\end{cases} \tag{17}$$

From this we get

$$A_mA_m^*=|A_m|^2=\frac{1}{4\pi} \tag{18}$$

The second equation (14) contains random variables. In order to solve this differential equation, we expanded the function $u_m(\theta)$ to be obtained according to the vibration mode $y_r(\theta)$ by letting

$$u_m(\theta) = \sum_{r=1}^{\infty} b_{m,r} y_r(\theta) \tag{19}$$

Substituting it into the original function multiplying $y_n(\theta)$ on both sides of the equation, and integrating, we obtain the following by using the orthogonality condition:

$$q_0^2(m^2-n^2)b_{mn} + \mu_m^2 b_{mn} = p_0^2 \int_{-\pi}^{\pi} P y_m y_n d\theta \tag{20}$$

when m = n, the frequency μ_m^2 obtained from equation (20) is

$$\mu_m^2 = p_0^2 \int_{-\pi}^{\pi} P y_m^2 d\theta = 2\pi p_0^2 (f_{2m} A_m^{*2} + f_{2m}^* A_m^2) \tag{21}$$

where the values of A_m and A_m^* can be given from equation (18) and f_{2m} and f_{2m}^* from equation (7). Let us assume

$$A_m = |A_m| e^{i\alpha_m}; \quad f_{2m} = |f_{2m}| e^{i\beta_{2m}}$$

then

$$\mu_m^2 = p_0^2 |f_{2m}| \cos(\beta_{2m} - 2\alpha_m) \tag{21'}$$

When m ≠ n, the coefficient b_{mn} of the vibration mode can be obtained from equation (20) as

$$b_{mn} = -b_{nm} = \frac{1}{m^2-n^2} \frac{p_0^2}{q_0^2} \int_{-\pi}^{\pi} P y_m y_n d\theta \tag{22}$$

Therefore,

$$u_m(\theta) = \sum_{\substack{n=1 \\ n \neq m}}^{\infty} b_{mn} y_n(\theta) \tag{23}$$

Following a similar method as in the previous section, we can obtain solutions for the third and fourth equations in (14) and the frequency obtained is:

$$\begin{aligned} \nu_m^2 &= q_0^2 \int_{-\pi}^{\pi} Q y_m'^2 d\theta = -q_0^2 m^2 |g_{2m}| \cos(\gamma_{2m} - 2\alpha_m) \\ \rho_m^2 &= -\lambda_m^2 \int_{-\pi}^{\pi} M y_m^2 d\theta = -\lambda_m^2 |h_{2m}| \cos(\delta_{2m} - 2\alpha_m) \end{aligned} \tag{24}$$

where $A_m = |A_m| e^{i\alpha_m}; \; g_{2m} = |g_{2m}| e^{i\gamma_{2m}}; \; h_{2m} = |h_{2m}| e^{i\delta_{2m}}$.

The expressions of the vibration modes are:

$$\left.\begin{aligned} v_m(\theta) &= \sum_{\substack{n=1 \\ n\neq m}}^{\infty} c_{mn} y_n(\theta) \\ w_m(\theta) &= \sum_{\substack{n=1 \\ n\neq m}}^{\infty} d_{mn} y_n(\theta) \end{aligned}\right\} \tag{25}$$

Furthermore

$$c_{mn} = -c_{nm}, \quad d_{mn} = -d_{nm} \tag{26}$$

V. THE NATURAL FREQUENCY, ITS AVERAGE AND SQUARE DEVIATION

The natural frequencies of various orders of the system can be obtained by combining equations (13), (15), (21) and (24). The natural frequency of m^{th} order of the system is:

$$\begin{aligned} \omega_m^2 &= \lambda_m^2 + \xi\mu_m^2 + \eta\nu_m^2 + \zeta\rho_m^2 \\ &= (p_0^2 + m^2 q_0^2) + \xi p_0^2 \int_{-\pi}^{\pi} P y_m^2 \, d\theta + \eta q_0^2 \int_{-\pi}^{\pi} Q y_m'^2 \, d\theta - \zeta\lambda_m^2 \int_{-\pi}^{\pi} M y_m^2 d\theta \\ &= (p_0^2 + m^2 q_0^2) + \xi p_0^2 |f_{2m}| \cos(\beta_{2m} - 2\alpha_m) - \eta m^2 q_0^2 |g_{2m}| \cos(\gamma_{2m} - 2\beta_m) \\ &\quad - \zeta (p_0^2 + m^2 q_0^2) |h_{2m}| \cos(\delta_{2m} - 2\alpha_m) \end{aligned} \tag{27}$$

In searching for the average value of the natural frequency, we have to consider that the average values of the functions P, Q and M are zero:

$$E[P(\theta)] = 0, \quad E[Q(\theta)] = 0, \quad E[M(\theta)] = 0$$

Hence, the average value of the natural frequency ω_m^2 is:

$$\begin{aligned} E[\omega_m^2] &= E[\lambda_m^2] + \xi p_0^2 \int_{-\pi}^{\pi} E[P(\theta)] \, y_m^2 d\theta + \eta q_0^2 \int_{-\pi}^{\pi} E[Q(\theta)] y_m'^2 d\theta \\ &\quad - \zeta\lambda_m^2 \int_{-\pi}^{\pi} E[M(\theta)] \, y_m^2 d\theta = \lambda_m^2 \end{aligned} \tag{28}$$

The average square value of the natural frequency ω_m^2 can be estimated in the following:

$$\begin{aligned} E[(\omega_m^2)^2] &= E[(\lambda_m^2)^2] + \xi^2 p_0^4 \int_{-\pi}^{\pi}\int_{-\pi}^{\pi} E[P(\theta_1)P(\theta_2)] y_m^2(\theta_1) y_m^2(\theta_2) d\theta_1 d\theta_2 \\ &\quad + \eta^2 q_0^4 \int_{-\pi}^{\pi}\int_{-\pi}^{\pi} E[Q(\theta_1)Q(\theta_2)] y_m'^2(\theta_1) y_m'^2(\theta_2) d\theta_1 d\theta_2 \\ &\quad + \zeta^2 \lambda_m^4 \int_{-\pi}^{\pi}\int_{-\pi}^{\pi} E[M(\theta_1)M(\theta_2)] y_m^2(\theta_1) y_m^2(\theta_2) d\theta_1 d\theta_2 \\ &\quad + 2\xi\eta \, p_0^2 q_0^2 \int_{-\pi}^{\pi}\int_{-\pi}^{\pi} E[P(\theta_1)Q(\theta_2)] y_m^2(\theta_1) y_m'^2(\theta_2) d\theta_1 d\theta_2 \\ &\quad + 2\xi\zeta \, p_0^2 \lambda_m^2 \int_{-\pi}^{\pi}\int_{-\pi}^{\pi} E[P(\theta_1)M(\theta_2)] y_m^2(\theta_1) y_m^2(\theta_2) d\theta_1 d\theta_2 \end{aligned}$$

$$+2\eta\zeta q_0^2\lambda_m^2\int_{-\pi}^{\pi}\int_{-\pi}^{\pi}E[Q(\theta_1)M(\theta_2)]y_m'^2(\theta_1)y_m^2(\theta_2)d\theta_1 d\theta_2$$

$$+2\lambda_m^2\left\{\xi p_0^2\int_{-\pi}^{\pi}E[P(\theta)]y_m^2(\theta)d\theta+\eta q_0^2\int_{-\pi}^{\pi}E[Q(\theta)]y_m'^2(\theta)d\theta\right.$$

$$\left.-\zeta\lambda_m^2\int_{-\pi}^{\pi}E[M(\theta)]y_m^2(\theta)d\theta\right\} \tag{29}$$

The square deviation of the natural frequency is:

$$\begin{aligned}\sigma_{\omega_m}^2=E[(\omega_m^2)^2]-\lambda_m^4=\frac{1}{2}\{&\xi^2p_0^4|f_{2m}|^2+\eta^2m^4q_0^4|g_{2m}|^2+\zeta^2\lambda_m^4|h_{2m}|^2\\&-2\xi\eta p_0^2q_0^2m^2|f_{2m}||g_{2m}|\cos(\beta_{2m}-\gamma_{2m})\\&-2\xi\zeta p_0^2\lambda_m^2|f_{2m}||h_{2m}|\cos(\beta_{2m}-\delta_{2m})\\&+2\eta\zeta m^2q_0^2\lambda_m^2|g_{2m}||h_{2m}|\cos(\gamma_{2m}-\delta_{2m})\}\end{aligned} \tag{30}$$

The above equation indicates that the standard deviation of the natural frequency is the vector sum of the three following vectors (Figure 2):

$$\xi p_0^2 f_{2m}\quad -\eta m^2 q_0^2 g_{2m}\quad -\zeta\lambda_m^2 h_{2m} \tag{31}$$

The standard deviation of the natural frequency can be estimated by the following approximation:

$$\sigma_{\omega_m}^2\leqslant\xi p_0^2|f_{2m}|+\eta m^2q_0^2|g_{2m}|+\zeta\lambda_m^2|h_{2m}| \tag{32}$$

We can see that the standard deviation σ_ω^2 of the natural frequency is on the same order of magnitude as the small infinitesimal quantities ξ, η, ζ, which is an infinitesimal quantity on the same order of magnitude as the standard deviations σ_p, σ_q, σ_m of local frequency scatter.

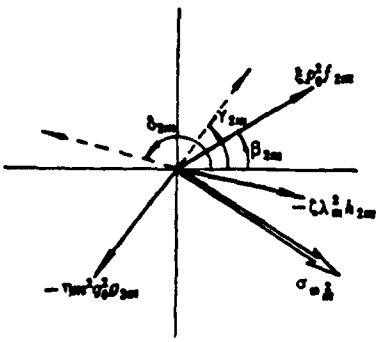

Fig. 2 Standard deviations of natural frequencies

AD-A127 840 ACTA AERONAUTICA ET ASTRONAUTICA SINICA(U) FOREIGN TECHNOLOGY DIV WRIGHT-PATTERSON AFB OH Y ZHENG ET AL. 04 MAR 83 FTD-ID(RS)T-1605-82 2/2

UNCLASSIFIED F/G 20/4 NL

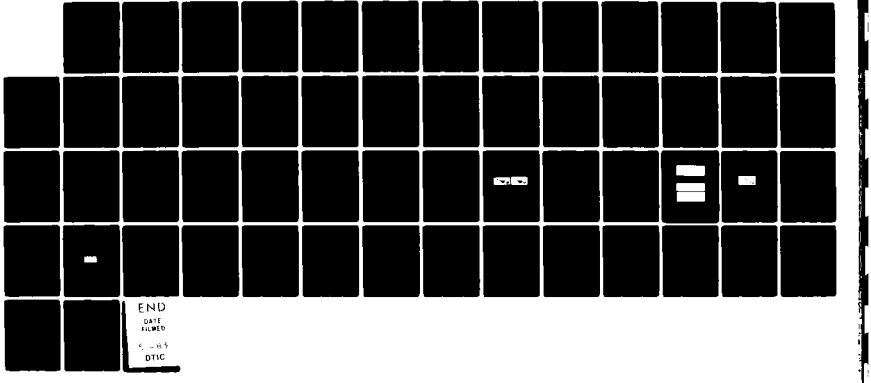

END
DATE FILMED
DTIC

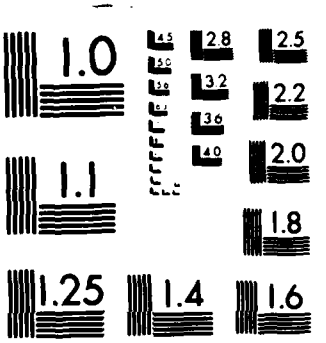

VI. NATURAL VIBRATION MODE AND ITS PHASE ANGLE

The vibration modes of various orders of the system can be obtained by combining equations (13), (16), (23) and (25). The m^{th} order natural vibration mode is

$$\begin{aligned} X_m(\theta) &= y_m(\theta)+\xi u_m(\theta)+\eta v_m(\theta)+\zeta w_m(\theta) \\ &= y_m(\theta)+\sum_{\substack{n=1 \\ n\neq m}}^{\infty}(\xi b_{mn}+\eta c_{mn}+\zeta d_{mn})y_n(\theta) \end{aligned} \tag{33}$$

Due to the complexity of the vibration mode expression (33), we can see that the nodal diameter of the vibration mode is changing from a symmetric distribution to an asymmetric distribution (Figure 3).

57

It can be proven that the vibration mode (33) satisfies the orthogonality condition:

$$\int_{-\pi}^{\pi} X_m X_{m'}\, d\theta = \delta_{mm'} = \begin{cases} 1 & \text{when } m=m' \\ 0 & \text{when } m\neq m' \end{cases} \tag{34}$$

As for the phase angle α_m of the natural vibration mode, when the structural parameters are constant, the phase angle α_m is a value to be determined by the initial condition. When the structural parameters are not constants but random quantities, the natural vibration mode phase angle α_m is determined by the variations of the structural parameters $P(\theta)$, $Q(\theta)$ and $M(\theta)$ and is not related to the initial condition.

In fact, in solving for the latter three equations in (14), the right hand side of the equation should not contain a "long term" term with spatial frequency m. Otherwise, a solution which increases with time will be found which is not rational.

In order to make sure that the solution $X_m(\theta)=y_m+\xi u_m+\eta v_m+\zeta w_m$ does not contain any term which increases with time, we must let the coefficients of the following equation be zero:

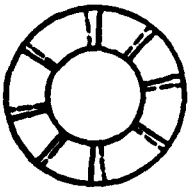

Fig. 3 Nodal diameters of natural modes (m = 3)
----symmetrical; ——asymmetrical.

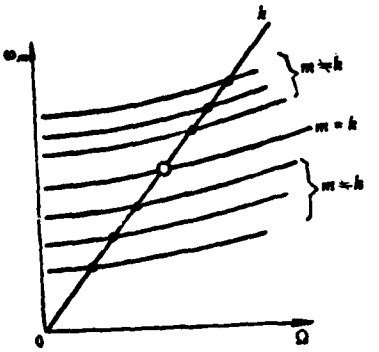

Fig. 4 Campbell diagram
○——violent resonance; ●——weak resonance.

$$\frac{1}{\sqrt{\pi}}\left\{-\frac{\xi p_0^2}{q_0^2}|f_{2m}|\sin(\beta_{2m}-2\alpha_m)+\eta m^2|g_{2m}|\sin(\gamma_{2m}-2\alpha_m)\right.$$
$$\left.+\zeta\lambda_m^2|h_{2m}|\sin(\delta_{2m}-2\alpha_m)\right\}\sin(m\theta+\alpha_m)=0$$

After expansion, we can obtain the formula to calculate the phase angle of the vibration mode:

$$\operatorname{tg}2\alpha_m=\frac{-\xi p_0^2|f_{2m}|\sin\beta_{2m}+\eta m^2 q_0^2|g_{2m}|\sin\gamma_{2m}+\zeta\lambda_m^2|h_{2m}|\sin\delta_{2m}}{-\xi p_0^2|f_{2m}|\cos\beta_{2m}+\eta m^2 q_0^2|g_{2m}|\cos\gamma_{2m}+\zeta\lambda_m^2|h_{2m}|\cos\delta_{2m}} \qquad (35)$$

VII. FORCED VIBRATION

In equation (1), let us assume that the exciting force $f(\theta,t)$ contains many harmonics:

$$f(\theta,t)=\sum_{k=1}^{\infty}f_k(\theta,t)=\sum_{k=1}^{\infty}m_{z_0}F_k(\theta)e^{ik\Omega t} \qquad (36)$$

Now, let us only consider the k^{th} harmonic of the exciting force, i.e., on the right hand side of equation (1) we only take

$$f_k(\theta,t)=m_{z_0}F_k(\theta)e^{ik\Omega t} \qquad (37)$$

For the convenience of writing without losing the generality, let us assume that the spatial distribution of the exciting force and the k^{th} harmonic of the vibration mode have the same phase angle, which is to assume that

$$F_k(\theta)=F_k y_k(\theta) \qquad (38)$$

Let us assume the special solution to the differential equation (1), i.e., the forced vibration is

$$x(\theta, t) = X(\theta)e^{i k\Omega t} \tag{39}$$

Substituting it into equation (1), we obtain the differential equation of forced vibration as

$$-(q^2X')' + \left[p^2 - \frac{m_x}{m_{x_0}}(k\Omega)^2\right]X + i\varepsilon k\Omega X = F_k y_k(\theta) \tag{40}$$

In the following, in order to simplify the derivation, let us assume $m_x(\theta) = m_{x0} = \text{const}$ which is to neglect the nonuniformity of mass distribution by assuming $\xi M(\theta) = 0$.

Let us assume that the solution to the differential equation (40) can be expressed as the sum of the various orders of natural vibration modes:

$$X(\theta) = \sum_{m=1}^{\infty} a_m X_m(\theta) \tag{41}$$

58

where the natural mode $X_m(\theta)$ can be found in equation (33). Substitute equation (41) into the differential equation (40). Multiply both sides by $X_m(\theta)$ and then integrate. By using the orthogonality condition (17) and neglecting higher orders of the infinitesimal amounts, we get

$$(\omega_m^2 - (k\Omega)^2 + i\varepsilon k\Omega)a_m = \begin{cases} F_k & (\text{when } m = k) \\ F_k(\xi b_{m,k} + \eta c_{m,k}) & (\text{when } m \neq k) \end{cases} \tag{42}$$

VIII. RESONANCE AMPLITUDE AND ITS AVERAGE AND SQUARE DEVIATION

The following is a consideration of the resonance amplitude. Please refer to the Campbell diagram in Figure 4.

(1) when the "triple point" condition is satisfied, i.e., when $\omega_m = k\Omega$ and m = k, from equation (42):

$$a_{m_0} = \frac{F_k}{i\varepsilon k\Omega} \tag{43}$$

This is the quantity of a defined mode. Under small damping conditions, the amplitude is very large and a very intense resonance is obtained.

(2) when the "triple point" condition is not satisfied, i.e., when $\omega_m = k\Omega$, but m ≠ k. From equation (42):

$$|a_m| = \frac{F_k}{\varepsilon k\Omega}(\xi b_{m-k} + \eta c_{m-k}) \tag{44}$$

At this time, the average of the vibration amplitude is zero:

$$E(|a_m|) = \frac{F_k}{2\pi\varepsilon k\Omega}\frac{1}{m^2-k^2}\int_{-\pi}^{\pi}\left\{\xi\frac{p_0^2}{q_0^2}E[P(\theta)]y_m y_k + \eta E[Q(\theta)]y'_m y'_k\right\}d\theta = 0 \tag{45}$$

The square deviation of the resonance amplitude is

$$\sigma_a^2 = E(|a_m|^2) = \frac{F_k^2}{2\pi(\varepsilon k\Omega)^2}\frac{1}{(m^2-k^2)^2}$$

$$\times\left\{\xi^2\frac{p_0^4}{q_0^4}\int_{-\pi}^{\pi}\int_{-\pi}^{\pi}E[P(\theta_1)Q(\theta_2)]y_m(\theta_1)y_k(\theta_1)y_m(\theta_2)y_k(\theta_2)d\theta_1 d\theta_2\right. \tag{59}$$

$$+\eta^2\int_{-\pi}^{\pi}\int_{-\pi}^{\pi}E[Q(\theta_1)Q(\theta_2)]y'_m(\theta_1)y'_k(\theta_1)y'_m(\theta_2)y'_k(\theta_2)d\theta_1 d\theta_2$$

$$\left.+2\xi\eta\frac{p_0^2}{q_0^2}\int_{-\pi}^{\pi}\int_{-\pi}^{\pi}E[P(\theta_1)Q(\theta_2)]y_m(\theta_1)y_k(\theta_1)y'_m(\theta_2)y'_k(\theta_2)d\theta_1 d\theta_2\right\} \tag{46}$$

The calculated results are:

$$\sigma_a = \frac{F_k^2}{2(m^2-k^2)^2(\varepsilon k\Omega)^2}\left\{\xi^2\frac{p_0^4}{q_0^4}|f_{m-k}|^2 + \eta^2 m^4|g_{m-k}|^2\right.$$

$$-2\xi\eta m^2\frac{p_0^2}{q_0^2}|f_{m-k}||g_{m-k}|\cos(\beta_{m-k}-\gamma_{m-k}) + \xi^2\frac{p_0^4}{q_0^4}|f_{m-k}|^2 \tag{47}$$

$$\left.+\eta^2 m^4|g_{m-k}|^2 + 2\xi\eta m^2\frac{p_0^2}{q_0^2}|f_{m-k}||g_{m-k}|\cos(\beta_{m-k}-\gamma_{m-k})\right\}$$

From the above complicated expression, we can see that the ratio of the standard deviation σ_α of the resonance amplitude and the resonance amplitude $|a_{m0}|$ under the triple point condition can be considered as the vector sum of the following vectors (Figure 5):

$$\xi\frac{p_0^2}{q_0^2}f_{m-k},\ \eta m^2 g_{m-k},\ \xi\frac{p_0^2}{q_0^2}f_{m-k},\ \eta m^2 g_{m-k} \tag{48}$$

This can be estimated approximately using the following equation:

$$\frac{\sigma_a}{|a_{m_0}|} < \left\{\left(\xi\frac{p_0^2}{q_0^2}|f_{m-k}| + \eta m^2|g_{m-k}|\right)^2 + \left(\xi\frac{p_0^2}{q_0^2}|f_{m-k}| + \eta m^2|g_{m-k}|\right)^2\right\}^{1/2} \tag{49}$$

From this we can see that this ratio is on the same order of magnitude as the small parameters ξ, η and the standard deviation σ_p, σ_q of the scatter of the local frequencies.

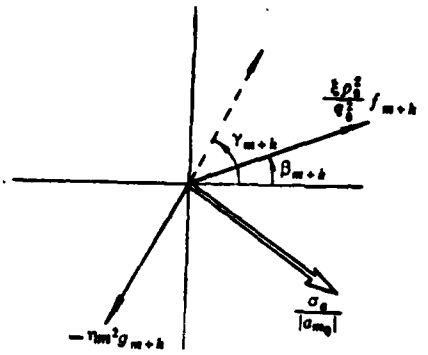

Fig. 5 Square deviations of resonance amplitude

IX. EXAMPLE

With respect to the mechanical model shown in Figure 1, let us choose the local frequency as:

$$p_0 = 110 \times 2\pi, \quad q_0 = 22 \times 2\pi$$

Usually, a turbine machinery factory establishes that the frequency scatter of the blades on a turbine cannot exceed ±4%. Now, let us take 1/3 of this value as the standard deviation of the frequency scatter, i.e.,

$$\xi = \eta = \sigma_p = \sigma_q = \frac{0.04}{3} = 0.01333$$

Assuming that the self-correlation function of the random structural parameters has the form of that of equation (10), let us also choose $\alpha = 1$. Using equation (49), let us calculate the extremes of the ratio of the standard deviation σ_n of resonance amplitude and the resonance amplitude $|a_{m0}|$ under the triple point conditions at various orders of harmonics k of the exciting force, and different main vibration mode nodal diameter numbers m are shown in Table 1. 60

From Table 1, we can see that, under the condition of the main mode with no nodal diameter (m = 0) and the first order harmonic exciting force (k = 1), $\sigma_n / |a_{m_0}| \leqslant 13.58\%$ Under other conditions,

Table 1 Limit values of ratio $\sigma_s/|\sigma_{m_0}|$

harmonic number	nodal diameter no. $m=0$	$m=1$	$m=2$	$m=3$	$m=4$
$k=0$	1	0.1413	0.0239	0.0092	0.0046
$k=1$	0.1358	1	0.0467	0.0112	0.0055
$k=2$	0.0206	0.0365	1	0.0271	0.0085
$k=3$	0.0067	0.0086	0.0231	1	0.0229
$k=4$	0.0028	0.0035	0.0060	0.0190	1
$k=5$	0.0015	0.0016	0.0026	0.0051	0.0177
$k=6$	0.0008	0.0010	0.0013	0.0023	0.0046

this ratio is extremely small which can be neglected. References [6-7] have reported the experimental results on the machine. They believed that the resonance amplitude of a circumferentially connected blade group was approximately $\frac{1}{10}$ -$\frac{1}{7}$ of the resonance amplitude of free blade. This result is on the same order of magnitude as the calculated result based on the above model.

X. CONCLUSIONS

1. For a periodic dynamic system with random structural parameters, to use a spectral method to find the solution is a feasible and convenient method. The random functions of the structural parameters are expanded into Fourier series to facilitate the calculation of the natural frequency, natural mode and resonance amplitude of the system, and to estimate their average values and the square deviations.

2. The analytical calculation with regard to a periodic dynamic system with random structural parameters indicated that its vibration characteristics have some special features different from those of a uniform periodic structure.

(1) the natural frequencies of various orders of a uniform structure are fixed quantities, while those of a random structure are random quantities. The standard deviation of the m^{th} order natural frequency is only related to the $2m^{th}$ order Fourier coefficient of the random parameter. Furthermore, it is the vector sum of the standard deviations of several deviations.

(2) the natural vibration modes of a uniform structure are of harmonic waveforms and all the nodal diameters are uniformly distributed. For a random structure, in addition to the harmonic waveforms of the natural frequencies of the various orders, there are various orders of harmonic waves with complicated shapes and uneven nodal diameter distribution. However, all the natural vibration modes satisfy the orthogonality condition.

(3) the phase angles of the natural modes of a uniform structure are parameters to be determined by the initial condition. However, the phase angles of the vibration modes of a random structure are related to the respective structural parameters which are not related to the initial condition.

(4) for a uniform structure, the "triple point" condition must be satisfied to create resonance. Under the condition that the "triple point" condition is not satisfied, it is impossible to create resonance. For a random structure, when the "triple point" condition is satisfied, very strong resonance will be created. However, even when the "triple point" condition is not satisfied, as long as $\omega_m = k\Omega$, even though $k \neq m$, it will create a weak resonance. In this paper we estimated the square deviation of the weak resonance amplitude. This square deviation is related to certain orders of the Fourier coefficients of the structural parameters.

REFERENCES

[1] Huang Wenhu, Zhao Yuchang, Den Lianchao. "The Analysis of Vibration of a Circumferentially connected Blade Group". Harbin Turbine Factory, Technical Promotion Office, 1974.

[2] Huang Wen hu, Deng Lianchao, Zhao Yuchang. "The analysis of Vibration of one Kind of Periodic Structures". Journal of Harbin Institute of Technology, vol. 3, 1979, pp 11-30.

[3] Huang Wenhu. Free and Forced Vibrations of Closely Coupled Turbomachinery Blades, AIAA Journal, vol. 19, no. 7, July 1981.

[4] Hoshiya, M. and Shah, H. C. Free Vibration of Stochastic Beam-Column, EM. Div., ASCE, Aug. 1971.

[5] Sing Kushen. "Random Vibration Analysis". Earth Publications, 1977.

[6] Yampol'skaya, R.G., and Arkad'yev, D.A. Determination of the vibration Characteristics of the Blading with Damper Connections. Energomashchinostroyeniye, No. 11, 1965.

[7] Arkad'yev, D.A. Influence of Couplings on the Vibration Strength of Turbine Blades. Energomashchinostroyeniye, No. 3, 1968.

A SPECTRAL APPROACH FOR ANALYZING THE VIBRATION OF A PERIODIC STRUCTURE WITH RANDOM PARAMETERS

Huang Wenhu

(Harbin Institute of Technology)

Abstract

In a periodic structural system such as blades in a circumferentially closed packet on a disk of turbo-machinery, the natural frequencies of individual blades can be randomly different from one another. From this arises the problem of vibration analysis of a periodic structure with random parameters. There is lack of general method for solving the differential equations with random parameters. This paper describes a spectral approach for analyzing the vibration of a periodic structure with random parameters. Suppose the standard deviations of random structural parameters are small so that a perturbation method can be used to reduce the differential equation with several random parameters to several differential equations with one parameter, and then these differential equations may be solved one by one. Suppose the spatial distributions of the random structural parameters are ergodic, and for concrete structure these distribution functions and their correlation functions can be determined by experiments. It is suggested in this paper to expand these spatial distribution functions of random parameters into Fourier Series. And then the relation between these Fourier coefficients and the correlation functions is established so that these Fourier coefficients can be determined by several ways. In this situation, these differential equations with random parameters can be solved. Thus natural frequencies of the structure are then obtained, and their standard deviations are estimated. Also, the expressions of natural modes are given, the orthogonality of natural modes is proved, and it is shown that the phase angles of natural modes are not arbitrary. Finally the special conditions of resonance of periodic structure with random parameters are discussed. It is shown that a violent resonance occurs when the number of harmonic of exciting force is equal to the number of nodal diameters of natural modes, and only a weak resonance appears when these two numbers are not equal. This phenomenon does not exist in the case of structures with homogeneous parameters. The standard deviations of amplitudes of weak resonance are estimated, Numerical examples show that the calculated results have the same order as the experimental results in literature.

A NEW METHOD OF FINITE ELEMENT STRUCTURE DISCRETIZATION

Liang Guowei*
Northwestern Polytechnical University

ABSTRACT

In this paper, the iso-parametric element geometric interpolation method was used to automatically generate the nodal coordinates of all the elements based on a small amount of input data. A "chessboard" mesh was used to facilitate the numbering of elements and nodal points. Simultaneously, a "front solver" method was used to solve the equations to simplify the numbering program.

This method has the advantages of little input data, ease of changing the mesh and the sufficient accuracy of the boundary nodal coordinates. It has been used for the two dimensional mesh of an axial symmetric body and the three dimensional mesh of a turbine blade. The results were satisfactory.

I. INTRODUCTION

In the finite element calculation work, the work load for the preparation of input data is very large. It mainly involves the determination of nodal point coordinates and number. If these data are obtained manually, it is very easy to make mistakes. Therefore, this will cause difficulties in testing the program and wasting computer time. Hence, automatic discretization becomes an actual problem to be resolved in the finite element computation work.

In the references [1-4] both here and abroad in the 70's, various methods to automatically form meshes were discussed; which were limited to planar triangular elements.

As we all know, under the same nodal point number the accuracy of a rectangular element (or hexagonal element) is higher than that of a triangular or (tetrahedral) element. Therefore, it is very

*received October 1981

imperative to develop a rectangular iso-parametric element which is applicable to the automatic generation of two-dimensional and three dimensional meshes. Furthermore, in the aforementioned literature, the emphasis was focused on the automation of the division of the element and the formation of the nodal point coordinates. As for the automatic numbering of the nodal points and elements, it was seldom considered in connection with the storage problem. In some references [5-6], although some methods for renumbering the nodal points and reducing the bandwidth were proposed, yet such methods would complicate the program.

In 1978, the author proposed a method to automatically form the nodal point coordinate using an interpolation function [7] together with a "front solver" method to solve the linear equations by considering the convenience of automatic numbering of the nodal points. The numbers of the nodal points were allowed to be discontinuous to simplify the program as well as to save the internal storage. During the numbering of the elements, some programming techniques were used to minimize the "wave front". After the discretization of the mesh, a huge amount of data was required to be checked. Undoubtedly, it is very time consuming. This method displays these data using the method most convenient for checking which consequently saves a lot of time.

II. MAIN POINTS OF THIS METHOD.

1. Automatic formation of nodal point coordinates using the interpolation function

Usually, geometric interpolation is used in an iso-parametric element to transform a rectangular (or hexagonal) element into a curve (curved surface) element. The coordinates of an arbitrary point P of the curve (or curved surface) element can be obtained by the nodal coordinate interpolations of the elements:

$$\left.\begin{aligned} x &= \sum_i N_i(\xi, \eta, \zeta) \cdot x_i \\ y &= \sum_i N_i(\xi, \eta, \zeta) \cdot y_i \\ z &= \sum_i N_i(\xi, \eta, \zeta) \cdot z_i \end{aligned}\right\} \qquad \text{(A)}$$

where (x_i, y_i, z_i) is the coordinate of nodal point i, (ξ,η,ζ) is the local coordinate of the point P, and $N_i(\xi, \eta, \zeta)$ is the shape function corresponding to the nodal point i as shown in Figure 1.

Through the transformation, the original linear mesh (the iso ξ, iso η lines on the left of Figure 1) is transformed into the curve mesh (the iso ξ and iso η lines in the x-y coordinate system on the right of Figure 1). If this iso-parametric element is the component we want to analyze (or part of a component), then the large amount of nodal point coordinates in the mesh can be obtained by interpolating the small amount of original nodal coordinates (x_i, y_i, z_i) using equation (A).

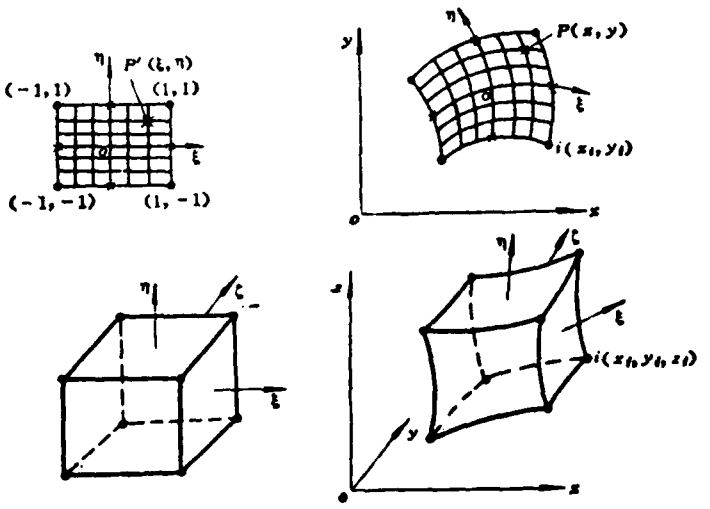

Fig. 1 2-and 3-dimensional iso-parametric elements

2. Actual procedures of nodal point coordinate interpolation

(1) Based on the boundary shape of the component, it is divided into several zones. For each zone, a proper parent element for each zone was chosen;

(2) in the body coordinate system, based on the boundary shape of the component, the nodal point coordinates (x_i, y_i, z_i) of the parent element was chosen;

(3) based on the degree of closeness of the discretized mesh, the local coordinates(ξ,η,ζ) of any nodal point on the parent element in the mesh in that zone are determined;

(4) from equation A), the coordinates (x,y,z) of all the nodal points of the mesh in that zone can be interpolated.

Now, let us use the disk in Figure 2 as an example to explain the above procedures.

First, based on the shape of the disk, let us divide it into 18 zones. The principle of zoning is that: a different boundary curve should be divided into two zones. For example, the a-b-c boundary in the figure, a-b is a line, b-c is a circular arc, then a-b-c should be divided at point b, and a-b is in zone 7 and b-c is in zone 8. 65

For each zone, a parent element is selected and its nodal points are determined by the boundary shape. For zone 7, the boundaries are straight lines and a four nodal point parent element is chosen (no. 1 in the figure) in order to ensure the accuracy of boundary interpolation. For zone 8, it is necessary to choose the no. 2 parent element to ensure the sufficient accuracy of the interpolated b-c boundary. The principle of selecting the parent element is that: under the premise of assurance of sufficient accuracy of boundary interpolation, the nodal points should be as few as possible in order to reduce the

input coordinate data. In the meantime, it should be ensured that the mesh in the neighboring zones is continuous.

Next, on the cross-section of the disk, the nodal point coordinates (R_i, z_i) in this zone are determined based on the nodal point distribution of the selected parent elements in each zone. For corner nodal points, their coordinates are fixed. As for nodal points located on the side, there is room for selection. The numbers and positions of the middle line nodal points would affect the error of the interpolated boundary curve greatly. Based on the experience of the author, for a second order curve, the use of 1-2 middle nodal points is sufficient. Furthermore, a uniform location distribution might be optimal. For a complicated shape such as the turbine blade, two middle nodal points are used. The maximum error of the interpolated boundary nodal point coordinates is within ±0.15 mm. With regard to stress analysis, it can be considered satisfactory. In this case, the middle nodal point positions may not be uniformly distributed. Incidentally, by changing the position of the middle nodal point, it is possible to change the density distribution of the mesh which is one of the advantages of the method. However, it should be noted that, if the distance between the middle nodal point and the corner nodal point is less than 1/4 (l is the length of the side), then the mesh is "wrinkled" [8-9].

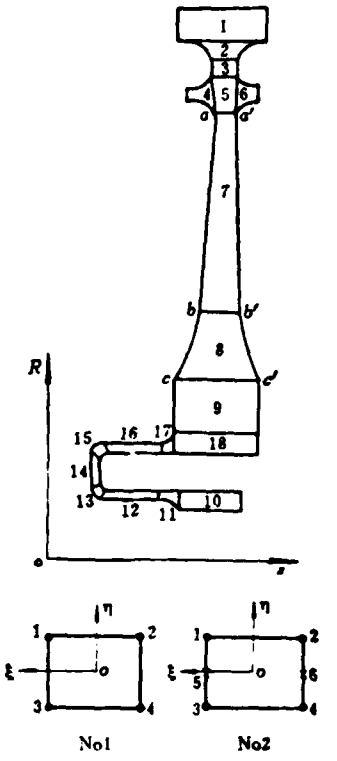

Fig 2 Division of a disk into several zones and their parent elements

The local coordinates (ξ,η,ζ) of any nodal point in the mesh are easily obtained in the parent element because the mesh is uniform in the parent element. As long as the longitudinal and transverse lines

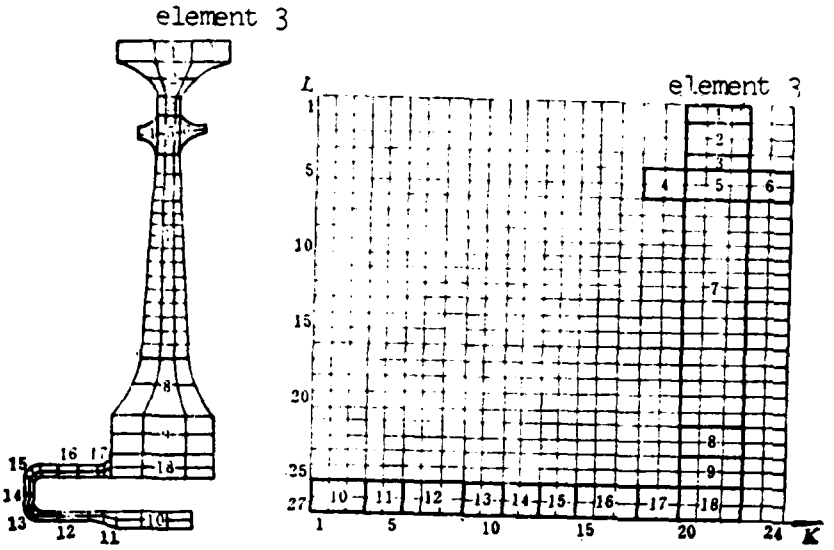

Fig. 3 Real mesh of a disk and its "Chessboard" mesh

of the mesh are chosen, it is not difficult to determine the partial coordinates of any nodal point.

Due to the fact that the distribution of the nodal points of the parent elements in each zone is irregular, the shape function $N_i(\xi,\eta,\zeta)$ can be directly derived using the method in [10].

3. The numbering of elements and nodal points

In designing the program, it is more complicated to number the nodal points. If optimized numbering is used to reduce the bandwidth, it would complicate the program further. The author adopted the "front solver" method to solve the set of linear operations. It has two advantages: "front solver" method itself can save the internal storage, besides, "front solver" method does not have a bandwidth requirement for the numbering of the nodal points. Even when the nodal point sequence is not continuous, it does not matter at all [11]. This makes it difficult to compile the program.

The procedures to number the nodal points are as follows:

COMPUTER RESEARCH ON DYNAMIC CHARACTERISTICS OF A SYNCHRO GENERATOR

Qian Zhenxiong and Xu Qiaobao

(Beijing Institute of Aeronautics and Astronautics)

Abstract

A P-transform matrix is applied to transforming the time-varying dynamic equations of a synchro generator into so-called P Park's equations, in result the state equations of one unit generator system are established. Owing to the nonlinear effect of the voltage regulator and the lagging of the a. c. exciter in an aircraft brushless a. c. generator, the forcing function of the main synchro generator $U_F(t)$ can be reduced to an exponential curve with a lagging t_E and an equivalent time constant T_{II}.

On the basis of the state equations above mentioned eight dynamic characteristics of the synchro generator are printed out separately on an electronic digital computer by four different methods: analysis; fourth-order Rungo-Kutta algorithm; exponential matrix (e^{AT}); and network topology. The computation accuracy and the stability region of these four methods are analyzed and their applicable range is established in conformity with their advantages. Then the following conclusions are drawn:

1. The characteristic roots of the coefficient matrix at no-load sudden short circuit are the dynamic parameters of the synchro generator, i.e. T_a, T_d'', T_d'', T_d'.

2. In symmetrical operation the synchro generator can be simplified as an one-order inertial link.

3. The dynamic characteristics of the a. c. exciter (t_E, T_{II}) have rather little effect on the maximum surge current of the synchro generator at sudden short circuit.

4. In consideration of the non-linearity of the magnetic circuit in the synchro generator, it is verified that the inductor flux ψ_L and the capacitor charges q_C are more suitable than i_L and u_C to be taken as the state variables.

REFERENCES

[1] P. M. Anderson (American) "Control and Stabilization of the Electrical System" Vol. 1, Hydroelectric Publications, 1979.

[2] Edited by Kao Chinde. "The analysis of the transition process and operating mode of an ac generator", Science Publication, 1963.

[3] Yang Huyen et al, editors. "Applied mathematics of the electronic computer", vol. 1, Metallurgical Publication, 1979.

[4] Lee Yunhua et al, editors. "Methods to solve the numerical solutions of differential equations", People Education Publication, 1980.

[5] Shu Tien Shin En et al (Japan). "Matrix theory in Automatic Control", Sciences Publication, 1979.

[6] Leon O. Chua, Pen-Min Lin. "Computer Aided Analysis of Electronic Circuits". 1978.

[7] Frannlin F. Kuo. "Circuit Analysis by Digital Computer", 1975.

[8] Zhang Wei lian et al, editors. "Computer assisted design of electronic circuits", Vol. 1, People Education Publication, 1979.

[9] Shu Fang Shen Yen et al (Japan). "Modern Control Engineering", Science Publication, 1976.

TECHNICAL EXCHANGE MEETING ON RELAYS AND CONTACTORS OF THE AERONAUTICAL SOCIETY OF CHINA

The China Society of Aeronautics and Astronautics held a meeting entitled "Technical Exchange Meeting on Relays and Contactors" in Zunyi between March 12-17, 1982. The meeting was organized by the 315th Factory of the Third Machinery Department. The delegates attending the meeting included 73 people from 35 organizations from the Third Machinery Department, the Fourth Machinery Department, the Seventh Machinery Department, the First Machinery Department, the Air Force and the Navy.

The conference received over 30 papers and technical reports. 17 were presented in the conference and over 10 were read in group meetings. The papers and reports covered a wide range of areas. Primarily, they are the results in theoretical design, new product development and exploratory directions in the relay field, such as the development of the computer assisted design and verification of the dynamic parameters of a magnetic relay system, the complete verification of the JKM sealed relay series, the 10 A 4 circuit magnetic maintenance relay, the 0.5 A 2 circuit miniature magnetically maintained relay, the square TO-5 transistor tube case sealed relay, and the spherical TO-5 relay as well as the development of new silver oxide contact materials.

During the meeting, the delegates conducted a panel discussion on the problem of the developmental direction of the relay. It was unanimously agreed upon that aeronautical relays and contactors should develop in the following three areas: (1) the maneuverability of attack aircraft, (2) the modernization of aircraft control system and engine control, and (3), the development of new aircraft power sources. In summary, efforts will be continued based on high reliability, high sensitivity, high velocity, low load capability, low power assumption and miniaturization.

Finally, the meeting suggested that the next technical exchange meeting be held in 1984.

Chen Chenghang*
Northwestern Polytechnical University

ABSTRACT

The computer aided design technique is an important development in computer applications and it is an important component of computer science. The special language for electronic circuit analysis is the foundation of computer aided design or computer aided circuit analysis (abbreviated as CACD and CACA) of simulated circuits.

Electronic circuit analysis language (ECAL) is a comparatively simple and easy to use circuit analysis special language which uses the Fortran language to carry out the explanatory executions. It is capable of conducting dc analysis, ac analysis, and transient analysis of a circuit. Furthermore, the results of the dc analysis can be used directly as the initial conditions for the ac and transient analyses.

The ECAL language describes the circuit by using input statements which are familiar to electronic circuit engineers. As for the allowable elements, in addition to the regular linear elements, such as resistors, capacitors, inductors, current sources and voltage sources, nonlinear elements, such as diodes, transistor triodes and nonlinear resistors, are also permitted. Hence, it is capable of circuit analysis for both linear and nonlinear circuits.

The ECAL language uses very simple output statements to control the output form of the resultant analyzed data. It may be tables or figures, depending on the various needs. Therefore, it is a very useful analytical tool for engineers.

INTRODUCTION

Computer aided design is an important aspect of computer applications which is also an important milestone in the development process of computer applications from elementary to advanced stages. As a branch of computer science, the computer aided design technique is a

*Received November 1981

special technique which is the simple application of the computer to a process or part of the design work. Even for a product, in spite of the fact that its design has been completed by a computer from the beginning to the end, if the program used was compiled specifically for the design of this product, it is still not possible to claim that the computer-aided design technique was adopted. In other words, computer aided-design technique has certain conditions as its label. These conditions are: 1) there is a suitable special language for this type of problem; 2) there is a data bank with various computational methods and applications data; 3) there is a combined software-hardware system with a certain dialog capability between man and machine to allow the designer to interfere with the work of the computer at any time. This allows the man and the machine to do their best to complete this task fast and well.

The electronic circuit analysis language ECAL was developed as an important component of the computer-aided design technique of electronic circuits. By taking into account the convenience of use for the circuit designer and the feasibility of a man-machine dialog, its input statement form is simple, which is consistent with the custom of the circuit analyst. Therefore, it is easy to learn and convenient to use.

The electronic circuit analysis language ECAL is a comparatively simple and easy to use language for circuit analysis which uses the Fortran language to carry out the explanatory executions. It includes a set of statements with simple structures. The statements have the 82
capability to describe the circuits. They also have the capabilities to designate the analysis range and the output form. In addition, they are also able to control whether the analysis should be repeated or to change the element parameters. It is capable of carrying out dc analysis, ac analysis, or transient analysis of a circuit. Furthermore, the results of the dc analysis can be directly used as the initial conditions of ac or transient analysis to switch into ac or transient analysis.

I. BASIC CHARACTERISTICS

Because ECAL uses the FORTRAN language to compile the explanatory program, it can be operated on any computer with a Fortran compiler. Its symbol group is a subgroup of the FORTRAN symbols. Its data format also agrees with that of the FORTRAN language.

The symbols are formed by the 25 capital alphabets of the English language and the 10 Arabic numerals from 0 to 9 and special symbols, such as "+", "−" "*", "." and a blank space.

The statements of the ECAL language are also composed by using cards just as in FORTRAN. However, each statement has only one line which corresponds to one card. There is no continuation card.

The foundation of electronic circuit analysis of the ECAL language is the nodal point method. Between nodal points, there are branches to create the connections. Each branch is composed of a sourceless element and several independent voltage sources, independent current sources and correlated current sources. Figure 1 shows a standard branch circuit formed by a sourceless element, independent power source and correlated power source. The entire analysis is carried out on the basis of the standard branch. The allowable elements are resistors, capacitors, inductors, independent voltage sources, mutual inductors, voltage controlled current sources (abbreviated as mutual conductance), current controlled current sources (or called the current amplification coefficient), semiconductor diodes, semiconductor triodes and nonlinear resistors.

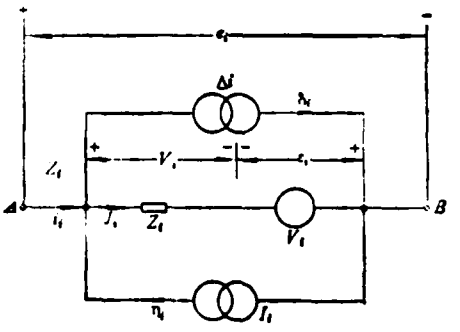

Fig. 1 Standard branch

The ECAL language uses a bending line method to describe nonlinear elements. The nonlinear resistor N can be used to describe a non-

linear element, such as a tunnel diode, field effect transistor, voltage stabilizing transistor, operational amplifier, etc.

There are seven output formats in the ECAL language. One is the standard format. When the format is not specified, this format is automatically used. It tabulates voltage at each nodal point, voltage and current in each branch, and the voltage and current of each element in a table form. If it is an ac analysis, it also provides the power of each branch and element. Obviously, this method may involve a huge amount of output data especially for circuits with more branches and nodal points or under the condition that the analysis frequency or the number time interval points is high. For this reason, there are three more table output formats with six nodal point voltages, branch current, or element voltage of interest as well as three curve output formats with three nodal point point, branch current, or element voltage of interest.

II. APPLICATION RANGE

The first application of ECAL is dc analysis. It can be used to analyze the working condition of the various serial and parallel voltage regulators at the various stages of different dc, ac amplifiers. It can also be used to analyze the amplification factor of a dc amplifier as well as the steady state voltage, current gains of the medium frequency equivalent circuits of ac or pulsed amplifiers.

In the dc analysis, originally it does not treat the energy storage elements--capacitors and indicators. However, in order not to destroy the completeness of the circuit, as well as to obtain the working points from dc analysis before ac or transient analysis, therefore, inductors and capacitors are allowed in the input. In the computation, the inductor is replaced by an 0.1 Ω resistor, while the capacitor is replaced by a 10 M Ω resistor instead. Consequently, it allows the input of the dc insulating capacitors, filtering capacitors or compensating inductors of a multi-stage amplifier into the computer without modification. In the computation of dc working points, the explanatory program automatically will use the aforementioned resistance values

83

instead. The computation of the working point will not be affected.

Another application of the ECAL language is ac analysis. It is capable of conducting frequency characteristics analysis on various wide band, narrow band amplifiers and filters with and without sources. For the AC analysis, the explanatory program carries out the analysis based on small ac signals. It is usually believed that nonlinear problems do not exist for small ac signals near the working points. Therefore, for a working point determined in the dc analysis, if the circuit is not redescribed after switching to ac analysis, a linear analysis will be carried out for the corresponding parameters of the nonlinear elements determined by that working point.

One important statement in ac analysis is the frequency range statement. It indicates the frequencies to be analyzed. Starting from the minimum value, it is increased algebrically or geometrically. After reaching or exceeding the maximum value, it is stopped. Usually, for a narrower analysis range, it is possible to use an equal increment. Thus, the results plotted form a linear coordinate. If a wide frequency range must be analyzed, such as the frequency characteristics of a wide band amplifier which is usually from several tens Hz to several tens mega Hz, then it is not suitable to use a linear coordinate or equal increment method. At this time, it is more suitable to use the common ratio increment method. Its pattern corresponds to a semi-log coordinate.

The ECAL language can also be used to conduct transient analysis on circuits and systems. Usually, a transient analysis is always done with respect to a specified input signal waveform. For example, the output waveform, when the input signal is an impulse, is called the impulse response. When the input signal is a unit step jump, the output is called a unit step response. These are very important output results in transient analyses. In addition, sometimes we are interested in the response of the system or circuit to a certain input waveform. For example, a ramp waveform (linearly increasing waveform) and exponentially increasing waveform, etc., are commonly used. The ECAL language provides the feasibility to describe the input signal which is

also comparatively simple. It involves the use of an input statement INPT. It uses the positions of four coordinate points to provide the variation of the input signal. Thus, it is possible to describe a step, a ramp, a square wave, a trianguar wave, a sawtooth wave and a trapezoidal wave. It is also possible to use three segments of straight lines to replace an exponential or logarithmic curve approximately.

III. PROGRAM FLOW CHART

In order to suit the batch process method [5] of the operating system of the Felix C-256 computer presently in use, the explanatory program of the ECAL language has also adopted a batch process form, i.e., several circuit analysis jobs can be processed at the same time. Each job is not mutually correlated. A job not only can perform a dc analysis, but also an ac or transient analysis. It is also possible to change the element parameters repeatedly. This format can be converted into the man-machine dialog format easily with user teletype terminals or CRT-keyboard terminals.

The explanatory program can be approximately divided into three parts: the main program--reading in the headings and the electronic circuit descriptive statements, filling out the table of elements and controlling the process of analysis; and two subroutines--calculating and providing output results of the dc, ac and transient analyses of the circuit, respectively.

The program flow chart is shown in Figure 2.

IV. EXAMPLES OF THE ANALYSIS

A low frequency amplifier, as shown in Figure 3, has 22 branch numbers and nine nodal point numbers. The nodal point number is circled to distinguish from the branch number. The 18th branch resistance is a negative feedback resistance. The circuit analysis program is shown in Table 1. The first execution statement EXEC carries out the dc analysis to calculate the working point. Then, the dc power supply

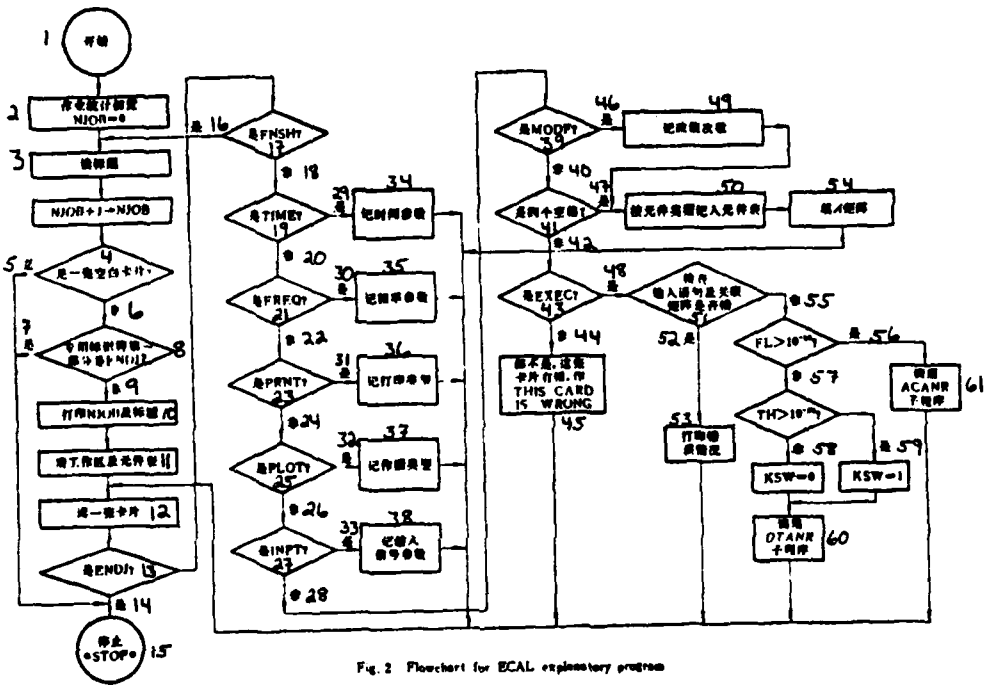

Fig. 2 Flowchart for ECAL explanatory program

KEY TO FIGURE 2 (page 133):

1--start; 2--initial job statistics; 3--read headings; 4--is it a blank card; 5--yes; 6--no; 7--yes; 8--is the first part of the special identification code ENDJ; 9--no; 10--PRINT NJOB and headings; 11--clear working area and element table; 12--read one card; 13--is it ENDJ; 14--yes; 15--stop; 16--yes; 17--is it FNSH; 18--no; 19--is it TIME; 20--no; 21--is it FREQ; 22--no; 23--is it PRNT; 24--no; 25--is it PLOT; 26--no; 27--is it INPT; 28--no; 29--yes; 30--yes; 31--yes; 32--yes; 33--yes; 34--note time parameter; 35--note frequency parameter; 36--note print type; 37--note plot type; 38--note input signal parameter; 39--is it MODF; 40--no; 41--is it four blank spaces; 42--no; 43--is it EXEC; 44--no; 45--none of the above. This card is wrong. PRINT "THIS CARD IS WRONG"; 46--yes; 47--yes; 48--yes; 49--note number of times of value charges; 50--enter the elements according to the type into the element table; 51--check for mistakes in the input statements and the correlation matrix; 52--yes; 53--situation when printing error occurs; 54--fill the matrice A; 55--no; 56--yes; 57--no; 58--no; 59--yes; 60--call subroutine DTANR; 61--call subroutine ACANR

V_{17} is removed and a 5mV ac voltage signal is added. At R_{18} = 10 MΩ, it corresponds to the situation that the negative feedback linkage is broken off to obtain the frequency characteristic curves. Then, R_{18} = 20 KΩ is used to obtain the frequency characteristic curve with the feedback. The range of analysis is from 1 Hz to 1 mega Hz. 86

The circuit for a single-shot trigger is shown in Figure 4. The trigger pulse is added to the 21^{th} branch. Different triggering capacitance has an effect on the output waveform. Here, a value change statement is used to change C_{13}. The response curves corresponding to C_{13} = 4000PF, 8000 PF and 12,000 PF were calculated. The trigger pulse is a square wave, 20 microseconds wide. The amplitude is four volts. The program is listed in Table 2.

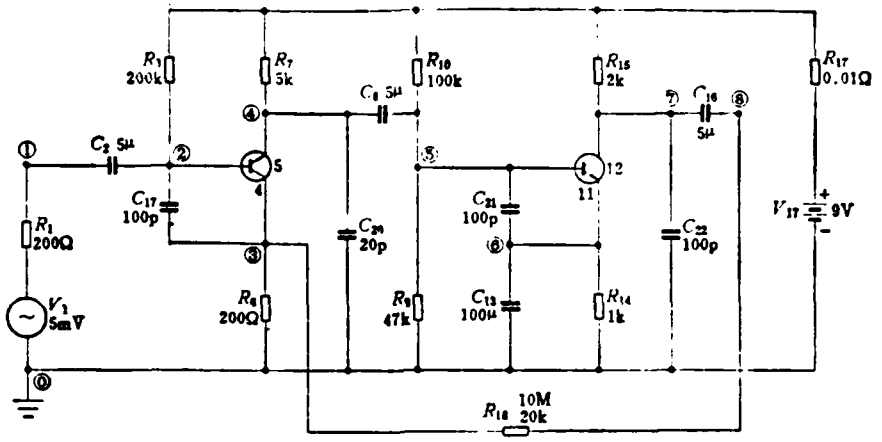

图 3　低频放大器电路图

Fig. 3　Circuit diagram for a low frequency amplifer

表 1　低频放大器分析程序

Table 1　Program of the analysis of a low frequency amplifier

```
THE ANALYSIS OF A LOW FREQUENCY AMPLIFIER
     R   1    0   1                200
     C   2    1   2              5E-6
     R   3    2   9                2E5
     R   6    3   0                200
     R   7    9   4               5000
     C   8    4   5               5E-6
     R   9    5   0              4.7E4
     R  10    5   9                1E5
     C  13    6   0               1E-4
     R  14    6   0               1000
     R  15    7   9               2000
     C  16    7   8              5E-6
     R  17    0   9               0.01
     V  17                          9
     R  18    8   3                1E7
     C  19    2   3             1E-10
     C  20    4   0             2E-11
     C  21    5   6             1E-10
     C  22    7   0             1E-10
     T   4    5   2   4   3      300   0.6          80   2E5
     T  11   12   5   7   6      300   0.6          80   2E5
EXEC
     V   1                       5E-3
     V  17
FREQ*                               1   1E7   1.1749
PLOT     1    5   8   9          -180   180           5
EXEC
     R  18    8   3                2E4
PLOT     1    5   8   9          -180   180           *
EXEC
FNSH
```

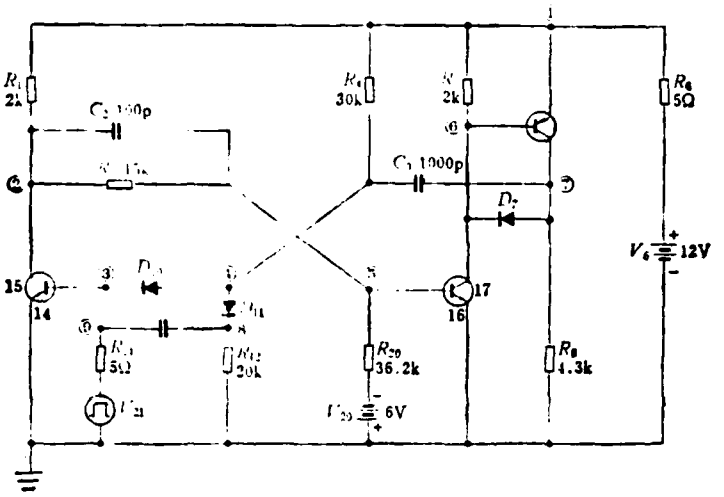

图 4　单稳态触发器电路图

Fig. 4　Circuit diagram for a Single-shot trigger

表 2　单稳态触发器分析程序

Table 2　Program of the analysis of a singleshot trigger

```
THE ANALYSIS OF A SINGLE-SHOT TRIGGER
      C   2   2   5                  1E-10
      R   1   1   2                  2E+03
      R   3   2   5                1.5E+04
      R   4   1   4                  3E+04
      R   5   1   6                  2E+03
      R   6   1   0                  5E+00
      V   6                        -12E+00
      D   7   7   6                  1E+01
      R   8   7   0                4.3E+03
      C   9   4   7                  1E-09
      D  10   4   3                  1E+01
      D  11   4   8                  1E+01
      R  12   8   0                  2E+04
MODFC C  13   8   9                1.0E-09  1.2E-08  4.0E-09
      T  14  15   3    2    0        1E+03  6.5E-01  1.5E+02  1E+05
      T  18  19   6    1    7        1E+03  6.5E-01  1.5E+02  1E+05
      R  20   5   0              3.62E+04
      V  20                          6E+00
      R  21   0   9                  5E+00
INPT     21   0   1   20   21            0     4E+00     4E+00        0
TIME                                    0     1E-04     1E-06
PLOT      1   7   4    8           -1E+01  1.2E+01
EXEC
FNSH
```

[1] D. A. Calahan. "Computer Aided Network Design", 1972.

[2] Leon O. Chua, Pen-Min Lin. "Computer Aided Analysis of Electronic Circuits", 1979.

[3] Zhang Hweikang, Chung Zangchun. "Computer Aided Design of Electronic Circuits", People's Education Publication, 1979.

[4] L. P. McNama. "Handbook of Circuit Analysis Languages and Techniques", 1978.

[5] Shi Shui Chiu, Lee Shuyang, Lee Lunghong. "FORTRAN Language of the FELIX C-256 Computer", Defense Industry Publications, 1980.

ELECTRONIC CIRCUIT ANALYSIS LANGUAGE(ECAL)

Chen Chenghang

(Northwestern Polyicchnical University)

Abstract

The computer-aided design (CAD) technique is one of important developments in computer application. CAD technique has already become an important branch of computer science. Special language for electronic circuit analysis is the foundation of computer-aided circuit design (CACD) and/or computer-aided circuit analysis (CACA).

Electronic circuit analysis language (ECAL), a special language for circuit analysis, is comparatively simple and convenient for engineering application. Statements of ECAL are executed explanatorily by FORTRAN language. So far, ECAL can be used to make DC, AC and transient analysis of a circuit, and the results of DC analysis can be regarded directly as initial conditions for AC and transient analysis.

Both linear and nonlinear elements can be taken into account in ECAL. Linear elements may consist of resistors, capacitors, inductors, mutual inductors, independent current sources, independent voltage sources and dependent current sources under voltage control or current control. Nonlinear elements may include diodes, transistors and nonlinear resistors. Therefore, this language is suitable to the analysis of linear circuits or systems as well as nonlinear ones.

AN EXPERIMENTAL INTERACTIVE COMPUTER GRAPHICS SYSTEMS FOR FREE-FORM SURFACE DESIGN

Zheng Huiling, Wang Zhisheng, Lu Hongjia and He Tianbao*
Shanghai Aircraft Manufacturing Factory

ABSTRACT

An interactive graphics system for free-form surface design is introduced in this paper. The system was established on the basis of the cubic uniform B-spline theory. In order to obtain better simulated results, the basic function with a quadruple knot at both ends was chosen. Its major functions are as follows:

1. It displays the three-dimensional model on a screen or a plotter. It also allows the three-dimensional coordinate system to undergo real time transformation with respect to the model.

2. Through the use of a method involving the fairing of the curvatures of discrete points sequentially, the external shape of the model is faired.

3. It provides two local modification methods for the model surface and also ensures C^2 continuity.

4. It permits the display of any arbitrary cross-section of the model.

A computer aided shape design interactive system was established using a DJS-6 computer and a model "751" optical pen graphics display which was developed and constructed by Sian Jiaotung University. Presently, it is taking its shape. However, perfection and further development are continuing. The B-splines method was chosen to form the curve (surface) because of considerations in geometric intuition, ease of computation and ease of control and modification. It is graphically called the "characteristic ployhedron surface design method". A brief introduction to the major functions, conclusions and application examples was presented in this paper.

*received June 1981

I. THE STRUCTURE AND DISPLAY OF THE CURVE (SURFACE)

With regard to the design of external shape, the use of a cubic uniform B-splines method is very suitable. In order to improve the end point characteristics, a basic function [1] with a quadruple knot at each end was used (Figure 1). In comparison to a usual cubic uniform B-splines curve, a difference only occurs in the two segment of curves on the ends. In the middle, they coincided completely (Figure 2). It has very good extrapolation conditions on the front end which satisfy

$$\vec{P}_1(0)=\vec{V}_1, \quad \vec{P}_1'(0)=3(\vec{V}_2-\vec{V}_1) \tag{1}$$

and

$$\vec{P}_1''(0)=3(\vec{V}_3-\vec{V}_2)+6(\vec{V}_1-\vec{V}_2) \tag{2}$$

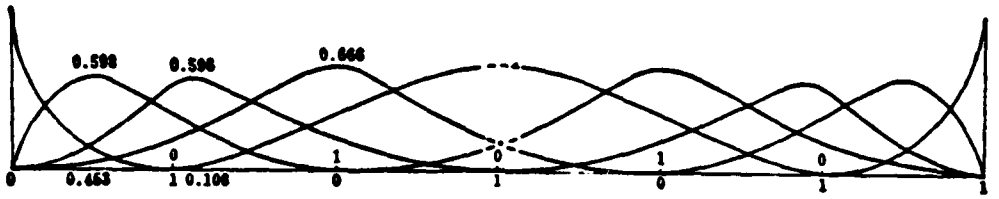

Fig. 1 B-splines with a quadruple knot at each end point

The rear end is similar to the front end. From equation (1) we can see that the curve passes through the front end point. Furthermore, it is tangent to the front (real) end. From equation (2) we can see that usually $\vec{P}_1''(0)$ is not equal to zero. Therefore, the method of using polygon equi-distance extension to ensure that the usual cubic uniform B-spline passing through the end points is superior.

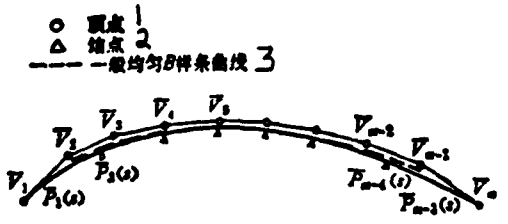

Fig. 2 The corresponding B-spline curve

Key: 1--vortex; 2--knot; 3--the usual uniform B-spline

From equation (1) we can also see that the conditions to be satisfied at the end point are consistent with those of the Bezier curve. Especially when only one segment of curve exists (four vertices), this type of curve rigorously deteriorated into the Bezier curve. Therefore, this system permits the combined use of both structuring methods.

For the convenience in use, a matrix expression of this type of curves under various conditions is derived from the deBoor-Cox interation equation. For example, when $m \geqslant 8$, the first two segments of curves can be expressed as:

$$\left.\begin{aligned}
\vec{P}_1(s) &= [s^3 s^2 s 1]\begin{bmatrix} -1 & 7/4 & -11/12 & 1/6 \\ 3 & -9/2 & 3/2 & 0 \\ -3 & 3 & 0 & 0 \\ 1 & 0 & 0 & 0 \end{bmatrix}\begin{bmatrix} \vec{V}_1 \\ \vec{V}_2 \\ \vec{V}_3 \\ \vec{V}_4 \end{bmatrix} \\
\vec{P}_2(s) &= [s^3 s^2 s 1]\begin{bmatrix} -1/4 & 7/12 & -1/2 & 1/6 \\ 3/4 & -5/4 & 1/2 & 0 \\ -3/4 & 1/4 & 1/2 & 0 \\ 1/4 & 7/12 & 1/6 & 0 \end{bmatrix}\begin{bmatrix} \vec{V}_2 \\ \vec{V}_3 \\ \vec{V}_4 \\ \vec{V}_5 \end{bmatrix}
\end{aligned}\right\} \qquad (3)$$

The last two expressions are

$$\left.\begin{aligned}
\vec{P}_{m-4}(s) &= [s^3 s^2 s 1]\begin{bmatrix} -1/6 & 1/2 & -7/12 & 1/4 \\ 1/2 & -1 & 1/2 & 0 \\ -1/2 & 0 & 1/2 & 0 \\ 1/6 & 2/3 & 1/6 & 0 \end{bmatrix}\begin{bmatrix} \vec{V}_{m-4} \\ \vec{V}_{m-3} \\ \vec{V}_{m-2} \\ \vec{V}_{m-1} \end{bmatrix} \\
\vec{P}_{m-3}(s) &= [s^3 s^2 s 1]\begin{bmatrix} -1/6 & 11/12 & -7/4 & 1 \\ 1/2 & -5/4 & 3/4 & 0 \\ -1/2 & -1/4 & 3/4 & 0 \\ 1/6 & 7/12 & 1/4 & 0 \end{bmatrix}\begin{bmatrix} \vec{V}_{m-3} \\ \vec{V}_{m-2} \\ \vec{V}_{m-1} \\ \vec{V}_m \end{bmatrix}
\end{aligned}\right\} \qquad (4)$$

The middle segments are consistent with the usual cubic uniform condition

$$\vec{P}_i(s)=[s^3 s^2 s 1]\begin{bmatrix} 1/6 & 1/2 & -1/2 & 1/6 \\ 1/2 & -1 & 1/2 & 0 \\ -1/2 & 0 & 1/2 & 0 \\ 1/6 & 2/3 & 1/6 & 0 \end{bmatrix}\begin{bmatrix} \vec{V}_i \\ \vec{V}_{i+1} \\ \vec{V}_{i+2} \\ \vec{V}_{i+3} \end{bmatrix} \quad (2<i<m-4) \tag{5}$$

Summarizing the coefficient matrices under various possible conditions (not limited by m and i), we discovered that there are only 18 different columns. In the program, these 18 columns are placed in a 4x18 group. Each time four columns are extracted based on the various m and i values to form the coefficient matrix of the B-spline of this segment. Thus, the number of operation is reduced and the internal storage capacity is saved. This 4x18 numeral group is

$$\begin{bmatrix} -1 & 7/4 & -11/12 & 1/6 & -1/4 & 7/12 & -1/2 & -1/6 \\ 3 & -9/2 & 3/2 & 0 & 3/4 & -5/4 & 1/2 & 1/2 \\ -3 & 3 & 0 & 0 & -3/4 & 1/4 & 1/2 & -1/2 \\ 1 & 0 & 0 & 0 & 1/4 & 7/12 & 1/6 & 1/6 \end{bmatrix} \tag{6}$$

$$\begin{bmatrix} 1/2 & -7/12 & 1/4 & 11/12 & -7/4 & 3 & -3 & -1 & 1 & 1 \\ -1 & 1/2 & 0 & -5/4 & 3/4 & -6 & 3 & 3/2 & -3/2 & 0 \\ 0 & 1/2 & 0 & -1/4 & 3/4 & 3 & 0 & 0 & 0 & 0 \\ 2/3 & 1/6 & 0 & 7/12 & 1/4 & 0 & 0 & 0 & 1/2 & 0 \end{bmatrix}$$

As for the curved surface, the range of boundary multiple knot effect is shown as the shaded area in Figure 3. So long as the curve is treated well, the curved surface problem is also naturally resolved.

Figure 4 is the characteristic polyhedron of an aircraft displayed by using the VVDP light button through the optical pen points. The point curved surface display light button SUDP can display an arbitrary projection of the curved surface.

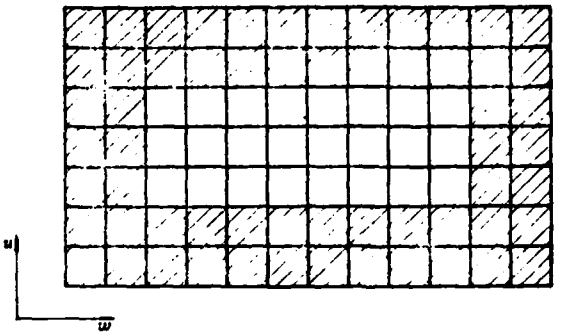

Fig. 3 The areas influenced by the multiple knots on a surface

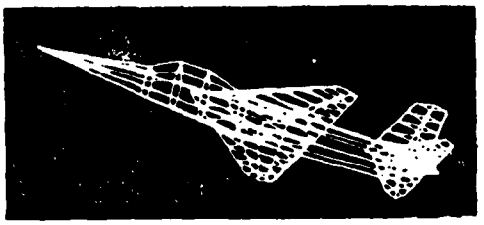

图 4 飞机的特征多面形

Fig. 4 The characteristic polyhedron of an aircraft

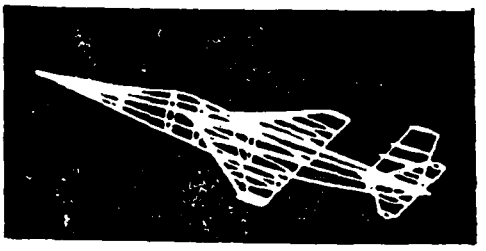

图 5 飞机的曲面显示

Fig. 5 Display of the surface of an aircraft

II. SOLVING FOR THE VERTEX AND DISPLAYING THE CHARACTERISTIC POLYHEDRON

In computer aided design and manufacturing, the composite problem is frequently encountered. It is necessary to start from the known, discrete vlaue point to solve for the vertex of the characteristic polyhedron. Subsequently, the B-spline curve passing through the above mentioned point is created.

This system considered the vertex problem in depth, including various shape value point numbers n(the effect of end point is different), the three end points condition--free end, the usual cubic uniform B-splines of the known tangential vector or equal distance extension and various combinations of them. There are 26 situations in total. For exmaple, when n > 5, the computation formula in solving for the vertex under the condition that both ends are free ends is

$$\begin{pmatrix} 1 & & & & & & & & \\ 8 & 15 & 3 & & & & & & \\ & \frac{1}{4} & \frac{7}{12} & \frac{1}{6} & & & & & \\ & & \frac{1}{6} & \frac{2}{3} & \frac{1}{6} & & & & \\ & & & \frac{1}{6} & \frac{2}{3} & \frac{1}{6} & & & \\ & & & & \ddots & \ddots & \ddots & & \\ & & & & & \frac{1}{6} & \frac{2}{3} & \frac{1}{6} & \\ & & & & & & \frac{1}{6} & \frac{7}{12} & \frac{1}{4} \\ & & & & & & & 3 & 15 & 8 & 1 \end{pmatrix} \begin{pmatrix} \vec{V}_1 \\ \vec{V}_2 \\ \vec{V}_3 \\ \vec{V}_4 \\ \vec{V}_5 \\ \vdots \\ \vec{V}_{m-3} \\ \vec{V}_{m-2} \\ \vec{V}_{m-1} \\ \vec{V}_m \end{pmatrix} = \begin{pmatrix} \vec{P}_1 \\ 27\vec{P}_2 - \vec{P}_3 \\ \vec{P}_3 \\ \vec{P}_4 \\ \vec{P}_5 \\ \vdots \\ \vec{P}_{n-3} \\ \vec{P}_{n-2} \\ 27\vec{P}_{n-1} - \vec{P}_{n-2} \\ \vec{P}_n \end{pmatrix} \tag{7}$$

In equation (7), the second row and the second last row come from the knot condition (choosing $s = \frac{1}{3}\left(\begin{matrix}2\\3\end{matrix}\right)^{(1)}$, of the first and last segments. At this time, m = n. Let us take the tangential vectors $\vec{D}_1$ and $\vec{D}_2$ of both ends, then the two rows should be changed to:

$$-3\vec{V}_1 + 3\vec{V}_2 = \vec{D}_1, \quad -3\vec{V}_{m-1} + 3\vec{V}_m = \vec{D}_2 \tag{8}$$

In addition, when m = n + 2, which corresponds to the equal distance extension condition, the first two rows should be changed to:

$$\vec{V}_2 = \vec{P}_1, \quad \vec{V}_1 - 2\vec{V}_2 + \vec{V}_3 = 0 \tag{8'}$$

The last two rows are similar with m = n + 2.

The vertex of a curved surface can be obtained through the shape value point after two such processes.

This system can also assure that the B-spline obtained from the vertex contains a pre-determined straight line segment, including the pre-assigned starting and end points. Furthermore, a C^2 continuity exists there (C^2 is a second order continuity). For a curved surface, this means that it is allowed to contain a pre-appointed plane.

III. PARTIAL MODIFICATION OF THE CURVE (SURFACE) AND THE DISPLAY OF THE MODIFIED POLYHEDRON

This is a power means of a computer aided external shape design system with man-to-machine dialog capability. It should be comparatively more effective in solving this problem by using the partial support characteristics of the B-splines.

Two types of partial modification capabilities were arranged in this system:

1. Direct modification of the vertex of the polyhedron. Through the optical pen and the keyboard to send in the corresponding modification information--we can change the vertex number, point number and its coordinate value until the shape is considered to be satisfactory. 93

2. Modification of the vertices of the polyhedron by using a new curve (surface) value. It is required that the new curve surface generated after the modification of the vertices must pass through the newly appointed points. Furthermore, C^2 continuity must still be ensured.

Because basically cubic uniform B-splines are used, the principle of modification is very simple. Using the curve modification in Figure 8 as an example, $\vec{P}_{C'}$、$\vec{P}_{D'}$、$\vec{P}_{E'}$ are the new given points. Our treatment is to discard the shape value control at B and F (which is frequently near a round angle transition; therefore, it is acceptable). The new vertices $\vec{V}_{C'}$、$\vec{V}_{D'}$、$\vec{V}_{E'}$ are solved simultaneously.

$$\begin{cases} \frac{2}{3}\vec{V}_{C'} + \frac{1}{6}\vec{V}_{D'} = \vec{P}_{C'} - \frac{1}{6}\vec{V}_B \\ \frac{1}{6}\vec{V}_{C'} + \frac{2}{3}\vec{V}_{D'} + \frac{1}{6}\vec{V}_{E'} = \vec{P}_{D'} \\ \frac{1}{6}\vec{V}_{D'} + \frac{2}{3}\vec{V}_{E'} = \vec{P}_{E'} - \frac{1}{6}\vec{V}_F \end{cases} \tag{9}$$

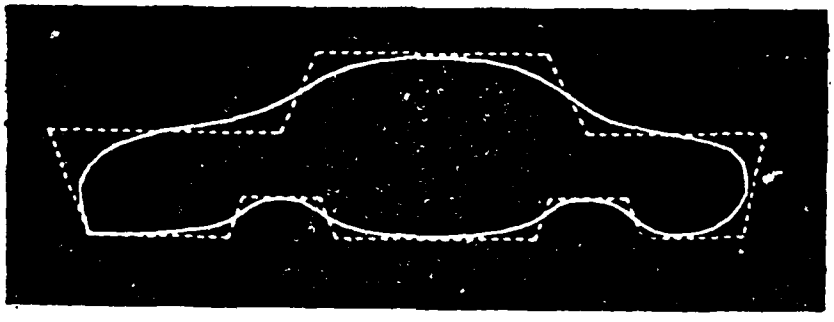

图 6　产生的截线仍不符合要求

Fig 6　The undesired section

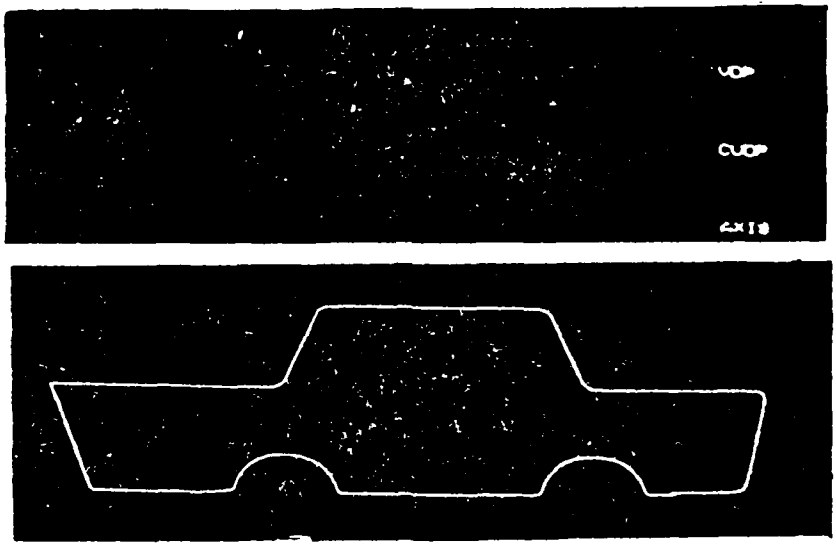

图 7　利用重顶点技巧的交替改顶点，产生出符合要求的截线

Fig 7　Modification of vertices with multiple vertex technique to produce the desired section

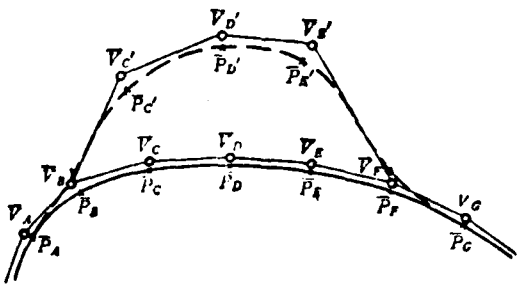

图 8　按指定的新型值点决定顶点

Fig. 8　Determination of the vertices by new given points

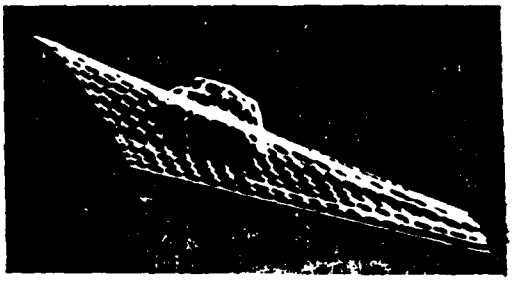

图 9　一个镶嵌上半球的机翼

Fig. 9　A semisphere inserted in a wing

Because only three vertices $\vec{V}_{C'}$、$\vec{V}_{D'}$、$\vec{V}_{E'}$ are changed, therefore, the new curve determined by the polyhedron $\cdots\cdots\vec{V}_A\vec{V}_B\vec{V}_{C'}\vec{V}_{D'}\vec{V}_{E'}\vec{V}_F\vec{V}_G\cdots\cdots$ can satisfy C^2 continuity. Only in the $\vec{P}_A\vec{P}_G$ segment, it deviates from the original curve. Furthermore, it rigorously passes through $\vec{P}_{C'}$、$\vec{P}_{D'}$、$\vec{P}_{E'}$; therefore, it agrees with the modification requirements. Moreover, the computational work load is very small. Similarly, it can be used on a curved surface. The corresponding surface knots can also be modified locally in order to save the computational time. It should be pointed out that the disadvantage of this treatment is that the convex boundary shape under surface modification cannot be satisfied (the modification zone is limited to above the rectangular region of the parametric plane). We computed an example which involved the insertion of a large hemisphere on a wing. After modifying 20 points, including the transition region between the hemisphere and the wing, we obtained very good results (Figure 9).

The fairing of the B-splines can be reduced to the fairing of the corresponding characteristic polyhedron vertex sequence [2]. We adopted the curvature method introduced in that book to carry out fairing with specific reference to the bad points of the vertex sequence of the polyhedron. Its basic principle is that the ordinate of the vertex must be modified in order to ensure the quadruple difference of the ordinate with respect to the arc length at that vertex is zero ($\Delta^4 y = 0$).

The so-called curvature K_i of point $\vec{P}_i$ is the curvature of the circle passing through the three points $\vec{P}_{i-1}$, $\vec{P}_i$, $\vec{P}_{i+1}$

$$K_i = \frac{4\Delta_i}{l_i l_{i+1} l_i^*} = -\frac{2\sin\varphi_i}{l_i^*} \tag{10}$$

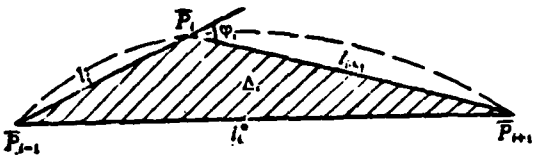

Fig. 10 The curvature of a specific circle of $\vec{P}_i$

where Δ_i is the algebraic area of the triangle formed by $\vec{P}_{i-1}, \vec{P}_i, \vec{P}_{i+1}$. Assuming that $\vec{P}_i$ is determined to be a bad point in Figure 11, then the modification quantity ρ_i has the following computational formula:

$$\rho_i = -\frac{l_i l_{i+1}}{g_i} D_i$$

$$g_i = 2\left[\mu_i \frac{l_i}{l_{i-1}+l_{i+2}} \sin\psi_{i+1} + \sin\psi_i + \lambda_i \frac{l_{i+1}}{l_{i-1}+l_i} \sin\psi_{i-1}\right] \tag{11}$$

$$\mu_i = \frac{l_i}{l_{i+1}+l_i} \qquad \lambda_i = \frac{l_{i+1}}{l_{i+1}+l_i}$$

$$D_i = \frac{(K_{i+1}-K_i)/l_{i+1} - (K_i - K_{i-1})/l_i}{l_{i+1}+l_i}$$ (sequence deviation of the the curvature)

Equation (11) was described in [2]. Its detailed proof, program flow chart and effectiveness were given in [5]. From the effectiveness, it is comparatively ideal. Furthermore, because the computational process does not involve the superpositioning of curves, the fairing speed is fast. As for a spatial curve, it is converted into two projection curves to be treated separately. 95

V. THE COMPUTATION AND SECTION DISPLAY OF AN ARBITRARY CROSS-SECTION

In order to rigorously control the external shape, especially some key positions, this function is also mandatory. Due to the inclination of the sectional coordinate system with respect to the surface coordinate system, many complicated details are brought into the computation of the section. In this system, the vertices and knots of the polyhedron are transformed into the sectional coordinate system based on the geometric invariance of the B-spline surface. Subsequently, the computation of the inclined sectional external shape is transformed into the normal section $(\tilde{y}=0)$. Therefore, it is much faster. Furthermore, it is more convenient for the digital controlled plotting of the sectional shape, computation of the incline angle and digitally controlled shape modifications. After the computation, the system can automatically transform the vertices and knots back to the surface coordinate system to be used for the next sectional computation. The sectional plane parameters are sent into the system by the keyboard. The step length of the extrapolation on the section line can provide the $\Delta\tilde{x}$ of the sectional coordinate system or the parametric increments ΔU or ΔW. It is selected by the user.

Figure 12 shows the inclined section of a wing bulge (see Figure 9). The step length chosen is $\Delta W = 0.2$.

VI. IDENTIFIED PROBLEMS

In addition to the aforementioned light buttons, functional keys, the present system also includes over 20 optical buttons and function keys such as picture change (magnification, reduction, displacement,

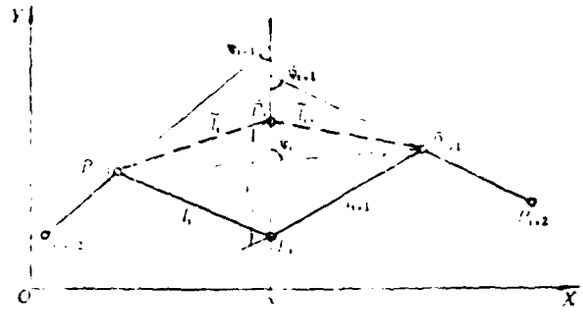

图11 确定$\vec{P}_i$点处的修改值P_i

Fig. 11 Determination of the modifying value P_i at $\vec{P}_i$

图12 在截面坐标系下的截线

Fig. 12 The section in a sectional coordinate system

rotation), automatic arrangement of the picture, graphics output and three-dimensional coordinate system transformation and three-dimensional surface symmetry, etc. The function mentioned above cannot meet the actual requirements yet. There is a lot of work to be done. For example, they include the further modification of the GSP software system, the establishment of a fast algorithm for the display of curve (surface), the formation of a transition surface, the continuity problem of the curve (surface), the surface plate problem of a non-quadrilateral surface...and other applied programs, such as the connection between the strength and aerodynamic computation programs.

In addition, the present hardware conditions are far less than those required to satisfy the requirements.

REFERENCES

[1] "Computer Aided Geometric Design" Symposium on the 1st International GAGD Conference, Foreign Aeronautical Editing Department, 1978.

[2] "Computational Geometry", authored by Su Boqing and Liu Denyuan. Shanghai Technical Publications, 1981.

[3] "Geometrical Concepts in Computer Graphics", J. A. Adams, author, translated from AD-750734 by Shanghai Aircraft Manufacturing Factory.

[4] I. D. Faux and M. J. Pratt. "Computational Geometry for Design and Manufacture", Ellis Horwood 1979.

[5] "An Introduction to a Discrete Point Fairing Method--the Curvature Method", Wang Zhisheng, Zheng Huiling, Technical Report of Shanghai Aircraft Manufacturing Factory, 1981.

AN EXPERIMENTAL INTERACTIVE COMPUTER GRAPHICS SYSTEM FOR FREE-FORM SURFACE DESIGN

Zheng Huiling, Wang Zhisheng, Lu Hongjia, He Tianbao

(Shanghai Aircraft Manufacturing Factory)

Abstract

An interactive computer graphics system for free-form surface design is described in this paper, and application of cubic uniform B-splines is suggested as the fundamental method of surface modeling. In order to obtain a better approximation, the basic function with a quadruple knot at each end point is utilized.

In respect of curve construction, there are only 18 columns in each of various coefficient matrices for the different numbers of vertexes and the different sequences of curve segments, and the matrix expressions of curves are also given. As a result, real benefit is gained for reducing the storage capacity and increasing the computational speed. In the inverse calculation for the vertexes 26 various composite cases are summarized, which permit to maintain the original straight line segments.

It is proposed to fair the given curves by fairing the curvature sequence of the discrete vertexes, and preliminary practical experience is also given.

This paper offers a simple and fast engineering algorithm for modifying of the surface data in a local region, while the surface still remains in second order continuity.

In the experimental system there are 20 functional buttons (embracing the functions of coordinate transform, 3-dimensional symmetry, construction of an arbitrary section etc.). A success has been made in surface modeling of aircraft, automobile and ship.

BEZIER PLOTTING THEOREM AND GEOMETRIC CHARACTERISTICS OF CUBIC BEZIER CURVES

Shi Fazhong and Wu Junheng*
Beijing Institute of Aeronautics and Astronautics

ABSTRACT

The geometric characteristics of the Bezier curve have been studied in depth by P. E. Bezier using the fast end curve [1] and by Su Boqing and Liu Dengyuan using simulated projection transformation [3-5]. The method presented in [1] by Bezier to find the points and their tangents on the Bezier curve using geometric plotting is the Bezier plotting theorem. This paper analyzed the geometric characteristics of plane cubic Bezier curves based on the plotting theorem. It pointed out that the λ, μ (or $\bar{\lambda}$, $\bar{\mu}$) shown in Figure 2 are a pair of invariant quantities determining the geometric characteristics. The complete plane diagram of λ, μ(or $\bar{\lambda}$, $\bar{\mu}$) was given (see Figure 3). Some geometric characteristics of the spatial cubic Bezier curves were discussed.

I. THE DERIVATION OF THE BEZIER PLOTTING THEOREM

The Bernstein expression of the n^{th} order Bezier curve is

$$\vec{P}(u)=\sum_{j=0}^{n} g_{n,j}(u)\cdot\vec{S}_j \qquad u\in[0,1] \tag{1a}$$

$$g_{n,j}(u)=c_n^j u^j(1-u)^{n-j} \tag{1b}$$

where $\vec{S}_j$ is the cusp vector of the Bezier characteristic polygon, $g_{n,j}(u)$ is the n^{th} Bernstein basic function.

The geometric plotting method presented by Bezier in [1] to find the points and their tangent on the curve is shown in Figure 1. We called it the Bezier plotting theorem. It can be expressed in terms of the following set of iteration equations:

$$\vec{P}(u)=\sum_{j=0}^{n-p} g_{n-p,j}(u)\cdot\vec{S}_j^{(p)}(u) \qquad p=0,1,\cdots,n \tag{2a}$$

*Received October 1981.

$$\vec{S}_i^{(r)}(u)=\vec{S}_i^{(r-1)}(u)+u\overrightarrow{S_i^{(r-1)}(u)S_{i+1}^{(r-1)}}(u) \quad (2b)$$

$$\vec{S}_i^{(0)}(u)=\vec{S}_i \quad (2c)$$

$$\vec{P}'(u)=n\overrightarrow{S_0^{(n-1)}(u)S_1^{(n-1)}}(u) \quad (2d)$$

$$\vec{P}''(u)=n(n-1)[\overrightarrow{S_1^{(n-2)}(u)S_2^{(n-2)}}(u)-\overrightarrow{S_0^{(n-2)}(u)S_1^{(n-2)}}(u)] \quad (2e)$$

Chang Gengzhe and Wu Junhen first provided the proof [2]. The following can also be derived directly.

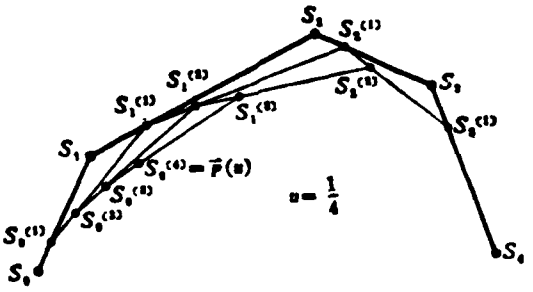

图 1　用作图定理求Bézier曲线上点及切线

Fig 1　Application of the plotting theorem to determining points and their tangents on the Bezier curve

Using $c_n^j=c_{n-1}^j+c_{n-1}^{j-1}$ and changing the index j, we can rewrite (1a) into

$$\vec{P}(u)=\sum_{j=0}^{n-1}c_{n-1}^j u^j(1-u)^{n-j}\vec{S}_j+\sum_{j=1}^{n}c_{n-1}^{j-1}u^j(1-u)^{n-j}\vec{S}_j$$

$$=\sum_{j=0}^{n-1}c_{n-1}^j u^j(1-u)^{n-j-1}[(1-u)\vec{S}_j+u\vec{S}_{j+1}]=\sum_{j=0}^{n-1}g_{n-1,j}(u)\vec{S}_j^{(1)}(u)$$

where $\vec{S}_j^{(1)}(u)=(1-u)\vec{S}_j+u\vec{S}_{j+1}=\vec{S}_j+u(\vec{S}_{j+1}-\vec{S}_j)=\vec{S}_j+u\overrightarrow{S_jS_{j+1}}$

Repeating the above process, we know that (2a)-(2c) are valid. Using (1b) to find its partial derivatives with respect to u, we get

$$g'_{n,j}(u)=n[g_{n-1,j-1}(u)-g_{n-1,j}(u)]$$

$$g''_{n,j}(u)=n(n-1)[g_{n-2,j-2}(u)-2g_{n-2,j-1}(u)+g_{n-2,j}(u)]$$

Again, finding the derivatives of (1a) with respect to u, and using the two above equations, we know (2d) and (2e) are valid. The higher order derivative vectors can be derived by further steps.

II. GEOMETRIC CHARACTERISTICS OF PLANAR CUBIC BEZIER CURVES

The equation of a plane cubic Bezier curve is

$$\vec{P}(u)=(1-u)^3\vec{S}_0+3u(1-u)^2\vec{S}_1+3u^2(1-u)\vec{S}_2+u^3\vec{S}_3,\quad u\in[0,1] \tag{3}$$

where $\vec{S}_j,\ j=0,1,2,3;\ \vec{a}_j=\vec{S}_j-\vec{S}_{j-1}=(x_j,\ y_j,\ 0),\ j=1,2,3$ correspond to the four co-planar vertices and three vectors of the characteristic triangle, respectively. If the lines coincide, then the curve becomes a straight line. No discussion will be necessary.

The geometric characteristics of a plane cubic Bezier curve include whether a single point (a cusp or a double point) or an inflexion point (an inflexion point or two inflexion points) exists or whether the curve is convex or not.

We used the two values λ, μ as shown in Figure 2 to express the geometric characteristics of a plane cubic Bezier curve. Once the observed λ,μ are determined, the geometric characteristics of the curve are determined. It is not related to the amplitude and direction of the vector of the sides. This indicates that λ,μ are a pair of invariant quantities or geometric characteristic control parameters which determine the geometric characteristics of the plane cubic Bezier curve.

Let $A_{ij}=(\vec{a}_i,\ \vec{a}_j)=\begin{vmatrix} x_i & x_j \\ y_i & y_j \end{vmatrix}$ and $A=(\overrightarrow{IS_1},\ \vec{a}_2)$, then we get

$$A_{12}=\frac{A}{1-\lambda},\quad A_{23}=\frac{A}{\mu},\quad A_{13}=-\frac{A}{\mu(1-\lambda)} \tag{4}$$

We are designating the parameters corresponding to the appearance of an inflexion point and a cusp on the plane cubic Bezier curve as u_I and u_c, respectively. The two parameters corresponding to the double point are noted as u_1 and u_2. Then, the equations of inflexion point, cusp and double point of the curve and their corresponding equations of the plotting theorem are the following:

9

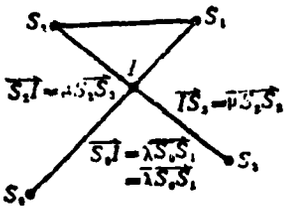

图 2　特征三边形的 λ、μ 与 $\bar{\lambda}$、$\bar{\mu}$

Fig. 2　The λ、μ and $\bar{\lambda}$、$\bar{\mu}$ of a characteristic trilateral

$$\lambda=\frac{A_{23}}{A_{13}}+1,\quad \mu=-\frac{A_{12}}{A_{13}} \tag{5}$$

inflexion point equation: $\vec{P}'(u_I)\times\vec{P}''(u_I)=\vec{0},\ \vec{P}'(u_I)\neq\vec{0},\ u_I\in(0,1)\Longrightarrow \overrightarrow{S_0^{(1)}(u_I)S_1^{(1)}}(u_I)\times\overrightarrow{S_1^{(1)}(u_I)S_2^{(1)}}(u_I)=\vec{0},\ \vec{S}_0^{(2)}(u_I)\neq\vec{S}_1^{(2)}(u_I)$ (6)

cusp equation $\vec{P}'(u_C)=\vec{0},\ u_C\in(0,1)\Longrightarrow\vec{S}_0^{(2)}(u_C)=\vec{S}_1^{(2)}(u_C)$ (7)

double point equation

$\vec{P}(u_1)=\vec{P}(u_2),\ 0\leqslant u_1<u_2<1$ 或 $0<u_1<u_2\leqslant 1\Longrightarrow\vec{S}_0^{(3)}(u_1)=\vec{S}_0^{(3)}(u_2)$ (8)

where the parameter region is unchanged. It is discussed separately in the following:

1. Inflexion point equation: From equation (6), we can get

$$(A_{12}+A_{23}-A_{13})u_I^2+(A_{13}-2A_{12})u_I+A_{12}=0$$

Using equation (4), the above equation can be rewritten as:

$$(2+\mu-\lambda)u_I^2-(1+2\mu)u_I+\mu=0 \tag{9}$$

when $\lambda=\mu+2$, we have $\vec{P}''(u_I)=\vec{0}\Longrightarrow S_0^{(1)}(u_I)S_1^{(1)}(u_I)=S_1^{(1)}(u_I)S_2^{(1)}(u_I)$

The curve becomes a single inflexion segment [6]. It is possible to conduct a simulated projection to transform it into a usual cubic polynominal [3]. Equation (9) has only one root:

$$u_I=\frac{\mu}{1+2\mu} \tag{10}$$

In order to let $u_I\in(0,1)$, it is necessary to have $\mu>0$ or $\mu<-1$. The curve has a single inflexion point at (0.1) as shown in Figure example 1.

When $\lambda\neq\mu+2$, then

$$u_I=\frac{1+2\mu\pm\sqrt{4\mu(\lambda-1)+1}}{2(2+\mu-\lambda)} \tag{11}$$

The determinant $\Delta = 4\mu(\lambda-1)+1$ has the following several situations:

(1) $\Delta > 0$, there are two real roots $u_{t_1} < u_{t_2}$, however, they may not all be on (0,1).

1) If $\mu > 0, \lambda \geqslant 1$ or $\mu \leqslant 0, \lambda < 1$, then:

$$\text{when } \mu > 0, \begin{cases} \lambda > 2+\mu & u_{t_1} < 0, \\ 1 < \lambda < 2+\mu \text{ at} & u_{t_2} > 1, \\ \lambda = 1 & u_{t_2} = 1, \end{cases}$$

$$\text{when } \mu = 0, \ \lambda < 1 \text{ 时}, \ u_{t_1} = 0,$$

$$\text{when } \mu < 0, \begin{cases} \lambda \leqslant 2+\mu & u_{t_1} \leqslant 0, \\ \text{at} & \\ 2+\mu < \lambda < 1 & u_{t_2} > 1. \end{cases}$$

10

i.e., there is always a root outside (0,1). There is only one inflexion point on (0,1) as shown in the diagrammatic examples 2-4. As a special case, when $\vec{a}_1 // \vec{a}_3$ $\lambda, \mu = \infty$ 或 $-\infty$, as shown in Example 5. Only at this time the inflexion point parameters cannot be expressed by λ, u. It is possible to assume $\vec{a}_3 = k\vec{a}_1, k > 0$, then we can obtain the following from equation (6):

$$u_t = \begin{cases} \dfrac{-1+\sqrt{k}}{k-1}, & k \neq 1 \\ 1/2, & k = 1 \end{cases} \qquad (12)$$

We define that after putting them in sequence, the vector of one side has a rotational angle with respect to the previous one of the same sign and its absolute value is always less than 180°; the plane polygon has an unchanged direction of rotation. Otherwise, its direction of rotation is changing. Then by summarizing the situation that the curve has an inflexion point on (0,1), we find the necessary and sufficient conditions for a plane cubic Bezier curve to have an inflexion point on (0,1) are that: $\mu > 0, \lambda \geqslant 1$ or $\mu \leqslant 0, \lambda < 1$, i.e., the corresponding characteristic trilateral changes its direction of rotation.

2) If $\mu>0,\ 1-\frac{1}{4\mu}<\lambda<1$, then the two real roots $u_{t_1}, u_{t_2}\in(0,1)$, i.e., the two inflexion points (also called the double inflexion point) must appear on (0,1). As a special case, when $S_0S_2//S_3S_1$. $0<\mu=\lambda<1$, then $u_{t_1}=\mu, u_{t_2}=1/2$. When the extension of the sides S_0S_2 and S_3S_1 intersects, i.e., when $0<\mu<\lambda<1$, there must be a double inflexion point as shown in example 6. $\mu>0, 1-\frac{1}{4\mu}<\lambda<1$ are the necessary and sufficient conditions for the plane cubic Bezier curve to have two inflexion points on (0,1).

(2) When $\Delta = 0$, there is a double root. From the following discussion on the cusp equation, we know that this is the

$$\vec{P}'(u_c)=\vec{0}\Longrightarrow \vec{S}_0^{(2)}(u_c)=\vec{S}_1^{(2)}(u_c)$$

condition. The two inflexion points coincide with each other which means it is a cusp as shown in examples 7-8. Therefore, we have

$$\left.\begin{aligned}&\lambda=1-\frac{1}{4\mu},\ \mu>0\\ &u_c=u_{t_1}=u_{t_2}=\frac{2\mu}{1+2\mu},\ \mu>0\end{aligned}\right\}\qquad(13)$$

The necessary and sufficient conditions for the plane cubic Bezier curve to have a cusp on (0,1) are: $\mu>0,\ \lambda=1-\frac{1}{4\mu}$.

(3) $\Delta<0\Longrightarrow\lambda<1-\frac{1}{4\mu},\ \mu>0$, there is no real inflexion point. From the following discussion on the double point equation, we know that when λ is above a certain lower limit, the curve will have a double point on [0,1) or (0,1].

2. Cusp equation. Here we will directly find the cusp from the cusp equation (7). From equation (7), we get:

$$\overrightarrow{S_1^{(1)}(u_c)S_2^{(1)}}(u_c)=\frac{u_c-1}{u_c}\overrightarrow{S_0^{(1)}(u_c)S_1^{(1)}}(u_c)$$

$$\Longrightarrow(\vec{a}_1-2\vec{a}_2+\vec{a}_3)u_c^2+2(\vec{a}_2-\vec{a}_1)u_c+\vec{a}_1=\vec{0}\qquad(14)$$

We can obtain $\lambda=1-\frac{1}{4\mu},\ u_c=\frac{2\mu}{1+2\mu},\ \mu>0$, which is consistent with (13).

3. Double point equation. From equation (8), we get

$$(\vec{a}_1-2\vec{a}_2+\vec{a}_3)(u_1^2+u_1u_2+u_2^2)+3(\vec{a}_2-\vec{a}_1)(u_1+u_2)+3\vec{a}_1=\vec{0}$$

we can obtain

$$u=\frac{1+2\mu\pm\sqrt{12\mu(1-\lambda)-3}}{2(2+\mu-\lambda)}\qquad(15)$$

which is the two parameters u_1, u_2 of the double point. The determinant $\Delta = 12\mu(1-\lambda) - 3$.

If $\Delta = 0$, it represents that the double point coincides itself. We have $\lambda = 1 - \frac{1}{4\mu}$, $\mu > 0$, $u_1 = u_2 = \frac{2\mu}{1+2\mu}$. This is consistent with equation (13) which shows that the cusp is the extreme case of a double point.

If $\Delta < 0 \Longrightarrow \lambda > 1 - \frac{1}{4\mu}$, $\mu > 0$, it indicates that there is no real double point. As shown before, there is a double inflexion point.

If $\Delta > 0 \Longrightarrow \lambda < 1 - \frac{1}{4\mu}$, $\mu > 0$, there are two real roots. However, only when both roots are on (0,1] or (0,1], the curve will have a double point on [0,1) or (0,1] as shown in examples 9-11. By letting $u_1 = 0$ in equation (15), we get

$$\left.\begin{aligned} \lambda = -\frac{(1-\mu)^2}{3\mu} \text{ or } \mu = \frac{2-3\lambda-\sqrt{3\lambda(3\lambda-4)}}{2}, \quad 0<\mu<1 \\ u_2 = \frac{1+2\mu}{2+\mu-\lambda} \end{aligned}\right\} \quad (16)$$

By letting $u_2 = 1$ in equation (15), we get

$$\left.\begin{aligned} \mu = \frac{\lambda^2-3\lambda+3}{3(1-\lambda)} \text{ or } \lambda = \frac{3(1-\mu)+\sqrt{3(3\mu^2-2\mu-1)}}{2}, \quad \mu>1 \\ u_1 = \frac{\lambda}{3-2\lambda} \end{aligned}\right\} \quad (17)$$

In a special case, when S_0 coincides with S_3, $u_1 = 0$, $u_2 = 1$, this already belongs to a convex curve case. Therefore, the necessary and sufficient conditions for a plane cubic Bezier curve to have a double point on [0,1) and (0,1] are

$$-\frac{(1-\mu)^2}{3\mu} \leqslant \lambda < 1 - \frac{1}{4\mu}, \quad 0<\mu<1$$

and

$$\frac{3(1-\mu)+\sqrt{3(3\mu^2-2\mu-1)}}{2} \leqslant \lambda < 1 - \frac{1}{4\mu}, \quad \mu>1$$

respectively.

4. Convex or not convex. The Bezier characteristic polygon is convex when the directional plane is on the same side as the vectors of the sides of the polygon and they do not coincide each other. The

definition of a plane directional convex curve is shown in [6].

According to the definition, the plane cubic Bezier curve is a convex curve provided that there is no cusp, inflexion point on (0,1) and no double point on [0,1) and (0,1]. Furthermore, the tangent of any end point does not intersect the curve itself on (0,1). Therefore, the characteristic trilaterals shown in examples 1-11 and their corresponding curves are not convex. When

$$\lambda < -\frac{(1-\mu)^2}{3\mu}, \quad 0 < \mu < 1$$

or

$$0 < \lambda < \frac{3(1-\mu) + \sqrt{3(3\mu^2 - 2\mu - 1)}}{2}, \quad \mu > 1$$

the characteristic trilateral is not convex and the corresponding curve is a nonconvex curve segment without singular point and inflexion point as shown in example 12. When $\lambda = \mu + 2, 1 \leqslant \lambda \leqslant 2$, the characteristic trilateral is convex; the corresponding curve is a single inflected convex curve segment with a single inflexion point as shown in example 13.

102

Summarizing the above, after eliminating the non-convex conditions of the characteristic trilaterals and curves, the remaining conditions are the convex trilateral and convex curve situations as shown in examples 14-15. Hence, the sufficient and necessary conditions for the plane cubic Bezier curve to be a convex curve are: $\lambda \leqslant 0, \mu \geqslant 1$ or $\lambda \geqslant 1, \mu \leqslant 0$, i.e., the corresponding characteristic trilateral is a convex trilateral.

5. The geometric characteristics of the plane cubic Bezier curve. We summarized the above results to compose a complete plane diagram of λ, μ as shown in Figure 3. From this figure, we can clearly see the division of various characteristic regions. It might be possible to use the pair of geometrically invariant quantities $\bar{\lambda} = \lambda$, $\bar{\mu} = 1 - \mu$ which reflect the "symmetry" of the curve as shown in Figure 2. Figure 3 plots the two coordinate axes $\bar{\lambda}$ and $\bar{\mu}$, which form the complete plane diagram of $\bar{\lambda}$, $\bar{\mu}$. Using Figure 3, it is possible to very conveniently determine the geometric characteristics of

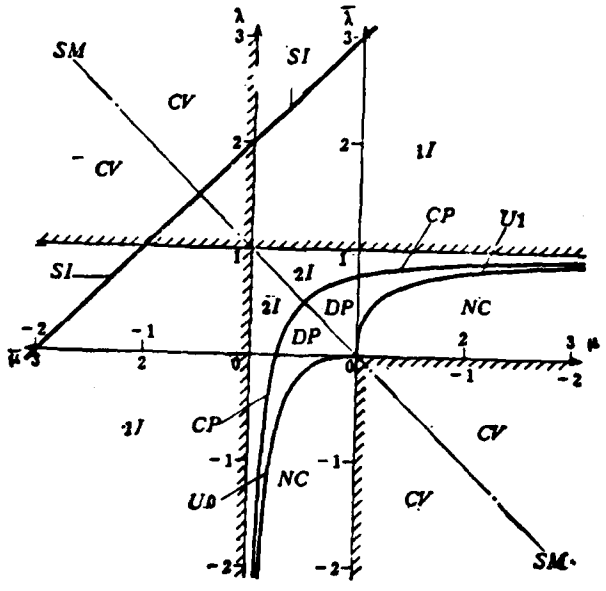

Fig. 3 Geometric characteristic diagram of plane cubic Bezier curves

$\overset{A}{B\,/\!/\!/\!/\,C}$ denotes that the boundary B is involved in region A, but not in C.

SM—symmetric axis; SI—'Single inflexion curve' line; CP—Cusp line;
$U0$—'Double point $u_1 = 0$' line; $U1$—'Double point $u_2 = 1$' line; CV—Convex curve region;
NC—Nonconvex curve region without singurity and inflexion; $1I$—Single inflexionregion;
$2I$—Double inflexion region; DP—Double point region.

the plane cubic Bezier curve corresponding to any plane characteristic trilateral. Furthermore, it is possible to design the curve segment we wanted.

103

III. GEOMETRIC CHARACTERISTICS OF A SPATIAL CUBIC BEZIER CURVE AND OTHER ASPECTS

When the four vertices of the characteristic trilateral are not co-planar, a corresponding spatial cubic Bezier curve is obtained. From the plotting theorem, we know that the three points $S_i^{(1)}$, $i = 0, 1, 2$ cannot be on the same line. Therefore, the curve will not show a pause point (i.e., $\vec{P}'(u) \times \vec{P}''(u) = \vec{O}$, cusp and double point. From the following equation, we get

$$\tau(u) = \frac{(\vec{a}_1, \vec{a}_2, \vec{a}_3)}{|(1-u)^2\vec{a}_1 \times \vec{a}_3 + u(1-u)\vec{a}_1 \times \vec{a}_3 + u^2\vec{a}_2 \times \vec{a}_3|^3}$$

where the numerator is a non-zero constant and the denominator is always positive. Therefore, the curve will not have any point with zero curvature. Let us introduce the direction of rotation: if $(\vec{a}_1, \vec{a}_2, \vec{a}_3) > 0$

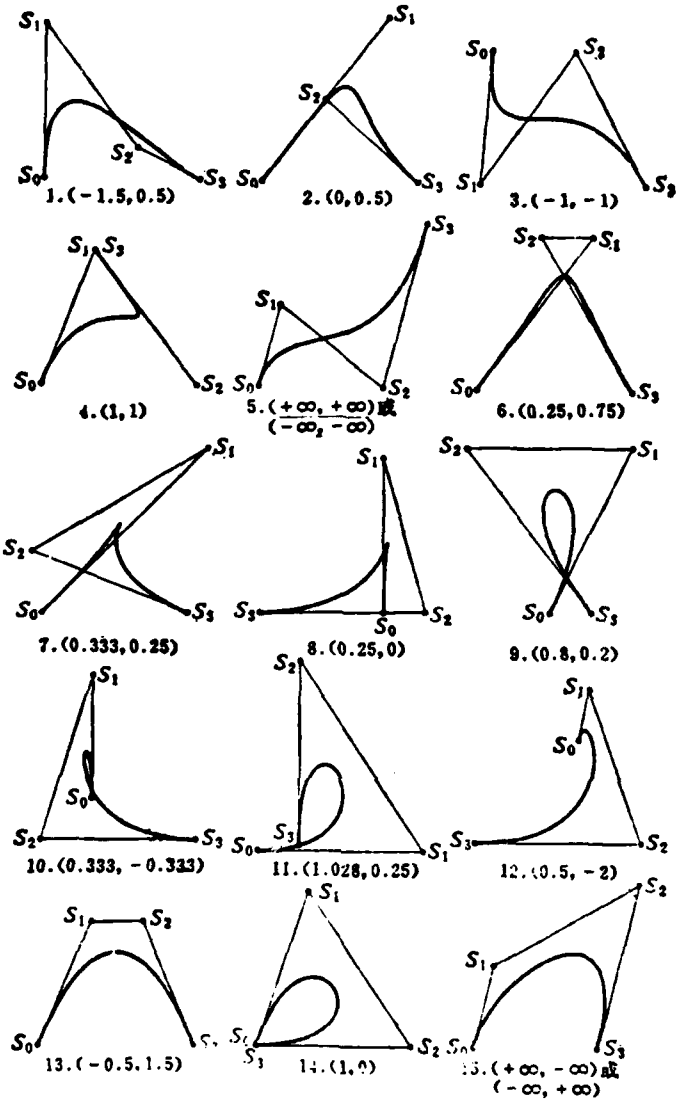

图 4　平面三次Bezier曲线图例1～15(μ，λ)

Fig. 4　Examples of plane cubic Bezier curves 1～15(μ, λ)

then the characteristic trilateral is right handed; if $(\vec{a}_1, \vec{a}_2, \vec{a}_3) < 0$, then it is left handed. Therefore, we have the conclusion that the direction of rotation of a spatial cubic Bezier curve is the same as that of its characteristic trilateral.

Comparing to other forms of parametric cubic curve segments, such as the Ferguson form, Hermite extrapolation form, parametric cubic spline segment and cubic B-spline segment, the Bezier form (through the characteristic trilateral) has the special feature of the most intuition from the point of view of the geometric characteristics of the curve. This is exactly what we hoped for in the practice of geometric design. In the matrix expression, they can be mutually transformed by a full order linear transformation. Hence, we can convert other forms into the Bezier form to subsequently obtain the corresponding Bezier characteristic triangles, to obtain the geometric characteristics of the known curve segment.

REFERENCES

[1] P. E. Bezier.. "Numerical Control-Mathematics and Applications", John Niley and Sons, London, 1972.

[2] Chang Genzhe and Wu Junhen. "The Mathematical Fundamentals of the Bezier Method", Computational Mathematics, 1980, 2, vol. 2.

[3] Su Boqing, Liu Dengyuan. "Computational Geometry", Shanghai Technical Publication, 1981.

[4] Su Boqing. "The Simulated Projection Invariance of the Bezier Curve", Computational Mathematics, 1980, 11, no. 4.

[5] Su Boqing, Hu He Sheng, et al. "Differential Geometry", People's Education Publication, 1980.

[6] Hu Tong Shipyard and Shantong University Hull Mathematical Modeling Research Group, "Single Inflexion Curve Spline Function", Journal of Applied Mathematics, vol. 2, 1977.

BÉZIER'S PLOTTING THEOREM AND GEOMETRICAL CHARACTERISTICS OF CUBIC BÉZIER CURVES

Shi Fazhong and Wu Junheng

(Beijing Institute of Aeronautics and Astronautics)

Abstract

In this paper, taking the plotting theorem as the point of departure, we analyze in detail the geometrical characteristics of plane cubic Bézier curves, including whether a cusp (a cusp of class one) or one inflexion point or two inflexion points exist on the (0 , 1); whether double point occurs on [0 , 1) or (0 , 1] and whether the curve is convex or not.

The geometrical characteristics of plane cubic Bèzier curve can be determined uniquely by two parameters λ , μ or $\bar{\lambda}$, $\bar{\mu}$ (see Fig. 2) on the diagram (fig. 3). The single inflexion curve in Fig. 3 represents the cases when the curve can be transformed into general cubic polynomial. The single inflexion region indicates the cases when the curve has only one inflexion point on (0 , 1) and another is not on (0 , 1).

We may obtain the parameter u_c of cusp, u_1 of inflexion point and u_1, u_2 of double point.

By using plotting theorem we can also make the conclusion that a space cubic Bèzier curve has not cusp, double point and its spiral direction doesn't change.

END

DATE
FILMED

5 -83

DTIC